Studies on Metal Extraction and Materials Preparation Using Chemical Vapor Transport

(化学気相輸送反応を利用した金属分離および材料調製に関する研究)

2000

Tetsuya Ozaki

Osaka University

Contents

General Introduction

As materials science has been developed, improvement in separation and purification processes of substances and materials preparation processes is required. Extraction of rare metals requires a series of complicated treatment, such as dissolution into acid or alkali, precipitation , filtration, drying, and calcination. Moreover, in the case of separation of rare earths, whose chemical properties are very similar with each other, difficulties arise not only in extraction of rare earth from ores or other sources, but also in mutual separation of them. In early times, fractional crystallization and fractional precipitation were used as separation methods of rare earths. Then ion-exchange chromatography and solvent extraction have been developed as new separation methods. These methods utilize complex formation of rare earth ion to enlarge difference in their properties. Accordingly, mutual separation efficiency between rare earths was remarkably improved [1]. However, all the methods mentioned above are so called wet methods for which large scale equipments and large amount of water are needed. As substitute for these methods, dry metal separation process using chemical vapor transport via gaseous halide complexes, which is applicable to both the extraction of metals and mutual separation of rare earths, has been attempted.

Gaseous halide complexes is volatile halogen-bridged compounds which are formed between two different metal halides.

$$m\,MX_x(s, l, g) + n\,LX_y\,(s, l, g) = M_mL_nX_{mx+ny}\,(g)\quad (X: \text{halogen}) \qquad (1)$$

where MX_x is a less volatile metal halide and LX_y called a complex former is an alkali halide or a Group-IIIA (Al, In, Ga) halide in most cases. The metal halides form the gaseous complexes at high temperature and the complexes dissociated into the metal halides at low temperature. Thermochemical and structural properties of many kinds of the gaseous complexes have been studied by means of Knudsen effusion mass spectrometry [2–6], spectrophotometry, and analysis of quenched equilibrium vapors. The RCl_3-$AlCl_3$ (R = Nd, Tb) gaseous complexes was investigated for the candidates of amplifier media in fusion laser systems [6]. The iodide gaseous complexes were already applied to activators of metal halide lamps [5].

It should be noted that apparent vapor pressure of less volatile halides such as rare earth

chlorides increases by the formation of the gaseous complexes. For example, Øye reported that the apparent vapor pressure of $NdCl_3$ was increased by a factor of $1x10^{13}$ and $3x10^7$ at 600 K and 800 K in the presence of 1 atm of Al_2Cl_6, respectively [2]. Reversible formation-dissociation of the gaseous complexes enable the metal halides to be transported chemically. In the presence of the complex formers, rare earth halides are transported along temperature gradient form high temperature side to low temperature side via the gaseous complexes. This chemical transport reaction is first applied to preparation and purification of anhydrous rare earth chlorides [3a]. On the basis of the difference in the stability of the gaseous complexes, each metal halide deposits at different temperature region: The more stable the gaseous complex, the lower temperature the chloride deposits at. It is possible to separate rare earth elements by taking advantage of the difference. Rare earth separation process using the chemical vapor transport via the gaseous complexes have been extensively studied [7–9]. The results of the recent studies on the mutual separation of rare earth elements using the chemical vapor transport was previously reviewed [7]. However, further research on this process with respect to the following points is required for its practical use. First, systematic study for mutual separation efficiency between rare earth elements including Sc and Y is needed. Second, factors, which contribute the chemical vapor transport of the metal halides is to be elucidated. This makes it possible to predict definitely the transport behavior.

It is well known that metal chlorides are easily formed by chlorination of the corresponding oxides with chlorine gas in the presence of carbon [24,28]. By chemical vapor transport in a flow of chlorine gas, metal oxides could be directly converted into volatile gaseous complexes and transported. Therefore direct extraction of rare earths from ores and concentrates by using chemical vapor transport is possible. This process is also applicable to metal recovery process from sludge, scrap, and wastes.

It should be noted that chlorination rate of each metal oxide is different. Such a difference of each element in chlorination rate has been observed not only for simple physical mixtures of two kinds of metal oxides but also for ores and concentrates, in which various metal components partly form solid solutions. This selectivity in chlorination and chemical vapor transport of metal oxides opened the another possibility of chemical vapor transport for materials processing. Bulk and surface modification of materials, in which a particular component of it is eliminated by chemical vapor transport, is also possible. Metastable phases, which have never been synthesized with the

conventional methods, may be obtained by using this process.

Meanwhile, metal halides decompose into the corresponding metal and halogen at high temperature [61]

$$MX_n\ (g) \rightarrow M\ (g) + n\ X\ (g) \quad (X: \text{halogen}) \qquad (2)$$

In the case of the iodides, the decomposition is initiated above about 1000 K. Since the metal vapor is obtained at much lower temperature than the melting point of the metal, the decomposition reaction, which has been applied to the metal halide lamps, has further possibilities of applications in combination with the chemical vapor transport.

The object of this study are as follows. The first is the elucidation of equilibrium and non-equilibrium factors having a influence on the chemical vapor transport behavior via the gaseous halide complexes by thermodynamic and kinetic investigations for the reaction. The second is development of effective rare earth separation process using the information obtained by the investigation of the chemical vapor transport. The third is the application of the chemical vapor transport to the surface modification of inorganic materials. The fourth is the elucidation of the decomposition behavior of the metal halides and halide gaseous complexes at high temperature.

This thesis consists of following chapters.

Chapters 1 and 2 deal with the application of the chemical vapor transport mediated by the gaseous halide complexes to rare earth extraction and separation. In **chapter 1**, for binary systems of rare earths including Sc and Y, chemical vapor transport efficiency and mutual separation characteristics were investigated using chloride or oxide mixtures as starting materials. The non-equilibrium factor resulting from physical diffusion was considered, and the prediction of the chemical transport behavior was attempted. Possibilities of decrease in reaction temperature and increase in chemical transport efficiency was also investigated with the gaseous iodide complexes, which is more volatile than the corresponding chloride complexes. In **chapter 2**, extraction of rare earths form the used polishing agent containing rare earth oxides as main components was actually attempted by using the identical process.

In **chapter 3**, surface modification process, in which particular element is eliminated from surface of inorganic materials by chemical vapor transport, was studied. The process was applied

to CeO_2-ZrO_2 mixed oxides and effect of the surface modification on the redox behavior was investigated.

In **chapter 4**, density distributions of vapor species in many kind of metal halide lamp systems containing metal iodides were simulated by comparing the thermodynamic data for the decomposition of the iodides with the experimental results and considering the effect of diffusion induced by the convection of mercury vapor.

List of Publications

1. The Characteristics of Chemical Vapour Transport and Mutual Separation for the Scandium, Yttrium and Lanthanum Mediated by the Corresponding Gaseous Rare Earth Chloride Complexes
   Jianzhuang Jiang, Tetsuya Ozaki, Ken-ichi Machida, and Gin-ya Adachi
   Journal of Alloys and Compounds, **264**, 157-163 (1998).

2. Mutual Separation Characteristics for the Yttrium and Lanthanides with Chemical Vapor Transport Process mediated by Metal Chloride Gaseous Complexes
   Tetsuya Ozaki, Jianzhuang Jiang, Kuniaki Murase, Ken-ichi Machida, and Gin-ya Adachi
   Journal of Alloys and Compounds, **265**, 125-131 (1998).

3. Extraction and Mutual Separation of Rare Earths from Used Polishes by Chemical Vapor Transport
   Tetsuya Ozaki, Ken-ichi Machida, and Gin-ya Adachi
   Metallurgical and Materials Transaction B, **30B**, 45-51 (1999).

4. Recovery of Rare Earths from Used Polishes by Chemical Vapor Transport Process
   Tetsuya Ozaki, Ken-ichi Machida, and Gin-ya Adachi
   Materials Science Forum, **315–317**, 297–305 (1999).

5. Thermodynamic Studies on Dissociation of Metal Iodides at High Temperatures in Metal Halide Lamps
   Tetsuya Ozaki and Gin-ya Adachi
   Journal of Applied Physics, **86**, 4723–4728 (1999).

6. Effects of Surface Modification by the Chemical Filing on the Redox Behavior of a Ceria-Zirconia Mixed Oxide
   Toshiyuki Masui, Tetsuya Ozaki, Ken-ichi Machida, and Gin-ya Adachi
   Journal of Alloys and Compounds, **292**, L8–L10 (1999).

7. Redox Behavior of Surface Modified CeO_2-ZrO_2 Catalysts by Chemical Filing Process
   Tetsuya Ozaki, Toshiyuki Masui, Ken-ichi Machida, Takao Sakata, Hirotaro Mori, and Gin-ya Adachi
   Chemistry of Materials, in press.

List of Supplementary Publications

1. Extraction and Mutual Separation of Rare Earths from Concentrates and Crude Oxides using Chemical Vapor Transport
   Kuniaki Murase, Tetsuya Ozaki, Ken-ichi Machida, and Gin-ya Adachi
   Journal of Alloys and Compounds, **233**, 96-106 (1996).

2. Extraction of Rare Earths and Thorium form Monazite by Chlorination with Carbon Tetrachloride
   Tetsuya Ozaki, Kuniaki Murase, Ken-ichi Machida, and Gin-ya Adachi
   Transaction of the Institution of Mining and Metallurgy, Section C, **105** (May-Aug.), C141–145.

3. Vapor Phase Extraction and Separation of Rare Earths from Bastnaesite Concentrate Mediated by Vapor Complexes
   Tetsuya Ozaki, Toshiki Miyazawa, Kuniaki Murase, Ken-ichi Machida, and Gin-ya Adachi
   Journal of Alloys and Compounds, **245**, 10-14 (1996).

4. Separation and Recovery of Rare Earths via a Dry Chemical Vapour Transport Based on Halide Gaseous Complexes
   Jianzhuang Jiang, Tetsuya Ozaki, Ken-ichi Machida, and Gin-ya Adachi
   Journal of Alloys and Compounds, **260**, 222-235 (1997).

5. Recovery of Vanadium, Nickel and Magnesium form a Fly Ash of Bitumen-in-water Emulsion by Chlorination and Chemical Transport
   Kuniaki Murase, Ken-ichi Nishikawa, Tetsuya Ozaki, Ken-ichi Machida, Gin-ya Adachi, and Taiichiro Suda
   Journal of Alloys and Compounds, **264**, 151-156 (1998).

6. Preparation of Ceria-Zirconia Sub-Catalysts for Automotive Exhaust Cleaning
   Toshiyuki Masui, Tetsuya Ozaki, Ken-ichi Machida, and Gin-ya Adachi
   Journal of Alloys and Compounds, in press.

Chapter 1

Mutual separation of rare earth elements using chemical vapor transport

1.1 Introduction

As mentioned, purification and separation process of rare earths become of importance, because the rare earths with high purity is required for advanced materials. In our laboratory, dry separation processes of rare earth elements using chemical vapor transport (CVT) via the gaseous complexes, $KRCl_4$ and RAl_nCl_{3+3n} (R: rare earths), have been attempted. The mutual separation efficiency has been studied in many kinds of binary systems using both rare earth chlorides and oxides as raw materials[7–9]. In addition, the other group have investigated the mutual separation characteristics of the neighboring rare earths in a similar stepwise chlorination-chemical vapor transport (SC-CVT) process, which consists of the chlorination at low temperature and the successive chemical vapor transport at high temperature[10–14]. In the CVT experiments of binary mixtures of lanthanide chlorides with KCl and $AlCl_3$ as complex formers [8], the larger the difference of the rare earths in atomic number, the higher the separation efficiency between their chlorides. However, the mutual separation efficiencies for the same binary systems are often largely different depending on the difference in starting materials (oxides or chlorides) and the other experimental conditions.

Scandium (Sc) and yttrium (Y) have much smaller atomic numbers than and different electronic configurations from the other rare earths. Ionic radius of the 6-coordinated Sc^{3+} ion (pm) is the smallest among rare earth trivalent ions, while that of Y^{3+} (90.0 pm) is close to those of Dy^{3+} (91.2 pm), Ho^{3+} (90.1 pm), and Er^{3+} (89.0 pm) [15], and separation of yttrium from the heavy rare earths in Xenotime, a kind of rare earth ores, is very difficult in conventional separation methods. However, it has not been investigated whether the rare earth ionic radii are decisive factors for CVT properties of rare earth chlorides.

Meanwhile, metal iodide gaseous complexes have the higher vapor pressure than the corresponding chloride gaseous complexes, because the covalency in the chemical bond in the metal halides increase in the following order: fluoride < chloride < bromide < iodide.

In this chapter, the CVT efficiencies of $ScCl_3$ and YCl_3 were investigated and compared with those of lanthanide chlorides. Mutual separation characteristics in the binary systems including Sc and Y were also studied using oxide and chloride mixtures as starting materials. The application of

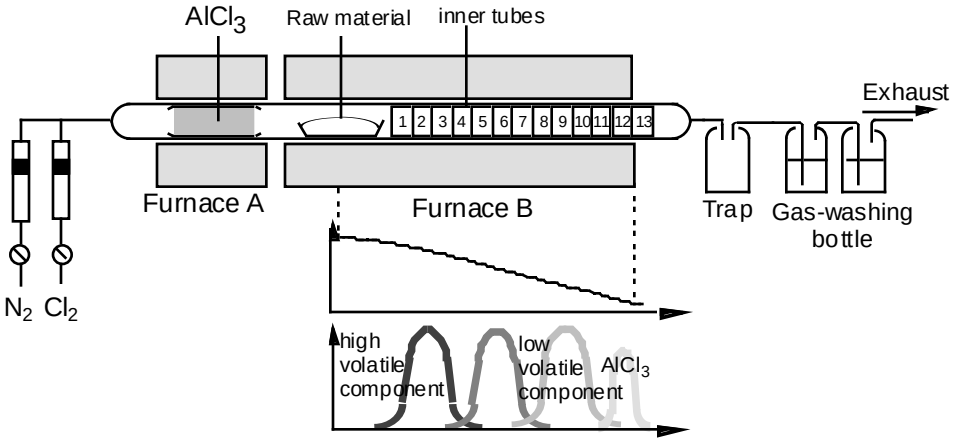

Figure 1.1. A Schematic diagram of the apparatus for the chemical vapor tranport reaction.

the iodide gaseous complexes to the separation process was also attempted.

1.2 Experimental details

The rare earth oxides, R_2O_3 (R = Sc, Y, La, Pr, Nd, Dy, Ho, Er) were obtained from Shin-Etsu Chemical Co. Ltd. The oxides, chlorides, and iodides of the rare earths were used as the starting materials for the CVT experiments. The Rare earth chlorides and iodides were synthesized by the solid-state reaction of the corresponding oxides with ammonium halides. In the synthesis of the pure chlorides, 2.00 g of the oxides were mixed with 8.00 g of ammonium chloride, NH_4Cl, for 30 min in alumina mortar in a N_2-filled glove box. The mixture was heated in a N_2 flow at 473 K for 2 h to remove moisture, and then the temperature was raised to 573 K for 2 h to complete the chlorination of the oxides. Finally, the excess NH_4Cl was removed in vacuo at 673 K for 3 h. In the synthesis of the pure iodides, the mixture of 1.00 g of the oxides and 20.00 g of ammonium iodide, NH_4I, was heated at 693 K for 3 h after dehydration at 473 K, and the excess NH_4I was removed in vacuo at 703 K for 3 h. The binary mixtures of the halides were synthesized in manners similar to the synthesis of the pure halides using the mixtures of the rare earth oxides as the starting materials. The product was identified by X-ray diffractometer (MAC Science M18XHF-SHA) using Cu-Kα radiation and its purity as rare earth iodide was determined by its solubility in deionized water.

An apparatus employed for the chemical vapor transport experiments is shown in Figure 1.1. The apparatus consists of two horizontal tubular furnaces A and B. Furnace B was devised for generating different kinds of temperature gradients by eight individual heating systems. Furnace A was used to generate gaseous Al_2Cl_6.

The starting materials (2.0×10^{-3} mol) mixed with active carbon (0.100 g) as a deoxidant was

loaded on a graphite boat, and the boat was set at the end of furnace B. Inside the reactor tube, 13 pieces of quartz inner tubes were put side by side next to the boat for recovery and analysis of the deposits. Mixture of N_2 and Cl_2 gases with flow rates of 15–50 and 6 cm^3min^{-1}, respectively, flow in the reactor as a carrier. In the case of iodide starting materials, only N_2 was introduced. $AlCl_3$ and KCl, KI, and K_2CO_3 were used as the complex formers for the CVT experiments using the chlorides, iodides, and oxides starting materials, respectively. KCl, KI, and K_2CO_3 were directly mixed with the starting materials. In the case of $AlCl_3$, gaseous Al_2Cl_6 was generated by heating $8.0x10^{-3}$ mol of $AlCl_3$ put in ample with small orifice at 353–453 K in furnace A. Rare earth oxides and K_2CO_3 were chlorinated by Cl_2 in the presence of carbon.

$$R_2O_3\ (s) + 3\ C\ (s) + 3\ Cl_2\ (g) \rightarrow 2\ RCl_3\ (s) + 3\ CO\ (g) \quad (1.1)$$

$$K_2CO_3\ (s) + 2\ C\ (s) + Cl_2\ (g) \rightarrow 2\ KCl\ (s) + CO\ (g) \quad (1.2)$$

Rare earth halides react with KX and $AlCl_3$ to form the gaseous complexes K_mRX_{3+m} and RAl_nCl_{3+3n}, respectively.

$$RX_3\ (s, l) + m\ KX\ (s, l) = K_mRX_{3+m}\ (g)\ (X = I, Cl) \quad (1.3)$$

$$RCl_3\ (s, l) + n/2\ Al_2Cl_6\ (g) = RAl_nCl_{3+3n}\ (g) \quad (1.4)$$

The gaseous complexes were transported along the temperature gradients, and the rare earth halides deposited by the reverse reaction. Deposits in the reactor were recovered from every inner tube, and the metal halides contained in the deposits and the residue were determined on the X-ray fluorescent spectrometer (Rigaku System 3270 A).

1.3. Results and Discussion

1.3.1 Chemical vapor transport reaction of rare earth chlorides

In the chemical vapor transport (CVT) from the high temperature to the low temperature, the rare earth halides deposit as a result of the decrease in the saturated vapor pressure of the gaseous complexes. The transported amount of the rare earth chlorides from temperature T to temperature T_1 is calculated as follows.

$$N = (P - P^\circ_{T1}) \cdot V / RT \quad (1.5)$$

where P is the partial pressure of the gaseous complexes, P°_{T1} is the saturated vapor pressure at T_1, R is gas constant, and V is total volume of the vapor species in the system. Although the carrier gases, the gaseous complexes, and each metal chloride exist in vapor phase, the volume of the carrier gas is much larger than those of the metal chlorides and the gaseous complexes.

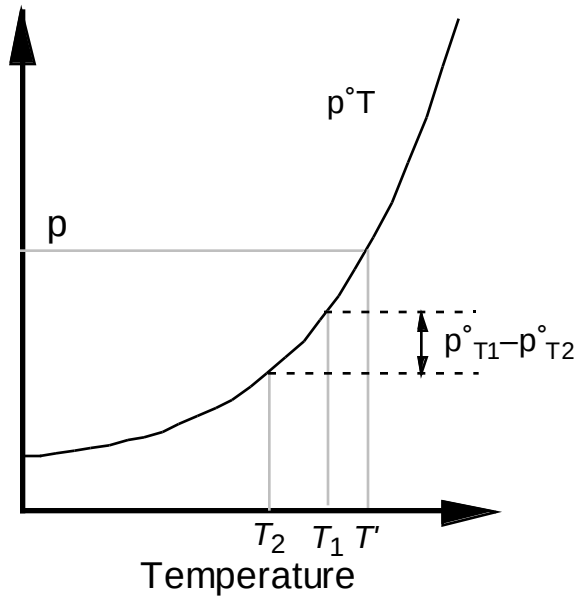

Figure 1.2 Relationship between saturated vapor pressure of gaseous complexes and deposition temperature of metal halides

$$V = V_c \cdot t + V_{\text{gaseous complex}} + V_{\text{KCl or Al2Cl6}} + V_{\text{RCl3}} \approx V_c \cdot t \qquad (1.6)$$

where V_c is the flow rate of the carrier gas and t is the reaction time. Since P°_{T1} is negligible at room temperature, the total transported amount from the reaction temperature to room temperature is

$$N_{\text{RCl3}} = P \cdot V_c \cdot t / RT \qquad (1.7)$$

Figure 1.2 explains the relationship between the saturated vapor pressure of the gaseous complexes and the deposition temperature of the rare earth chlorides when only the formation-dissociation equilibrium of gaseous complexes is considered for the CVT process. In the equilibrium condition, the dissociation of the gaseous complexes and the subsequent deposition of the rare earth chlorides begin at the temperature T' at which P equals to P°_T, and the deposited amount in the temperature region from T_2 to T_1 ($T_2 > T_1$) is

$$N_{T1-T2} = (P - P^\circ_{T1}) \cdot V_c \cdot t / RT \qquad (T_2 > T' > T_1) \qquad (1.8)$$

$$N_{T1-T2} = (P^\circ_{T2} - P^\circ_{T1}) \cdot V_c \cdot t / RT \qquad (T' \geq T_2)$$

However, the deposition temperature of rare earth chlorides is actually affected by the non-equilibrium factors and depends on various experimental conditions.

(1) Chemical vapor transport of pure rare earth chlorides with KCl

It has been reported that predominant gaseous complex formed between RCl_3 and KCl is $KRCl_4$ (g) for all rare earths. Murase et al. proposed C_{2v}-type structure shown in Figure 1.3 for $KNdCl_4$ (g) [80]. Gaseous complexes $KRCl_4$ (g) are formed according to the following reaction.

$$RCl_3 \text{ (s, l)} + KCl \text{ (s, l)} \rightarrow KRCl_4 \text{ (g)} \qquad (1.9)$$

Figure 1.4 shows the transported amount of the rare earth chlorides RCl_3 (R = Y, Dy, Ho, Er) in the CVT experiment of the pure rare earth chlorides with KCl complex former. The transported amount increased in the following order.

$$Dy < Y < Ho < Er$$

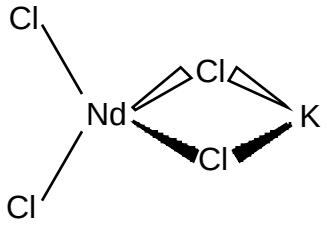

Figure 1.3 Proposed structure for $KNdCl_4$ (g) [80]

Except for YCl_3, the linear relationship between the transported amount and the ionic radii of 6-coordinated trivalent rare earth ions R^{3+} [15] was observed. The transported amount depends on the vapor pressure of $KRCl_4$ (g). The vapor pressure is calculated from the gibb's energy change for the formation reaction of the gaseous complexes (Eq. (1.9)).

$$P^{\circ}_{KRCl4,\,T} = K_p = \exp(-\Delta G/RT) \qquad (1.10)$$

where K_p is the equilibrium constant for Eq. (1.9). The enthalpy and entropy changes (ΔH, ΔS) for

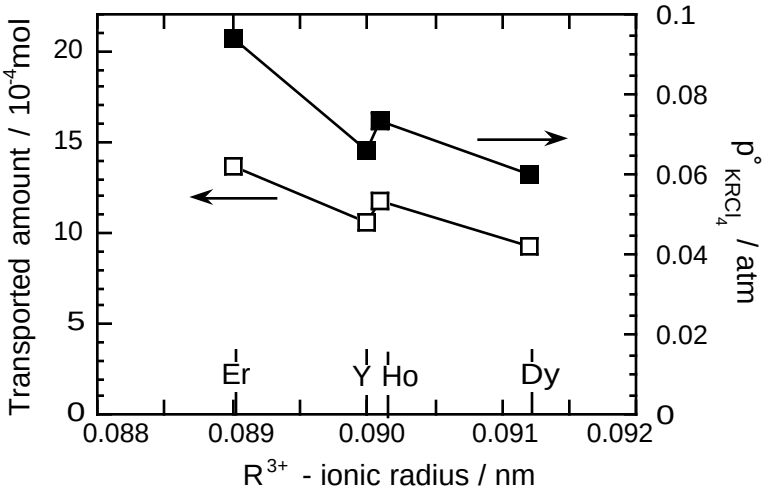

Figure 1.4 Variation in total transported amounts of RCl_3 for the chemical vapor transport with KCl complex former and vapor pressure of $KRCl_4$ at 1273 K calculated from thermodynamic quantities.

Eq. (1.9) were calculated from those for the following reactions (Table 1.1).

$$RCl_3\ (s, l) \rightarrow RCl_3\ (g) \qquad \cdots\cdots\Delta H_1,\quad \Delta S_1 \qquad (1.11)$$

$$KCl\ (s, l) \rightarrow KCl\ (g) \qquad \cdots\cdots\ \Delta H_2,\quad \Delta S_2 \qquad (1.12)$$

$$RCl_3\ (g) + KCl\ (g) \rightarrow KRCl_4\ (g) \qquad \cdots\cdots\ \Delta H_3 \quad \Delta S_3 \qquad (1.13)$$

$$\Delta H = \Delta H_1 + \Delta H_2 + \Delta H_3 \qquad \Delta S = \Delta S_1 + \Delta S_2 + \Delta S_3$$

where the thermodynamic quantities for Eqs. (1.11) and (1.12) have been reported [81, 82], and those for Eq. (1.13) are [6]

$$\Delta H_3 \approx -240 \pm 40\ \text{kJ mol}^{-1},\ \Delta S_3 \approx -135 \pm 20\ \text{J mol}^{-1}\text{K}^{-1}$$

The Gibb's energy change ΔG for equation (1.9) at temperature T was then calculated using the relationship $\Delta G = \Delta H - T\Delta S$. Figure 1.4 also shows the saturated vapor pressure of $KRCl_4$ (R = Y, Dy, Ho, Er) at 1273 K calculated from ΔG by using Eq. (1.10). It was demonstrated that the amount of RCl_3 transported with KCl depends on the saturated vapor pressure

$$N_{RCl3} = k\cdot(V_c\cdot t / RT)\ P^{\circ}_{KRCl4,\ 1273} \qquad (1.14)$$

where the average of the k values for RCl_3 (Y, Dy, Ho, Er) is $3.00\text{x}10^{-1}$.

Table 1.1 Enthalpy and entropy changes for formation reaction of gaseous complexes $KRCl_4$ (eq. (1.9))

Chlorides	ΔH (kJ mol^{-1})	ΔS (JK^{-1}mol^{-1})
YCl_3	236.95	167.56
$DyCl_3$	225.73	157.97
$HoCl_3$	223.47	157.82
$ErCl_3$	220.99	157.91

The distributions of the deposits of pure rare earth chlorides RCl_3 (R = Y, Dy, Ho, Er) transported with KCl under the linear temperature gradient (28 K/cm, Figure 1.5 (a))are described in Figure 1.5 (b)–(d). The higher the vapor pressure of the gaseous complexes, the lower the deposition temperature. The deposited amount calculated from the transported amount N_{RCl3} and the saturated vapor pressure $P^{\circ}_{KRCl4,\ T}$ by using eq. (1.8) is also shown in Figure 1.5 (b)–(d). The rare earth chlorides deposit in the lower temperature side compared to the calculated distribution, because the rare earth chlorides are in fact further diffused physically by the carrier gas to lower temperature. Therefore, if the whole temperature region consists of n fractions, the deposited amount in the k th

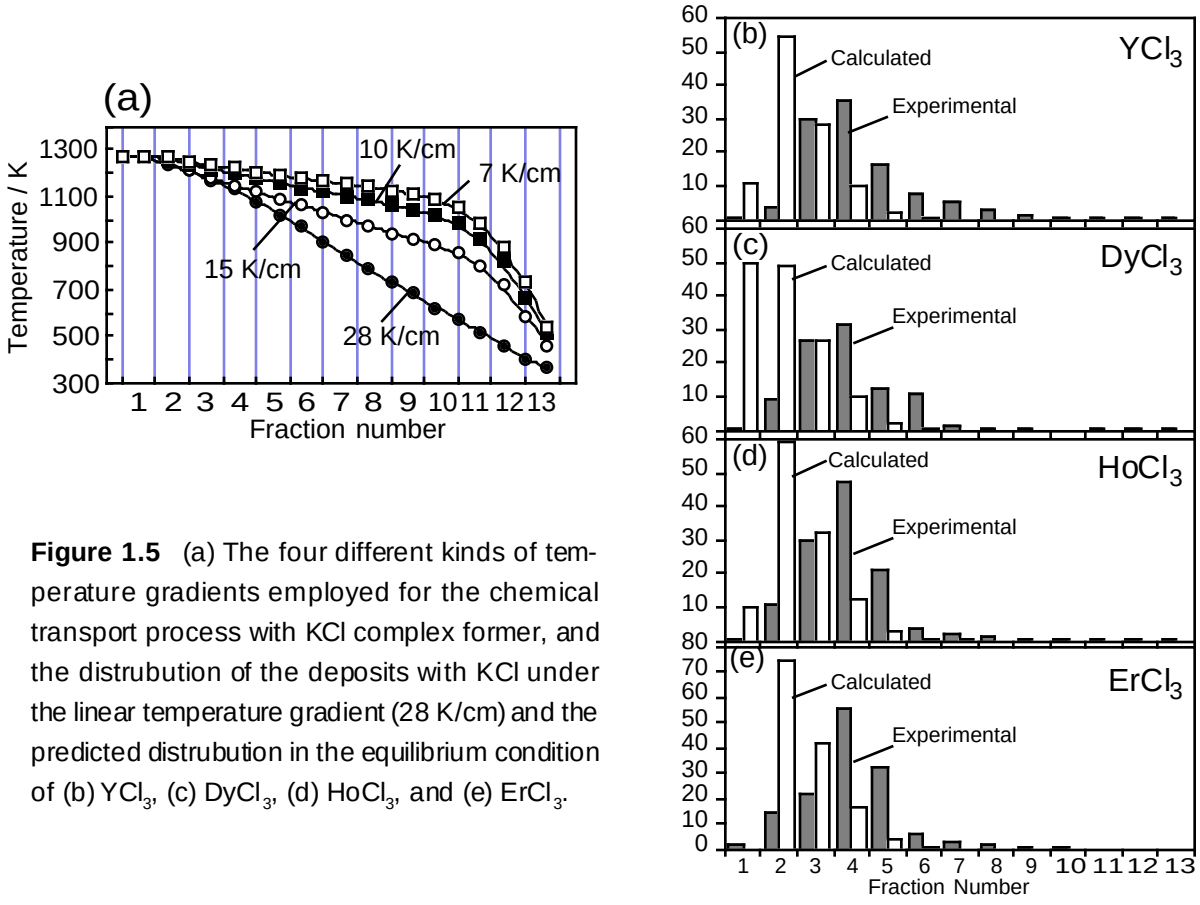

Figure 1.5 (a) The four different kinds of temperature gradients employed for the chemical transport process with KCl complex former, and the distrubution of the deposits with KCl under the linear temperature gradient (28 K/cm) and the predicted distrubution in the equilibrium condition of (b) YCl_3, (c) $DyCl_3$, (d) $HoCl_3$, and (e) $ErCl_3$.

fraction is expressed as

$$N_k' = N_k + \sum_{i=1}^{k-1} \Delta N_{i \to k} - \sum_{i=k+1}^{n} \Delta N_{k \to i} \qquad (1.15)$$

where N_k is the calculated deposited amount in the k th fraction in the equilibrium condition, and $\Delta N_{i \to j}$ is the amount diffused physically from i th fraction to j th fraction. By comparison between the experimental and the calculated distributions, $\Delta N_{i \to j}$ is found to be expressed using the following empirical equation.

$$\Delta N_{i \to j} = N \cdot \alpha \cdot (\Delta T/\Delta x)_{av} (\Delta T/\Delta x)^{-1} (1/\Delta x^2) \qquad (1.16)$$

where ΔT and Δx are temperature differences and distance between i th and j th fractions, respectively, and $(\Delta T/\Delta x)_{av}$ is the average temperature gradient in the temperature region where the rare earth chloride deposits obtained by

$$(\Delta T/\Delta x)_{av} = \Sigma N_k (\Delta T/\Delta x)_k / \Sigma N_k \qquad (1.17)$$

where N_k and $(\Delta T/\Delta x)_k$ is the calculated deposited amount and the temperature gradient in k th fraction, respectively. The coefficient α in Eq. (1.16) calculated for the rare earth chlorides are

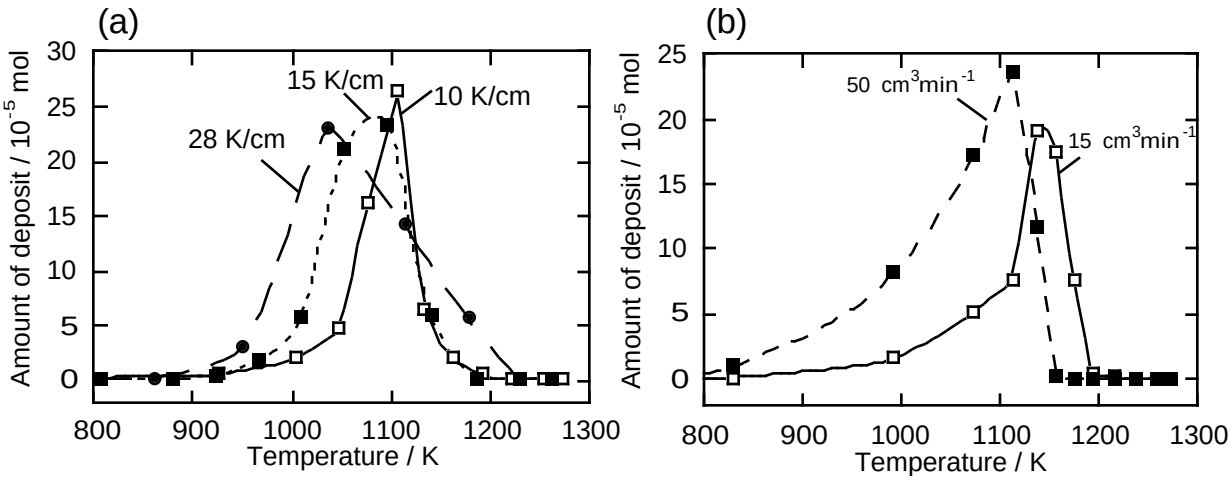

Figure 1.6 Relationship between amount of YCl_3 deposit and temperature for the chemical vapor transport with various temperature gradients

summarized in Table 1.2. The value for YCl_3 was much larger than those for $DyCl_3$, $HoCl_3$, and $ErCl_3$. Diffusion ability of substance is generally inversely proportional to its weight. YCl_3 is subject to physical diffusion by the carrier gas because of its smaller molecular weight (196.27) compared to $DyCl_3$ (268.86), $HoCl_3$ (271.29), and $ErCl_3$ (273.62). The deposition temperature depends on the experimental conditions because of the effect of the physical diffusion.

Table 1.2 Coefficients α of Eq. (1.16) for the rare earth chlorides in the present work

chlorides	YCl_3	$DyCl_3$	$HoCl_3$	$ErCl_3$
α	6.43	4.82	4.80	4.64

Relationships between the amount of deposited YCl_3 and the deposition temperature with three kinds of temperature gradients (10, 15, 28 K/cm, Figure 1.5 (a)) and two kinds of N_2 flow rate (15, 50 cm^3min^{-1}) in the chemical vapor transport experiments were indicated in Figure1.6 (a) and (b), respectively. The deposition temperature shifted to the higher temperature side with decreasing the temperature gradient and to the lower temperature side with increasing the N_2 flow rate.

(2) Chemical vapor transport of pure rare earth chlorides with $AlCl_3$

Gaseous complexes RAl_nCl_{3+3n} are formed according to the gas-solid reaction shown in Eq. (1.4). It has been reported that four kinds of gaseous complexes are formed between RCl_3 and $AlCl_3$: $RAlCl_6$, RAl_2Cl_9, RAl_3Cl_{12}, and RAl_4Cl_{15}. Wang et al. concluded that RAl_3Cl_{12} complex is predominant gaseous complex in the temperature range from 500 to 900 K for R = La – Lu, while that RAl_2Cl_9 is predominant gaseous complex for R = Sc and Y in the same temperature range [20]. Different coordination structures are suggested for RAl_3Cl_{12} of early and end series of lanthanides.

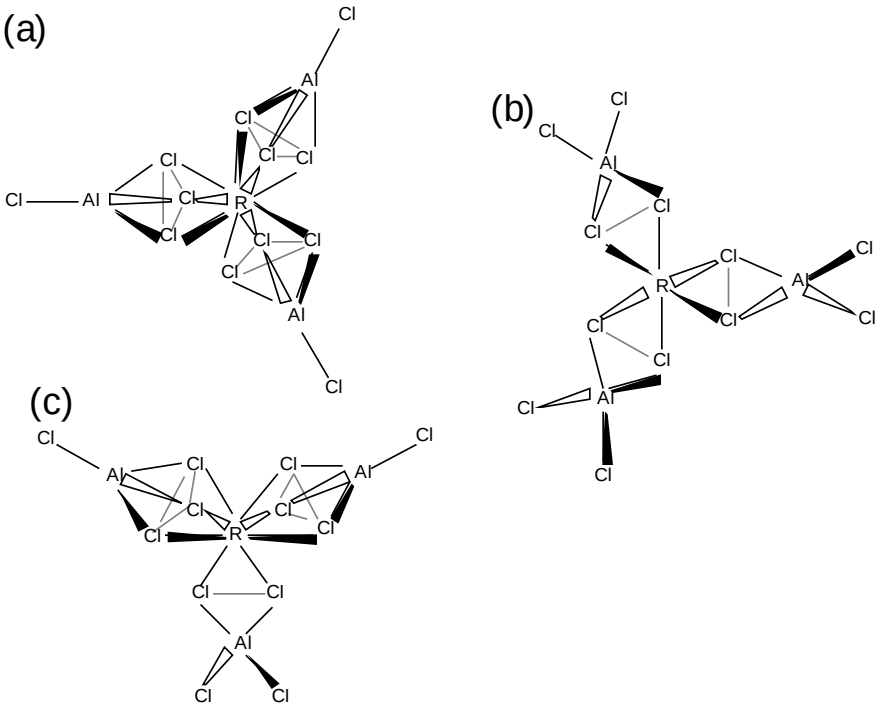

Figure 1.7 Proposed structure for RAl_3Cl_{12} (a) R = Nd–Eu (b) R = Ho–Yb (c) R = Tb [6].

Figure 1.7 (a), (b), and (c) describe the proposed structures of RAl_3Cl_{12} for Nd–Eu, Ho–Yb, and Tb, respectively [6].

Equilibrium constant K_P for Eq. (1.4) is

$$K_P = P_{RAlnCl3+3n}/(P_{Al2Cl6})^{n/2} \tag{1.18}$$

where $P_{RAlnCl3+3n}$ and P_{Al2Cl6} are partial pressure of RAl_nCl_{3+3n} and Al_2Cl_6, respectively. Therefore, vapor pressure of RAl_nCl_{3+3n} depends on vapor pressure of Al_2Cl_6 as well as Gibbs energy change ΔG and temperature T.

$$P_{RAlnCl3+3n} = (P_{Al2Cl6})^{n/2} \cdot K_P = (P_{Al2Cl6})^{n/2} \exp(-\Delta G/RT) \tag{1.19}$$

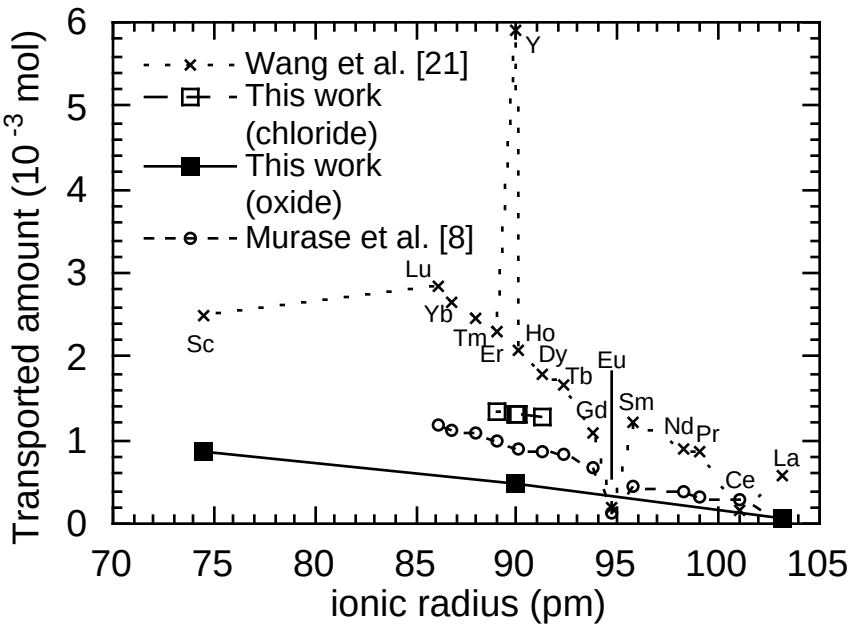

Figure 1.8 Variation in total transported amounts of RCl_3 for chemical vapor transport with $AlCl_3$ complex former

The CVT properties of RCl_3 mediated by gaseous complex RAl_3Cl_{12} (R = La–Lu) was previously investigated in our laboratory [8]. On the other hand, Wang's group carried out the chlorination-CVT experiment using the pure rare earth oxides from Sc_2O_3 to Lu_2O_3 as starting materials and $AlCl_3$ as a complex former [21]. In the present work, the CVT property for pure YCl_3, $DyCl_3$, $HoCl_3$, and $ErCl_3$ and the chlorination-CVT property for pure Sc_2O_3, Y_2O_3, and La_2O_3 was investigated. The results of these CVT experiments are compared in Figure 1.8. In all the results, the transported amount of lanthanoid chlorides increased with increasing atomic number. However, the different tendency was observed for the chemical vapor transport property of $ScCl_3$ and YCl_3 between the Wang's work and this work. The transported amount of YCl_3 was between those of $HoCl_3$ and $ErCl_3$ in this work, while it was the largest among the rare earth chlorides in the result reported by Wang's group. From eq. (1.19), the dependency of the pressure of $ScAl_2Cl_9$ and YAl_2Cl_9 on the pressure of Al_2Cl_6 is different from those of RAl_3Cl_{12}. The transported amount of YCl_3 is therefore larger than that of the lanthanide chlorides with low partial pressure of Al_2Cl_6 and comparable to them with high partial pressure of Al_2Cl_6. In the CVT experiments with oxide starting materials, the transported amount of $ScCl_3$ was less than YCl_3 in the Wang's result, while was larger than YCl_3 in this work. Gibb's energy changes for the reaction $RCl_3 + Al_2Cl_6 \rightarrow RAl_2Cl_9$ for R = Sc and Y at 1273 K are 25.6 and 33.2 kJ mol^{-1}, respectively [20]. The ratio of the vapor pressure of the gaseous complexes is

$$P_{ScAl2Cl9}/P_{YAl2Cl9} = \exp(-\Delta G_{Sc}/RT)/\exp(-\Delta G_{Y}/RT) = 2.045$$

Therefore, the transported amount of $ScCl_3$ with $AlCl_3$ is essentially larger than that of YCl_3. The

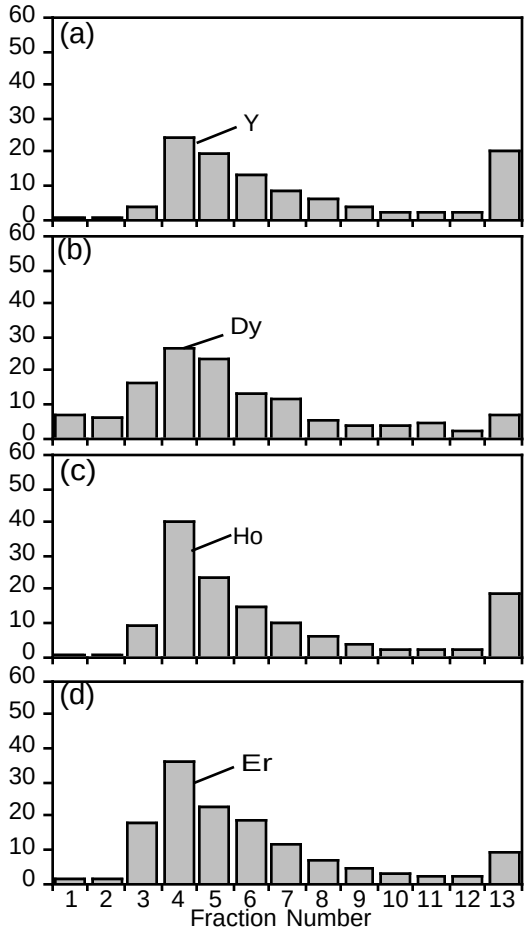

Figure 1.9 Distrubution of the deposit of (a) YCl_3, (b) $DyCl_3$, (c) $HoCl_3$, and (d) $ErCl_3$ in the CVT experiment using chloride starting materials with $AlCl_3$.

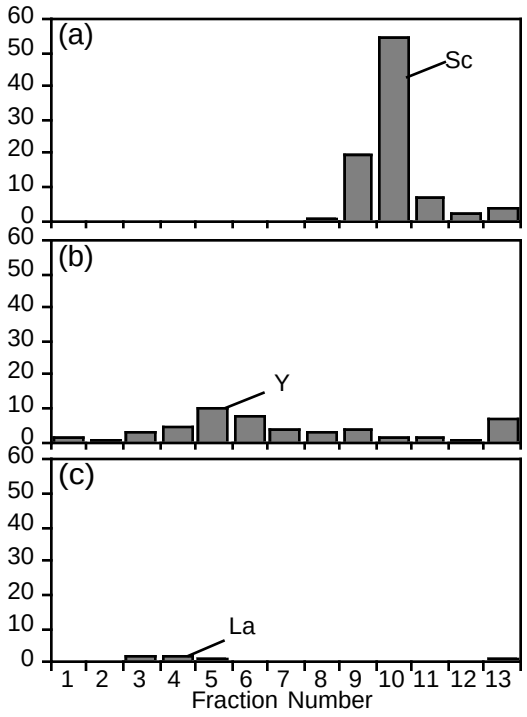

Figure 1.10 Distrubution of the deposit of (a) $ScCl_3$, (b) YCl_3, and (c) $LaCl_3$ in the CVT experiment using oxide starting materials with $AlCl_3$.

difference observed above indicates that the chlorination rate also affects the transported amount. The Gibb's energy changes for the chlorination reactions of Sc_2O_3 and Y_2O_3 (Eq. (1.1)) are –41.6 and –62.1, respectively, and Sc_2O_3 is less subject to chlorination than Y_2O_3. The difference in the chlorination rate is larger than that at high temperatures. Chlorination temperature in Wang's and our experiments is 700 K and 1273 K, respectively. Therefore, the transported amount of Sc_2O_3 in the former is lower than that in the latter.

The distribution of deposit for the transport experiments using chloride and oxide starting materials are shown in Figure 1.9 and 1.10, respectively. The deposition temperature regions of YCl_3, $HoCl_3$, $DyCl_3$, and $ErCl_3$ were closed to each other. On the other hand, $ScCl_3$, YCl_3, and $LaCl_3$ were deposited in remote temperature region from each other. This agrees with the general relationship between the vapor pressure of the gaseous complex and the deposition temperature. The stability of the gaseous complexes increase in the following order.

$$ErAl_3Cl_{12} > YAl_2Cl_9 > HoAl_3Cl_{12} > DyAl_3Cl_{12}$$
$$ScAl_2Cl_9 > YAl_2Cl_9 > LaAl_3Cl_{12}$$

Above findings show that the linear relationship between the ionic radii and the transported amount observed for the CVT experiment using $AlCl_3$ was incidentally obtained, and that the ionic radii was not the decisive factors for the transport properties in both chemical vapor transport using $AlCl_3$ and KCl.

1.3.2 Mutual separation between yttrium and heavy rare earths by chemical vapor transport

(1) Mutual separation characteristics in binary systems of yttrium and heavy rare earth chlorides with KCl

The CVT experiments of the binary mixtures of YCl_3 and $LnCl_3$ (Ln = Dy, Ho, Er) were carried out using the complex formers KCl and $AlCl_3$. When molar fraction of R_1Cl_3 and R_2Cl_3 in the raw mixture are x and $1–x$, respectively, the transported amounts of R_1Cl_3 and R_2Cl_3 are

$$N_{R1Cl3} = x \cdot P_{R1} \cdot V_c \cdot t/RT \quad (1.20)$$

$$N_{R2Cl3} = (1 - x) \cdot P_{R2} \cdot V_c \cdot t/RT \quad (1.21)$$

To evaluate the mutual separation efficiency between the two elements in the CVT process, we defined the separation factors as follows. With the temperature region divided into the high tem-

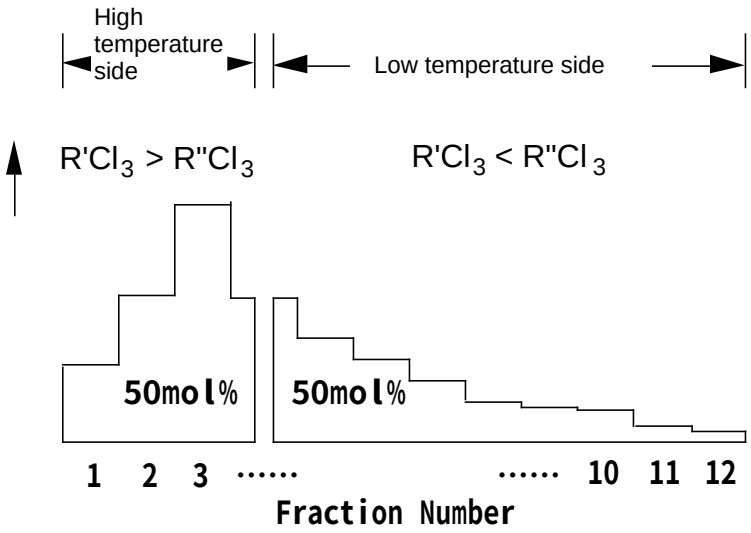

Figure 1.11 Definition of higher and lower temperature zones for calculation of separation factors

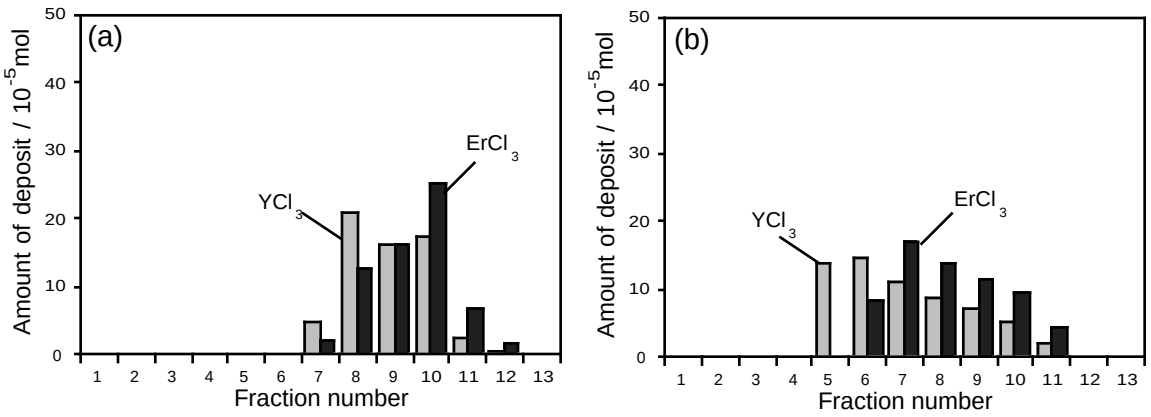

Figure 1.12 (a) Experimental and (b) calculated distribution profiles of rare earth chlorides for the YCl_3-$ErCl_3$ system with 7 K/cm temperature gradient and KCl complex former

perature zone and the low temperature zone so that the total deposited amounts in both the zones are equal (Figure1.11), the separation factor of R_1 in the high temperature zone ($\beta_{R1/R2}$) and that of R_2 in the low temperature zone ($\beta_{R2/R1}$) in the R_1Cl_3-R_2Cl_3 binary systems are

$$\beta_{R1/R2} = (N_{HR1}/N_{HR2}) / (N_{0R1}/N_{0R2}) \quad (1.22)$$

$$\beta_{R2/R1} = (N_{LR1}/N_{LR2}) / (N_{0R2}/N_{0R1}) \quad (1.23)$$

where N_{HR} and N_{LR} are the molar quantities of the deposits transported to the high- and low-temperature zones, respectively, and N_{0R1} and N_{0R2} are the R_1 and R_2 contents of the initially loaded raw mixture.

Mutual separation in the CVT processes is based on the difference in the temperature region in which each rare earth halide deposits. However, the deposition temperature varies with the experimental condition, because the rare earth chlorides are physically diffused, being affected by the carrier gas (see Section 1.3.1 (1)).

The distribution profile in the CVT experiment using the YCl_3 and $ErCl_3$ binary mixture with KCl under the 7 K/cm temperature gradient are compared with the estimated distribution from the calculated transported amount N_{YCl3} and N_{LnCl3} by using eq. (1.8) in Figure 1.12. The separation factors $\beta_{Y/Er}$ for the experimental and the calculated profiles were 1.62 and 1.52, respectively, suggesting that the experimental condition affects not only the deposition temperature but also the mutual separation characteristics in the binary systems. The effect of the experimental condition on the mutual separation efficiency was studied using the four kinds of temperature gradients, 7, 10, 15, and 28 K/cm (Figure 1.5 (a)). The relationship between the temperature gradient and the separation factor obtained for the experimental and calculated distribution profiles are shown in Figure1.13. For the both profiles, the separation factor increased with decreasing the temperature gra-

dient. It is obvious from Eq. (1.16) that the larger the temperature gradient, the larger the effect of the diffusion on the transport of the rare earth chlorides. Since YCl_3 is more subject to the physical diffusion than $ErCl_3$, the deposition temperature of YCl_3 approaches that of $ErCl_3$ with increase in the temperature gradient, and the mutual separation efficiency was lowered.

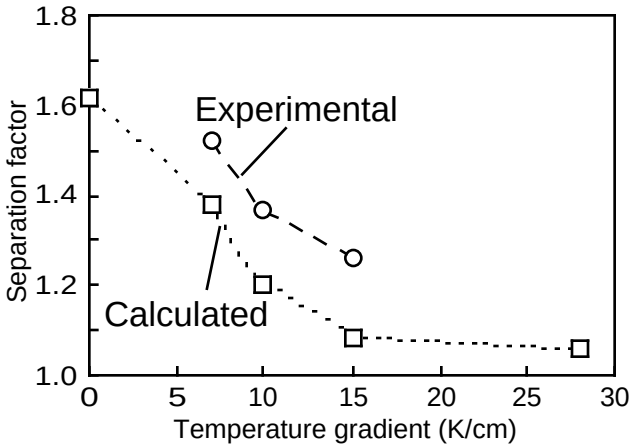

Figure 1.13 Relationship between separation factor and temperature gradient in the YCl_3-$ErCl_3$ system estimated by calculation considering the effect of diffusion.

For the other binary systems (YCl_3-$DyCl_3$ and YCl_3-$HoCl_3$ systems), the highest separation efficiency was obtained using the same optimized transport condition as the YCl_3-$ErCl_3$ system. $DyCl_3$ deposited at the higher temperature region than YCl_3, while $HoCl_3$ and $ErCl_3$ deposited at the lower temperature region (Figure 1.14). This is predictable from the vapor pressure of the gaseous complexes$KRCl_4$ at 1273 K shown in Figure 1.4.

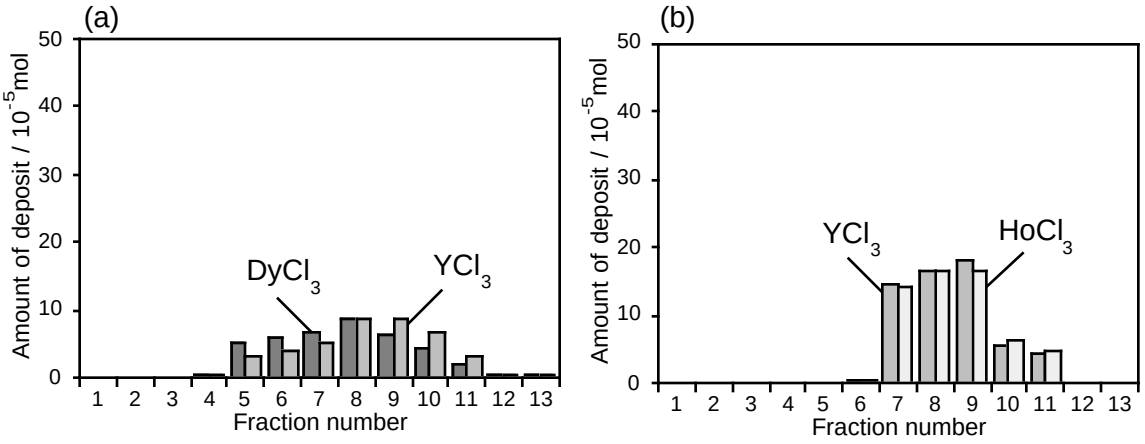

Figure 1.14 Distrubution profiles of the rare earth chloride deposits for the chemical transport experiments with the optimized condition in (a) YCl_3-$DyCl_3$ and (b) YCl_3-$HoCl_3$ binary system.

Table 1.3. Separation factors of YCl_3-$LnCl_3$ (Ln =Dy, Ho, Er) system with different temperature gradient

Slope of temperature gradient (K/cm)	Y/Er system		Y/Dy system		Y/Ho system	
	$\beta_{Y/Er}$	$\beta_{Er/Y}$	$\beta_{Dy/Y}$	$\beta_{Y/Dy}$	$\beta_{Y/Ho}$	$\beta_{Ho/Y}$
4	1.27	1.27	1.24	1.23	1.02	1.01
7	1.44	1.52	1.32	1.35	1.01	0.99
10	1.35	1.37	1.24	1.24	1.01	1.05
15	1.25	1.26	–	–	–	–
28	1.30	1.20	–	–	–	–

(2) Mutual separation characteristics in binary systems of yttrium and heavy rare earth chlorides with $AlCl_3$

The distribution of rare earth chloride deposits and the separation factors for the YCl_3-$LnCl_3$ (Ln = Dy, Ho, Er) binary systems in CVT experiments using $AlCl_3$ as a complex former are indicated in Figure1.15 and Table 1.4, respectively. $DyCl_3$ and $HoCl_3$ are deposited at higher temperature region than YCl_3, while $ErCl_3$ deposited at lower temperature region. This agrees with the

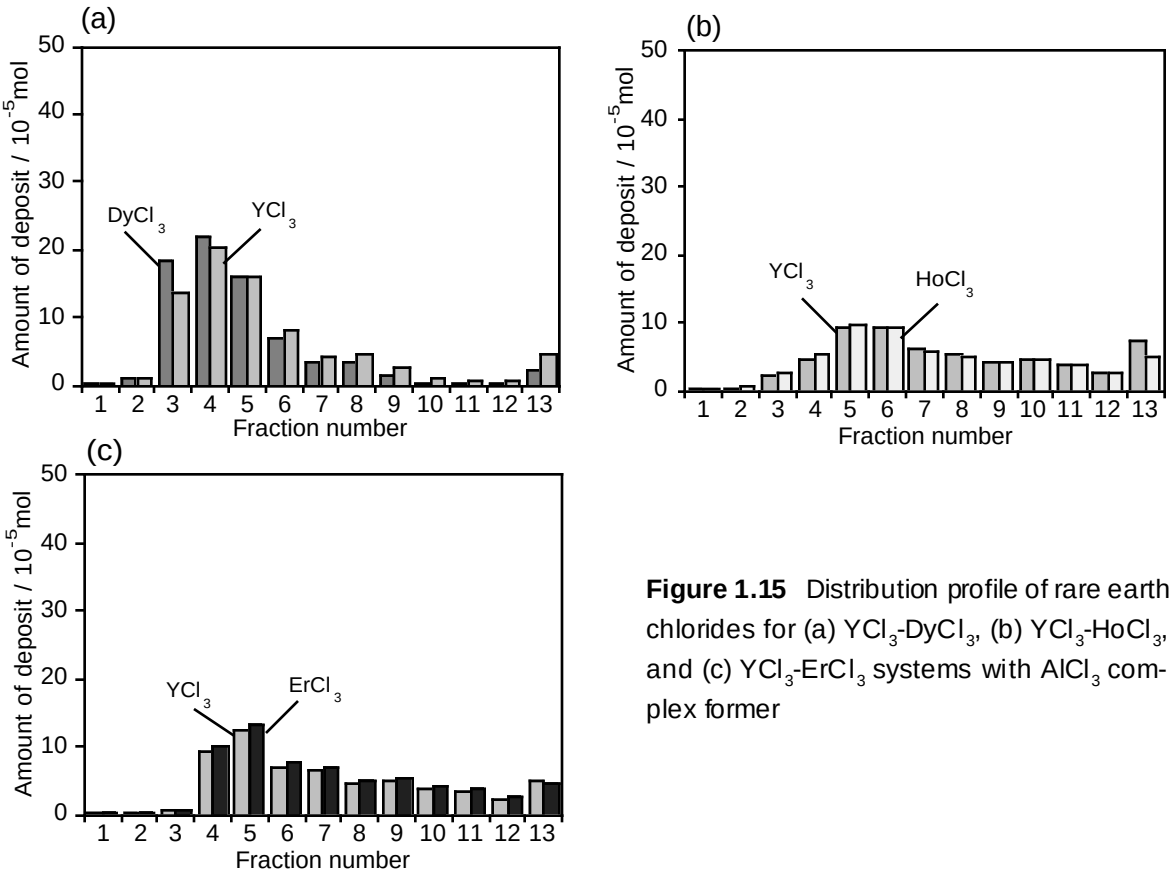

Figure 1.15 Distribution profile of rare earth chlorides for (a) YCl_3-$DyCl_3$, (b) YCl_3-$HoCl_3$, and (c) YCl_3-$ErCl_3$ systems with $AlCl_3$ complex former

Table 1.4 Separation factors for YCl_3-$LnCl_3$ (Ln = Dy, Ho, Er) binary systems with $AlCl_3$ complex former

Ln	Dy	Ho	Er
$\beta_{Y/Ln}$	1.19	1.07	1.00
$\beta_{Ln/Y}$	1.22	1.11	1.00

result of the CVT experiment of the pure chlorides (see Section 1.3.1 (2)). The higher separation factors were obtained for the YCl_3-$HoCl_3$ system compared to those obtained in the CVT experiment using KCl. For the YCl_3-$DyCl_3$ and YCl_3-$ErCl_3$ systems, however, the mutual separation efficiency was lowered. Contrary to the result with KCl, YCl and $ErCl_3$ were hardly separated with $AlCl_3$ from each other. It is difficult to predict the mutual separation characteristics in the CVT of rare earth chlorides with $AlCl_3$ is complicated, because YCl_3 and the heavy rare earth chlorides

form the different kinds of the gaseous complexes (see Section 1.3.1 (2)). The order of the transported amount in the CVT experiments of the pure chlorides is $DyCl_3 > HoCl_3 > YCl_3 > ErCl_3$, suggesting that the vapor pressure of the gaseous complexes increase according to the following order: $DyAl_3Cl_{12} < HoAl_3Cl_{12} < YAl_2Cl_9 < ErAl_3Cl_{12}$. Their difference in the vapor pressure is relatively small, and they are expected to be essentially deposited at the close temperature region. As in the case of KCl, however, the physical diffusion affects the deposition temperature of the chlorides, and the diffusion ability of YCl_3 is higher than those of the heavy rare earth chlorides. Therefore, the difference in the deposition temperature region between YCl_3 and $ErCl_3$ compensated, and those between YCl_3 and $HoCl_3$ or $DyCl_3$ is broadened. Generally, RCl_3-$AlCl_3$ gaseous complexes are more stable than RCl_3-KCl complexes at low temperatures, and the mutual separation efficiency is poorer in many binary systems.

(3) Mutual separation process between yttrium and heavy rare earths using oxide mixtures as starting materials

Using equimolar mixtures of the corresponding oxides as starting materials, separation of Y from Dy, Ho, Er using the chlorination-CVT was attempted with a manner similar to the CVT experiments using the chloride starting materials. In these experiments, K_2CO_3 was used as a precursor of complex former KCl, because the directly mixing of KCl with the oxide starting materials results in sole vaporization of KCl prior to the complex formation. It was found that chlorination rate of K_2CO_3 was most closest to that of the rare earth chlorides among many kinds of potassium salts [9]. By using it, therefore, it is expected the simultaneous formation of rare earth chlorides and KCl by chlorination and efficient CVT via the gaseous complex $KRCl_4$. The optimized transport condition in the CVT experiments using the chloride starting materials with KCl was adopted. The distribution of the rare earth chlorides and the separation factors for each binary system are shown in Figure1.16 and Table 1.5, respectively.

Table 1.5. Separation factors for the Y-Ln (Ln = Dy, Ho, Er) binary systems..

raw materials	separation factors		
	$\beta_{Dy/Y}$	$\beta_{Ho/Y}$	$\beta_{Er/Y}$
YCl_3-$LnCl_3$	1.35	1.01	1.52
Y_2O_3-Ln_2O_3	1.47	1.11	1.54

For the YCl_3-$DyCl_3$ and YCl_3-$HoCl_3$ systems, remarkable improvement in the mutual separation efficiency was observed. It should be mentioned that in the YCl_3-$HoCl_3$ system, $HoCl_3$ deposited at lower temperature side than YCl_3 using the chloride as starting materials, while the reverse

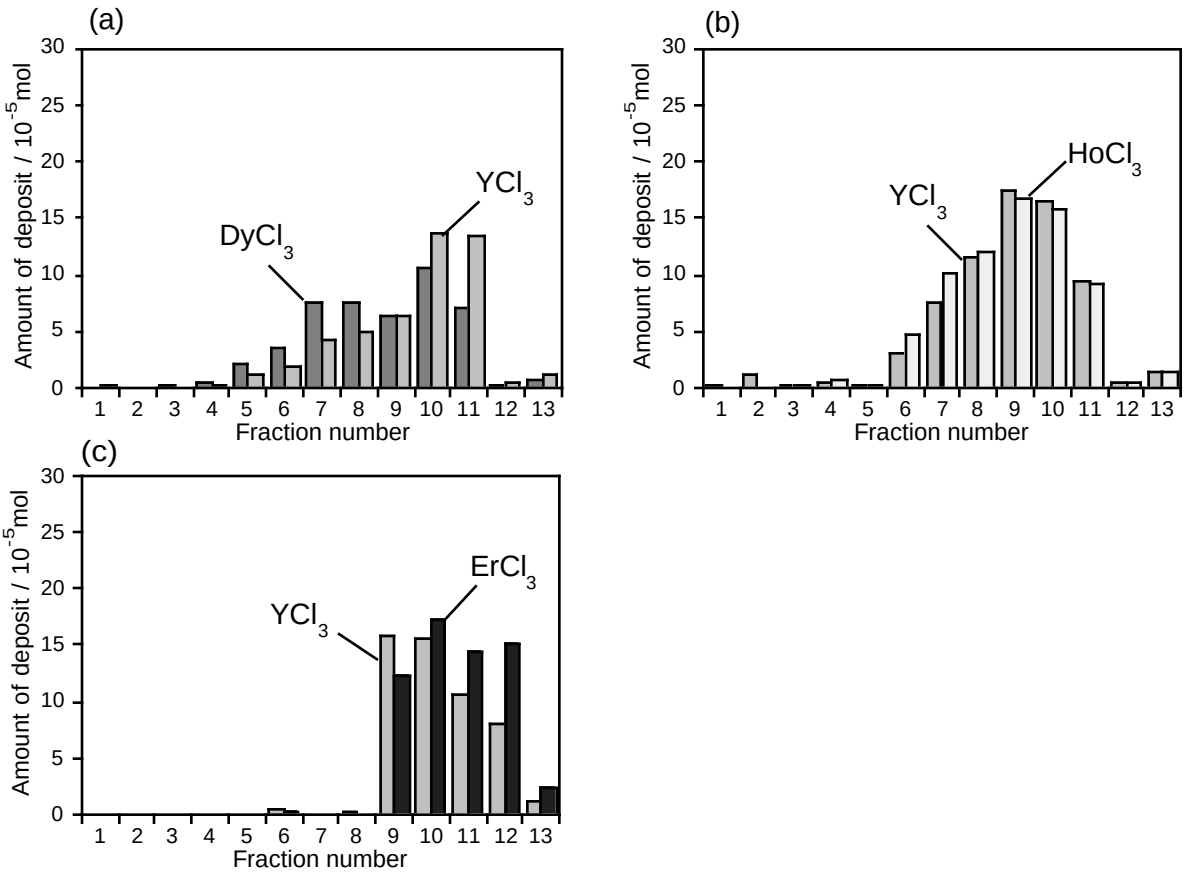

Figure 1.16 Distribution profile of rare earth chloride deposits for chemical vapor transport experiments using (a) Y_2O_3-Dy_2O_3, (b) Y_2O_3-Ho_2O_3, and (c) Y_2O_3-Er_2O_3 as starting materials.

tendency was observed using the oxide as starting materials.

Figure 1.17 shows Gibbs free energy changes for the chlorination reaction of rare earth oxides in the presence of carbon (eq. (1.1)) [25, 26]. In the whole temperature region from 300 K to 1300 K, the chlorination of Y_2O_3 is thermodynamically more feasible than Er_2O_3, and less feasible than Dy_2O_3 and Ho_2O_3. Therefore, the chlorination rate of the rare earth oxides increase according to the following order.

$$Dy_2O_3 > Ho_2O_3 > Y_2O_3 > Er_2O_3$$

This difference in the chlorination rate affects the mutual separation characteristics between yttrium and the heavy rare earths. In the R_1–R_2 binary system, the partial pressure of KR_1Cl_4 and KR_2Cl_4 are

$$P'_{R1} = x_{R1}P_{R1} \quad P'_{R2} = x_{R2}P_{R2} \tag{1.24}$$

where x_{R1} and x_{R2} are the molar fraction of R_1Cl_3 and R_2Cl_3 in raw mixtures, and P_{R1} and P_{R2} are the vapor pressure of the pure KR_1Cl_4 and KR_2Cl_4, respectively. In the Y_2O_3-Dy_2O_3 binary mixture, for example, the chlorination of Dy_2O_3 proceeds more rapidly than that of Y_2O_3, and the molar fraction

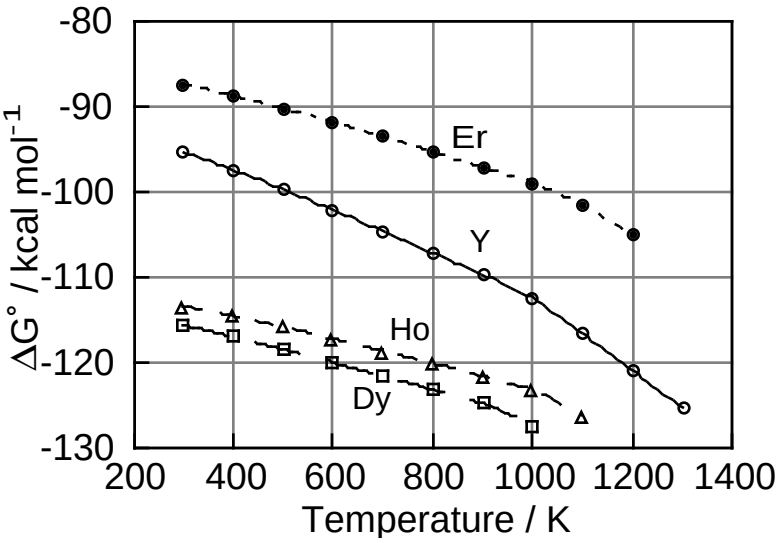

Figure 1.17 Gibb's free energy changes for the chlorination reactions of the rare earth oxides with Cl_2 in thepresence of carbon (eq.(1.1)).

of $DyCl_3$ in the raw material is much larger than that of YCl_3 in the initial stage of the reaction. The vapor pressure of $KDyCl_4$ using Y_2O_3-Dy_2O_3 as a starting material is larger than that using YCl_3-$DyCl_3$ for the same transport time. Therefore, $DyCl_3$ deposits at higher temperature compared to the case of the chloride starting materials. On the other hand, YCl_3 is gradually chlorinated, and its deposition temperature is not so much different from that with the chlorides. Since $DyCl_3$ deposits at high temperature side, the mutual separation efficiency between Y and Dy is improved compared to the CVT experiments using the chlorides. The reverse of the deposition temperature in the YCl_3-$HoCl_3$ system is also due to the higher chlorination rate of Ho_2O_3 compared to Y_2O_3.

Most of the rare earth raw materials is the oxides. Therefore, direct separation of the rare earths from the oxide is of great value on the industrial point of view. Higher mutual separation efficiency in CVT process with oxide raw materials compared to that with chloride raw materials is advantageous for practical use of this process.

(4) Comparison of mutual separation efficiency with the conventional processes

The separation factors for the binary system between yttrium and the heavy rare earth obtained in the present work is compared with the values for the solvent extraction method, which is an industrial method for rare earth separation (Table 1.6). The separation factors in the present work are comparable to those in solvent extraction methods with two kinds of extractant, suggesting that the chemical vapor transport process has enough separation efficiency for practical use.

Table 1.6 Comparison of the separation factors in the YCl_3-$LnCl_3$ systems between the chemical vapor transport and the solvent extraction methods.

	separation factor		
separation method	$\beta_{Dy/Y}$	$\beta_{Ho/Y}$	$\beta_{Er/Y}$
chemical vapor transport	1.47	1.11	1.57
solvent extraction			
(extractant: quaternary ammonium salt)	1.61	1.15	1.30
(extractant: D2EHPA)	3.19	1.65	1.37

1.3.3 Mutual separation for the scandium, yttrium, and lanthanum by chemical vapor transport

Figure 1.18 shows the distribution profiles of rare earth chloride deposits for chemical vapor transport experiments of $ScCl_3$-YCl_3, $ScCl_3$-$LaCl_3$, and YCl_3-$LaCl_3$ binary systems using the oxide mixtures as starting materials with $AlCl_3$ complex former. The higher temperature gradient (1273 K) and reaction time (6 h) were adopted. Table 1.7 summarizes the total transported amount of each rare earth chloride and the separation factors for the binary systems. From these distribution profiles, it is obvious that $ScCl_3$ distributes in the lower temperature region below 1023 K and well separated from YCl_3 or $LaCl_3$ concentrated in the higher temperature region, which is identical to the transport results of the chemical vapor transport efficiency measurement for the pure R_2O_3 (R=Sc, Y, La). Among the three binary systems, YCl_3 and $LaCl_3$ shows the worst separation effect. These results indicated the specificity of $ScCl_3$ among the rare earth chlorides, and that it is easy to make separation of $ScCl_3$ from other rare earths by the identical process, because chemical vapor transport property of YCl_3 with $AlCl_3$ complex former is similar to those of the heavy rare earths (see Section 1.3.2 (2)). However, the contamination of $ScCl_3$ with YCl_3 was still observed for the $ScCl_3$-YCl_3 binary system, resulting in the lowering of the $ScCl_3$ purity.

Figure 1.19 exhibits the distribution profiles for the $ScCl_3$-YCl_3 and $ScCl_3$-$LaCl_3$ binary systems with the $AlCl_3$ complex former under the lower temperature gradient (1073 K). The corresponding data such as separation factors and the transport yields are organized in Table 1.8. The transported amount of $ScCl_3$ is not lowered by decreasing reaction temperature for the both systems of $ScCl_3$-YCl_3 and $ScCl_3$-$LaCl_3$. On the contrary, only a very small part of YCl_3 or $LaCl_3$ transformed from their oxide species is transported because of the low vapor pressure of the gaseous complexes YAl_2Cl_9 and $LaAl_3Cl_{12}$ at 1073 K. As a result, the purity and the separation factors of $ScCl_3$ were improved for the both systems. It is necessary to mention that the composition of low molecular weight gaseous species such as $RAlCl_6$ (R=Sc,Y,La) or $LaAl_2Cl_9$ will increase to some

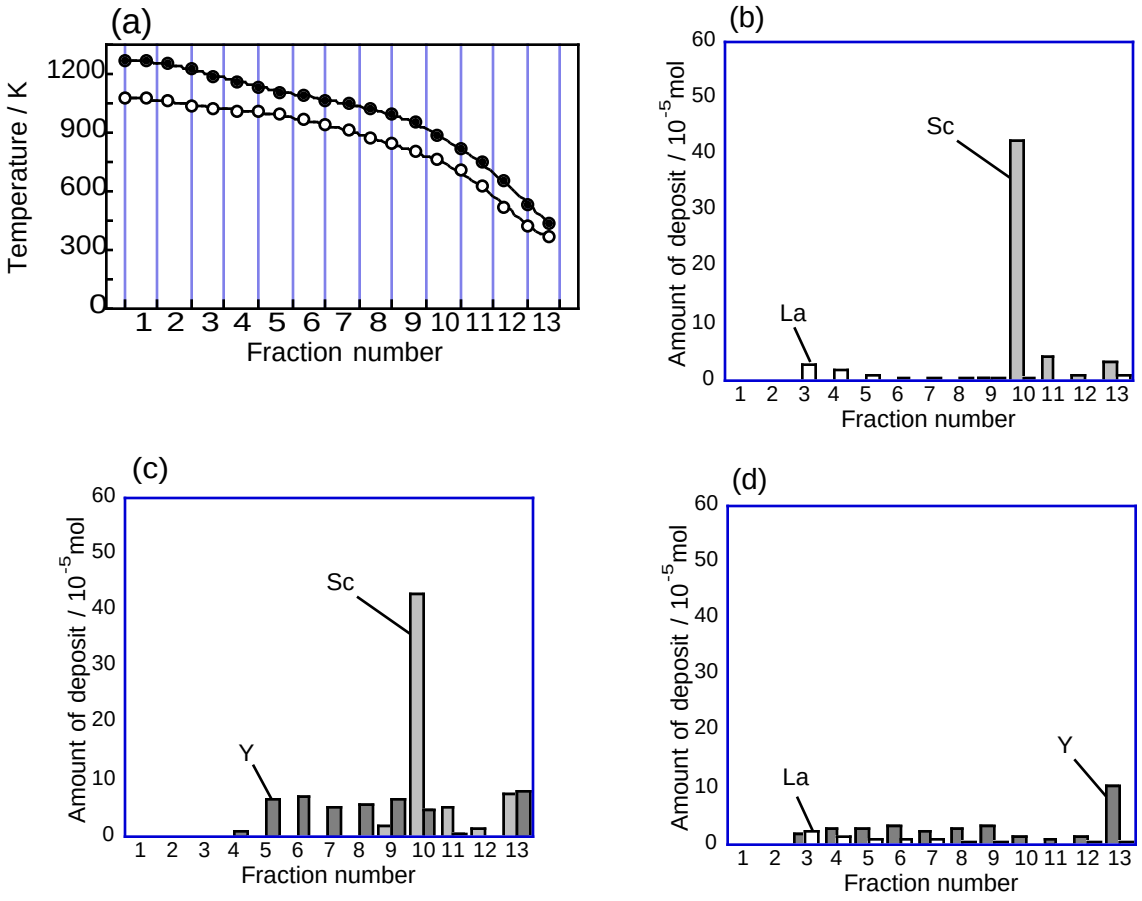

Figure 1.18 Temperature gradients employed for mutual separation between Sc, Y, and La and the distribution profiles of RCl_3 and $R'Cl_3$ ($R \neq R$ = Sc, Y, La) with $AlCl_3$ complex former from (b) Sc_2O_3-La_2O_3, (c) Sc_2O_3-Y_2O_3, and (d) Y_2O_3-La_2O_3 binary systems under the higher temperature gradient (1273 K).

Table 1.7. The purity, transported amount, and separation factors for binary systems R_2O_3-R'_2O_3 ($R \neq R$ = Sc, Y, La) with $AlCl_3$ coplex former under the higher temperature gradient (1273 K)

	Sc/La system		Sc/Y system		Y/La system	
	$ScCl_3$	$LaCl_3$	$ScCl_3$	YCl_3	YCl_3	$LaCl_3$
Purity (%)	95.2	95.4	80.1	94.4	82.3	56.8
Transport amount (10^{-5} mol)	52.1	10.1	59.0	94.9	35.5	10.0
Separation factors	19.83	20.74	4.03	16.9	4.65	1.31

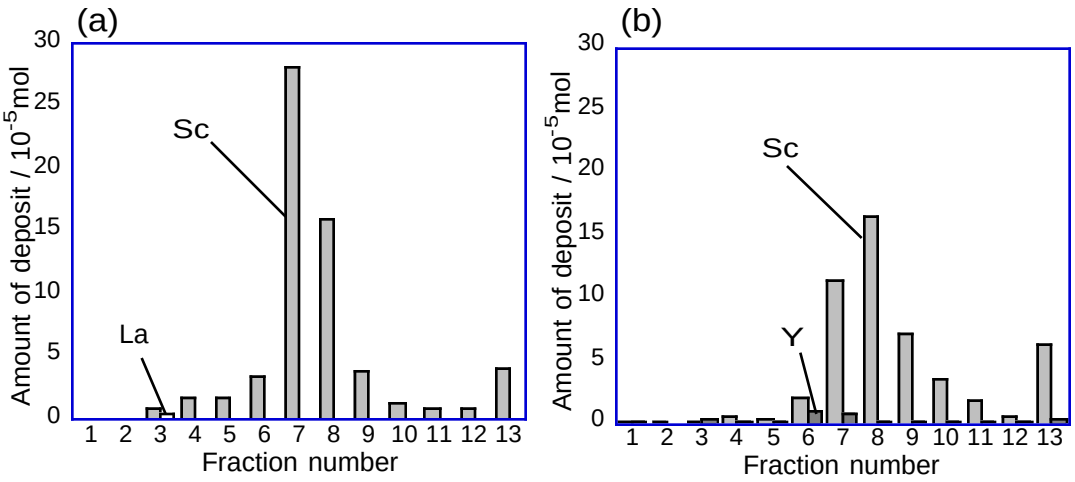

Figure 1.19 The distribution profiles of $ScCl_3$ and RCl_3 (R = Y, La) with $AlCl_3$ complex former from the binary systems Sc_2O_3-R_2O_3 (R = Y, La) under the lower temperature (1073 K).

Table 1.8. The purity, transported amount, and separation factors for binary systems R_2O_3-R'_2O_3 (R ≠ R = Sc, Y, La) with $AlCl_3$ coplex former under the higher temperature gradient (1073 K)

	Sc/La system		Sc/Y system	
	$ScCl_3$	$LaCl_3$	$ScCl_3$	YCl_3
Purity (%)	98.7		94.1	
Transport amount (10^{-5} mol)	62.5	0.8	50.0	3.0
Separation factors	75.92		15.95	

degree according to the thermodynamic characteristics at such a high temperature. The large fraction of YCl_3 or $LaCl_3$ remained in the sample boat could be further transported by another CVT process with a higher temperature gradient or treated by the simple dissolution method, providing the pure anhydrous rare earth chloride, RCl_3 (R=Y, La), or hydrated rare earth chloride, $RCl_3 \cdot nH_2O$ (R=Y, La). From the very low transport yield of YCl_3 or $LaCl_3$ for the binary systems of $ScCl_3$-RCl_3 (R=Y, La) under this lower temperature gradient, it could be also concluded that it is not appropriate for the mutual separation of YCl_3 and $LaCl_3$ under this lower temperature gradient.

As indicated in the previous section, KCl provides much better separation effect in many cases compared with $AlCl_3$ complex former for the rare earths. For these the binary systems, a comparative CVT process with K_2CO_3 as a precursor of KCl complex former under the 1273 K temperature gradient then is conducted to compare their mutual separation characteristics with those obtained using $AlCl_3$ complex former. Table 1.9 list the purity and the transport amounts of the chlorides as well as the separation factors for the binary systems.

Transported amounts of YCl_3 an $LaCl_3$ for these three binary systems were larger than those with the $AlCl_3$ complex former under the same temperature gradient. Separation factors for YCl_3 and $LaCl_3$ were also improved. These results indicates that the KCl complex former is more effec-

Table 1.9. The purity, transported amount, and separation factors for binary systems R_2O_3-R'_2O_3 ($R \neq R$ = Sc, Y, La) with KCl complex former under the higher temperature gradient (1273 K)

	Sc/La system		Sc/Y system		Y/La system	
	$ScCl_3$	$LaCl_3$	$ScCl_3$	YCl_3	YCl_3	$LaCl_3$
Purity (%)	98.3	95.5	93.2	95.7	92.6	76.0
Transport amount (10^{-5} mol)	48.6	16.5	44.0	54.2	64.3	10.9
Separation factors	57.82	21.12	13.71	22.26	12.51	3.17

tive than $AlCl_3$ complex former for the mutual separation of binary rare earth chlorides by the chemical vapor transport process. However, in the case with KCl complex former the transported $ScCl_3$ concentrates in the higher temperature region compared with that using $AlCl_3$ complex former, which may suggests that the gaseous complex $KScCl_4$ is not as stable as $ScAl_nCl_{3n+3}$ and starts to dissociate at a higher temperature.

1.3.4 Chemical vapor transport reaction of rare earth iodides and its application to rare earth separation process

CVT efficiency and mutual separation characteristics of equimolar mixtures of PrI_3 and NdI_3 was investigated using KI as a complex former. Pr–Nd pair is most difficult to be separated among the neighboring rare earths. Two kinds of linear temperature gradients with respective reaction temperature of 1273 and 1173 K were adopted. Table 1.10 summarizes the transported amount of the rare earth iodides and the separation factors for the Pr–Nd binary system. The transported amount and the mutual separation efficiency were compared with that obtained for the vaporization of the iodides in absence of the KI complex former and that for the CVT of the corresponding chlorides with KCl complex former. Transported amount of the rare earth iodides slightly increased in the presence of KI, suggesting the volatility enhancement by the formation of gaseous complex between RI and KI. The transported amount is also sparingly larger than that of the chlorides in the $PrCl_3$-$NdCl_3$ systems with KCl. On the other hand, under the temperature gradient with the lower reaction temperature (1173 K), the transported amount of the iodides with KI as complex former was not largely altered compared to that under the higher temperature gradient, while the transported amount of iodides without KI and that of the chlorides with KCl significantly decreased. These results indicates that the difference in the vapor pressure between the RCl_3-KCl gaseous complex and the RI-KI gaseous complexes increased with decreasing the temperature and the vola-

tility enhancement by the complex formation also increased. However, the obvious improvement in mutual separation efficiency of the iodide system compared to the chloride system was not observed. This is due to the higher stability of the iodide complexes. The iodide complexes dissociate at lower temperature side than the chloride complexes, resulting in the enlargement of the deposition temperature range and the decrease in the total separation efficiency.

Table 1.10. Separation factor and transported amount for the Pr-Nd binary system

Reaction temperature / K	raw materials	complex former	separation factor	transported amount / 10^{-5} mol	
				Pr	Nd
1273	PrI_3-NdI_3	–	1.13	43.3	42.3
	PrI_3-NdI_3	KI	1.03	50.4	52.7
	$PrCl_3$-$NdCl_3$	KCl	1.02	41.6	47.6
1173	PrI_3-NdI_3	–	1.19	8.4	7.6
	PrI_3-NdI_3	KI	1.14	44.3	48.4
	$PrCl_3$-$NdCl_3$	KCl	1.03	5.8	6.7

1.4 Conclusions

It was found from chemical transport experiments of yttrium and heavy rare earth chlorides that the ionic radii was not the decisive factors for the transport properties in chemical vapor transport mediated by gaseous complexes. The mutual separation efficiency between yttrium and the heavy rare earths depends on the transport experiment conditions because of the difference in the diffusion ability. In many cases, the mutual separation efficiency was improved by using oxide mixtures as starting material instead of the chloride mixtures. The iodide gaseous complexes have higher chemical transport ability compared to the corresponding chloride complexes.

Chapter 2

Recovery and separation of rare earths from used polishes by chemical vapor transport

2.1 Introduction

Rare earth ores or concentrates occur in only limited countries and are currently imported by several countries. For a good supply of rare earths, sludge, scrap, and wastes are noted as new sources. Development of recovery process of rare earths from them is expected. In chapter 1, it was demonstrated that mutual separation between rare earths was successful by the chemical vapor transport using oxide mixtures as starting materials. This process is also applicable to the recovery of rare earths from scraps, sludges, and wastes.

Rare earth based polishing agents have been widely used for polishing glass substrates [22, 23]. They are recognized as superior polishing products to any others in terms of chemical as well as mechanical polishing action of cerium oxide. The Japanese glass industry uses 2000 tons per year of the polishes. During the polishing operations, the polishes are contaminated by compounds of Si and Al, and their effectiveness for polishing is gradually reduced. A large portion of the polish is thrown away after their polishing lifetime is due.

In this chapter, chlorination of used polishes with Cl_2-N_2 gas mixture and extraction of rare earths from them by formation of gaseous complexes were investigated. Mutual separation of rare earths was also attempted.

Table 1.1 Composition of the used polishes (weight percent)

Sample	La_2O_3	CeO_2	Pr_6O_{11}	Nd_2O_3	F	SiO_2	CaO	SrO	P_2O_5	SO_3	Fe_2O_3
A	28	50	7.4	4.0	9.5	0.62	0.71	–	0.085	0.27	0.28
B	28	38	3.8	10	12	1.7	1.3	0.46	1.7	2.2	0.18

2.2 Experimental details

Two kinds of used polishes were used in this work, and they were sample A and B, which were provided by Mitsui Mining and Smelting Co., Ltd.. They were dried at 373 K to constant weight prior to the experiment. Their composition was investigated by means of X-ray fluorometry

and inductively coupled plasma-atomic emission specrometry as given in Table 2.1. The used polishes contain alkaline-earth elements, Si, Fe, F, P, and S as well as light rare earth elements, but the content of the rare earth elements in the two samples was different. The La/Ce molar ratio of sample A and B was 0.56 and 0.74, respectively. The X-ray powder diffraction showed that the rare earths exist as oxides or oxyfluorides, while SiO_2 was amorphous.

The apparatus employed for the chemical vapor transport was same as that described in Section 1.2. The chlorination behavior was realized using a mixture of 0.5 g of the used polishes and 0.5 g of active carbon as a raw material. The mixture was heated to 1273 K under the N_2-Cl_2 mixed gas flow. The flow rates of N_2 and Cl_2 were 30 to 70 and 5 cm^3min^{-1}, respectively. Metal components contained in the polishes were gradually chlorinated by Cl_2, active carbon acting as a deoxidant. After 0.25 to 82 hours of chlorination reaction, the chlorinated sample was dissolved in deionized water. The resulting metal chloride, which is soluble in water, was analyzed by X-ray fluorometry, and the insoluble residue was dried, calcined to remove excess active carbon, and weighed.

The general procedure of chemical vapor transport experiment is similar to that of chlorina tion experiments, but aluminum chloride, Al_2Cl_6, and potassium chloride, KCl, were used as the complex former in the experiment. Al_2Cl_6 was generated by chlorination of γ-Al_2O_3 with active carbon at 573 to 1023 K in furnace A. As treated later it takes about an hour to chlorinate a large portion of the raw material. After heating the raw material for 2 h, Al_2Cl_6 was introduced into the reactor to avoid reaction between rare earth oxide and Al_2Cl_6 and resulting formation of Al_2O_3 on the surface of sample

$$R_2O_3 + Al_2Cl_6 \rightarrow 2\,RCl_3 + Al_2O_3 \qquad (2.1)$$

When KCl was used as a complex former, $1.0x10^{-3}$ mol fo K_2CO_3 was directly mixed with the raw material. K_2CO_3 and the raw material were chlorinated simultaneously during the experiments. Rare earth chlorides reacted with KCl and $AlCl_3$ to form vapor complexes. The vapor complexes were chemically transported. The recovery and determination of deposits were same procedure described in Section 1.2.

2.3 Results and discussion

2.3.1 Kinetics of chlorination of used polish

Figure 2.1 shows the parcentage weight loss during chlorination of the used polish at 1273 K. More than 80 % of the sample was chlorinated within 1 h. However, chlorination of the remaining portion proceeded quite slowly after that, and the weight loss after 82 h was 93.2 %. This result suggests that components, which are hard to chlorinate, exist in the sample. The X-ray diffraction

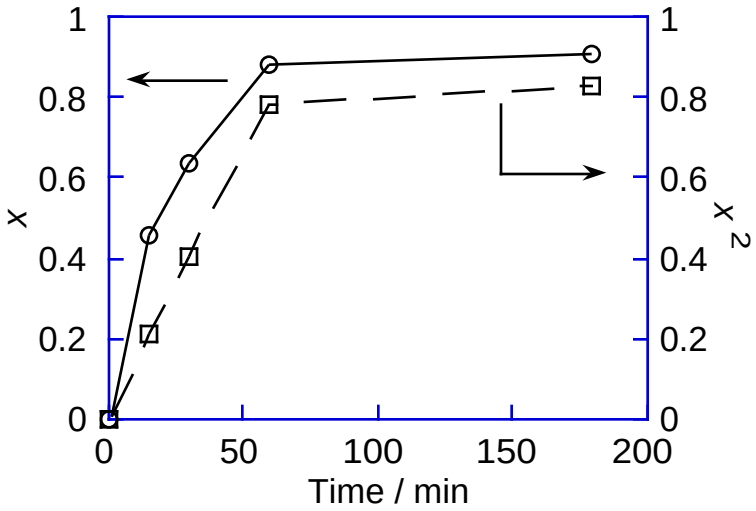

Figure 2.1. Fraction reacted, *x*, of the used polish with time during chlorination with Cl_2 and plot of x^2 against reaction time.

pattern of the used polihses wihtout any treatment shows peaks assigned to rare earth oxide and oxyfluoride, while that of the sample after chlorination for 1 hour shows only peaks of rare earth fluoride (Figure 2.2). It seems that the chlorinated residue mostly consists of rare earth fluoride. Equations (2.2) and (2.3) have been proposed as the reaction scheme for chlorination of Ln_2O_3 and CeO_2, respectively.

$$Ln_2O_3 + 2\,C + 3\,Cl_2 \rightarrow 2\,LnCl_3 + 3\,CO \qquad (2.2)$$

$$2\,CeO_2 + 4\,C + 3\,Cl_2 \rightarrow 2\,CeCl_3 + 4\,CO \qquad (2.3)$$

And we concluded in previous work that the most plausible reaction scheme for chlorination of rare

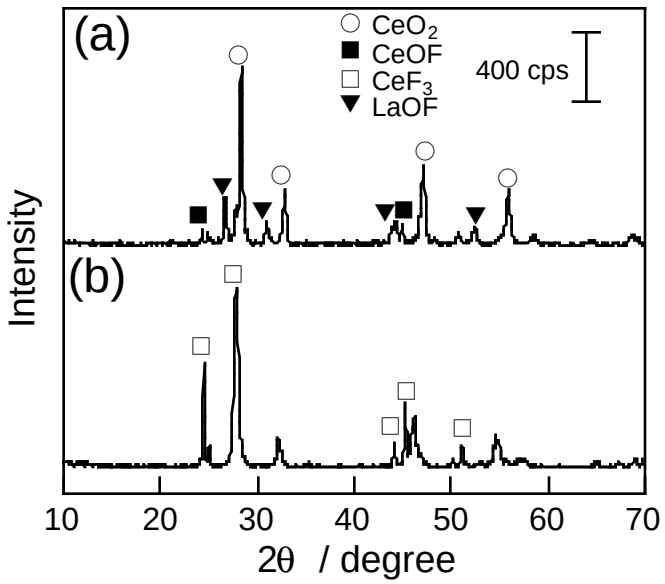

Figure 2.2 The X-ray diffraction pattern of (a) original used polish and (b)solid residue from the chlorination for 1h

earth oxyfluorides was

$$LnOF + C + 2\ Cl_2 \rightarrow LnCl_3 + CO + ClF \quad (2.4)$$

On the other hand, Eqs. (2.5) and (2.6) are expected for the reaction scheme for chlorination of rare earth fluorides.

$$RF_3 + 3\ Cl_2 \rightarrow RCl_3 + 3\ ClF \quad (2.5)$$

$$RF_3 + 3/2\ Cl_2 \rightarrow RCl_3 + 3/2\ F_2 \quad (2.6)$$

The Gibbs free energy changes of these reactions are shown in Figure 2.3 as a function of temperature from 273 to 1273 K [25–27]. These thermodynamic values indicate that the chlorination of La_2O_3, CeO_2, and LaOF with Cl_2 are thermodynamically feasible in the presence of carbon between 273 and 1273 K, and that chlorination of LaF_3 is not thermodynamically favorable in the same temperature range. Therefore, rare earth oxides and oxyfluorides are rapidly chlorinated, while it is difficult to chlorinate rare earth fluorides. The result of X-ray fluorescence spectrometry suggests that SiO_2 as well as rare earth fluorides remained in the residue. The following equation was found to hold for chlorination of the used polish for chlorinating time within 1hour (Figure 2.1):

$$kt = x^2 \quad (2.7)$$

where k = constant, t = chlorination time (min), and x = extent of reaction. This equation was applied for a gas-solid reaction of the sample with the shape of flat plate controlled by pore diffusion [28]. We previously investigated chlorination of monazite with carbon tetrachloride, and the

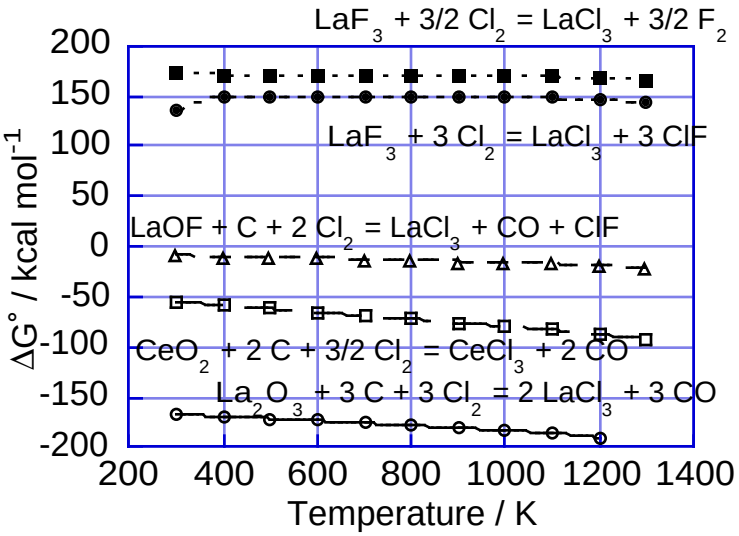

Figure 2.3 Gibbs energy change for chlorination reaction of La_2O_3, CeO_2,LaOF, and LaF_3 as a function of temperature

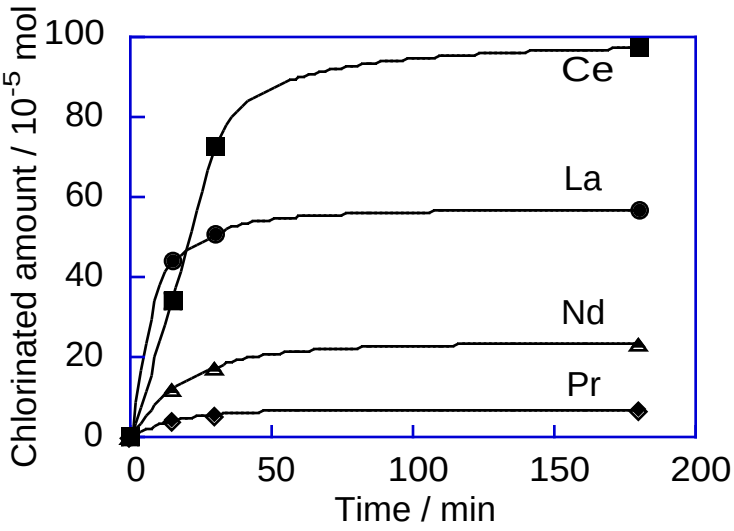

Figure 2.4 Chlorinated molar quantity of rare earth components.

data of the chlorination rate are best fitted to Eq. (2.8), which describes a reaction of a spherical sample controlled by the chemical reaction

$$kt = 1 - (1 - x)^{1/3} \tag{2.8}$$

However, the sample used in the present work has small particle size and high density, and its shape is regarded as flat plate. It is impossible to fit the chlorination rate of used polishes to one equation, and detailed consideration for the reaction is difficult because of the existence of a sparingly chlorinated portion in it. In the discussion, this portion is neglected.

Figure 2.4 shows the chlorinated amount of each rare earth element contained in the polish. The chlorination rate of the rare earths increases according to the following order:

$$\text{La} > \text{Pr} > \text{Nd} > \text{Ce} \tag{2.9}$$

It has been reported that the chlorination rate of rare earths generally decreases with increasing atomic number. However, this is not applicable to Ce. Chlorination of Ce is much slower than that of Pr and Nd, because the chlorination of CeO_2 was accompanied by the reduction from Ce (IV) to Ce (III). The Gibbs free energy change of both the chlorination reaction (Figure 2.3) also supports the experimental result that CeO_2 is less subject to chlorination by chlorine than La_2O_3.

2.3.2 Transport efficiency of rare earth chlorides

Transport efficiency of rare earth chlorides by chemical vapor transport using $AlCl_3$ as the complex former was investigated in different transport conditions. The total deposited amount yield of rare earth chloride was defined as follows:

$$\text{Yield (\%)} = N_{total} / (N_{total} + N_{boat}) \qquad (2.10)$$

where N_{total} and N_{boat} are the molar quantity values of the total transported rare earth chloride and the residual rare earth chloride in the boat, respectively. The transported amount consists of solely evaporated amount and chemically transported amount via the vapor complexes. Both partial pressure of complex former Al_2Cl_6 and flow rate of carrier gas N_2 affect the amount of formed vapor complexes. The effect of gas flow rate on the tranpsort efficiency was investigated. The effect of reaction temperature of furnace A, where gaseous Al_2Cl_6 was generated, on the transport efficiency was also investigated. Figure 2.5 shows the relationship between transported amount of rare earth chloride and N_2 flow rate with constant Furnace A temperature of 573 K. The transported amount passes through a maximum at about 50 cm^3min^{-1}. When the N_2 flow rate is too large, partial pressure of $AlCl_3$ decreases and the amount of vapor complexes formed also decreases. Table 2.2 summerizes the yields of rare earth chlorides at the various temperatures of furnace A with 50 cm^3min^{-1} of N_2 flow rate. Amount of $AlCl_3$ generated increases with increasing reaction temperature. It seems that the larger the introduced amount of $AlCl_3$, the larger is the amount of vapor complex formed. However, excess $AlCl_3$ inhibited vaporization and chemical transport of rare earth chlorides because of formation of alumina layer on the surface of samples by reaction of $AlCl_3$ and

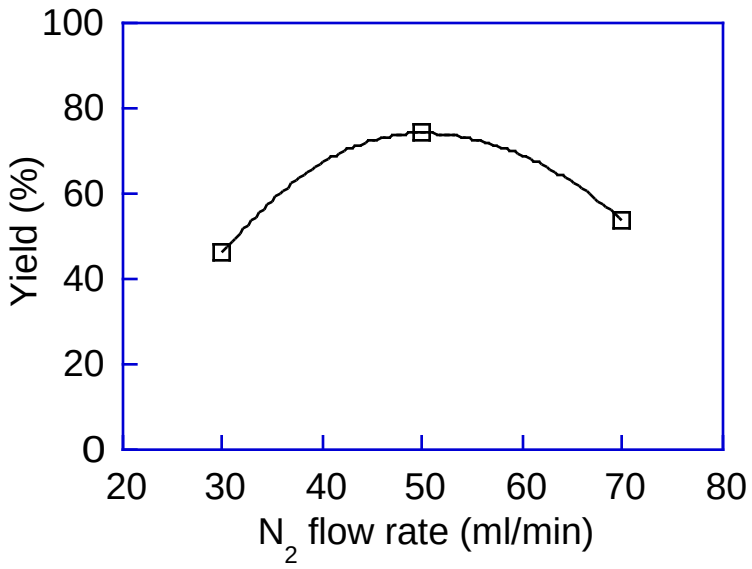

Figure 2.5 Effect of N_2 flow rate on the yield of rare earth chlorides

rare earth oxides (eq. (2.1)).

Table 2.2. The yield of rare earth chlorides for CVT Experimentts with Various Temperature of Furnace A

Temperature of	Yields/%				
Furnace A / K	Total	La	Ce	Pr	Nd
573	74	59	84	84	81
773	82	65	89	93	87
873	75	57	83	86	82

The highest yield was obtained when N_2 flow rate was 50 cm^3min^{-1} and temperature of furnace A was 773 K. Therefore, the CVT experiments after this were performed with these transport conditions. Yields of total and each rare earth chloride vs time curves are shown in Figure 2.6 (a). The yield of rare earth chloride totaled 94 % after CVT experiment for 82 hours. Transport reaction rate of rare earth chlorides increased according to the following order:

$$LaCl_3 < NdCl_3 < CeCl_3 < PrCl_3 \qquad (2.11)$$

In the RCl_3-$AlCl_3$ (R = La–Nd) systems, it was found that the dominant vapor complex species is RAl_3Cl_{12}. Gibbs energy changes for eq. (2.12) at 1273 K,

$$RCl_3\,(s, l) + (3/2)\,Al_2Cl_6\,(g) = RAl_3Cl_{12}\,(g) \qquad (2.12)$$

are 38.0, 39.0, 36.7, and 38.8 kJ mol^{-1} for R= La, Ce, Pr, and Nd, respectively [17]. The equilibrium constant K_P for Eq. (2.12) is

$$K_P = P_{RAl3Cl12}/(P_{Al2Cl6})^{3/2} \qquad (2.13)$$

Where $P_{RAl3Cl12}$ and P_{Al2Cl6} are partial pressures of RAl_3Cl_{12} and Al_2Cl_6, respectively. When N_2 gas flow rate was 30 cm^3min^{-1} and the temperature of furnace A was 773 K, the vapor pressure of Al_2Cl_6 was calculated to be $6.38x10^{-2}$ atm from weight loss of γ-Al_2O_3 in furnace A. The K_P value was calculated with previously described Gibbs energy changes and the ralationship

$$\Delta G = RT \ln K_P \qquad (2.14)$$

where R is the gas constant and T is the reaction temperature. The molar fraction of La, Ce, Pr, Nd in the raw material was 0.34, 0.69, 0.047, and 0.12, respectively. If the composition of each rare earth was maintained after chlorination, the partial pressure of each vapor complex could be expressed approximately by the following equation:

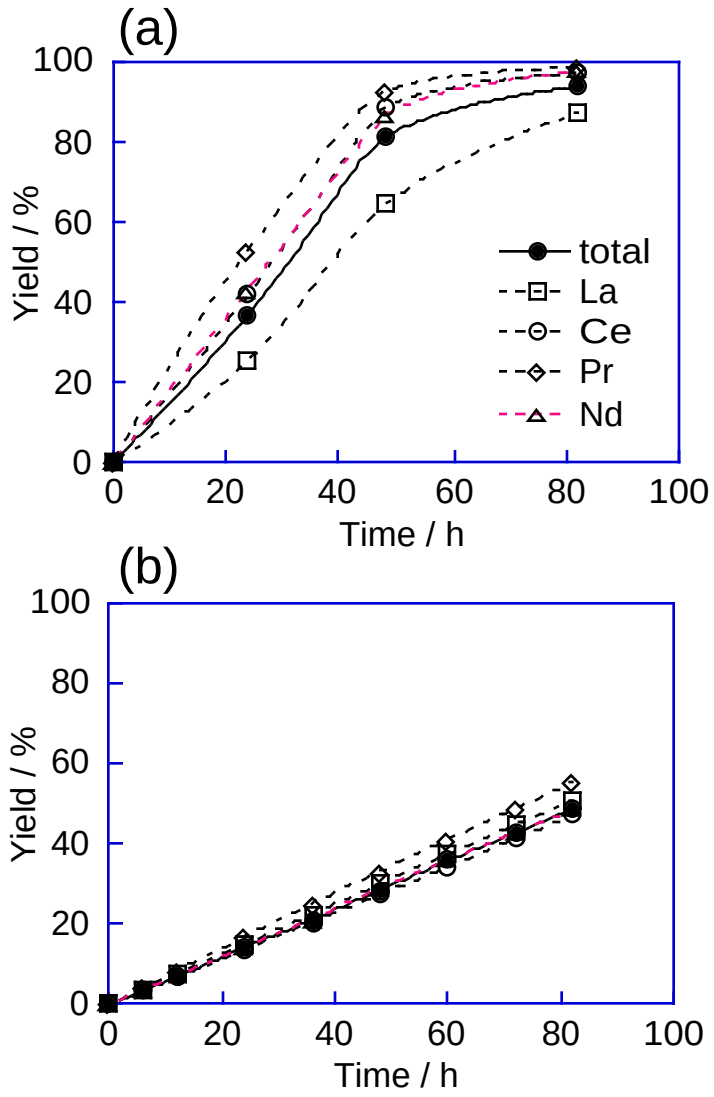

Figure 2.6 (a) Yields of rare earth chlorides under the optimized CVT condition as a function of time and (b) that calculated from thermodynamic data

$$P'_{RAl3Cl12} = x_R \cdot P_{RAl3Cl12} \quad (2.15)$$

where x_R is the molar fraction of the rare earth element. The transported amount of rare earth chlorides via vapor complexes with Al_2Cl_6 was obtained using the ideal gas equation:

$$n_R = PV/RT = P'_{RAl3Cl12} \cdot (10^{-6} \cdot V_{N2} \cdot t)/RT \quad (2.16)$$

where V_{N2} is N_2 gas flow rate (cm^3min^{-1}) and t is reaction time (minutes). Figure 2.6 (b)shows the calculated yields of rare earth chlorides. A large difference was observed between the experimental and calculated values. This deviation may arise from the following factors. First, the effect of a solely vaporized amount of rare earth chlorides is not negligible at 1273 K. Indeed, the vapor pressure of rare earth chlorides with Al_2Cl_6 at relatively low temperatures. However, the volatility

enhancement by formation of a vapor complex is small at temperatures higher than 1000 K. In the present work, because the partial pressure of Al_2Cl_6 is not so high, a considerable amount of rare earth chlorides may vaporize and transport to lower temperature regions simultaneously with the CVT reaction. The kinetic factor also affects the transport efficiency. As the complexation reaction between rare earth chloride and aluminum chloride is a gas-solid reaction, it is impossible to explain the reaction completely by equilibrium, and density and shape of sample also affect the reaction. The chemical tranport rate of each rare earth chloride is larger than the calculated value. The differences in stability of vapor complexes between rare earths estimated form thermodynamic data are small. So these differences are based on the differences in volatility of rare earth chlorides or the kinetic factor.

On the other hand, yields of rare earth chlorides for the CVT experiments using KCl as complex former were 34.2 %. Such a large difference in transport efficiency between the two complex formers was due to the higher vapor pressure of RCl_3-$AlCl_3$ gaseous complexes compared with the vapor pressures of the RCl_3-KCl gaseous complexes.

2.3.3 Extraction of Rare Earths from Used Polish

Two temperature gradients were adopted in the chemical vapor transport experiments: one was the linear gradient (28 K/ cm) and the other was the smaller gradient (10 K/ cm), which mainly occurred in the higher temperature region (Figure 2.7). First, separation characteristics between rare earths and the other elements and the yields of rare earth chlorides were investigated for the CVT processes using KCl or $AlCl_3$ as complex former under the linear temperature gradient. Figure 2.8 shows distribution of deposition for rare earth chloride and other metal chlorides of sample B versus the fraction number (FN). In both experiments, reaction time was 82 h. Deposits obtained by the experiment using sample A showed similar distribution. When $AlCl_3$ was used as complex former, rare earth chlorides was mainly deposited at FN = 3–8 (1213–733 K), while $AlCl_3$ and $FeCl_3$ was deposited at FN = 13 (< 413 K), and $SrCl_2$ and $CaCl_2$ were scarcely transported and remained in the residue. Other elements contained in the polishes, such as Si, seemed to remain in the residue as an oxide. Consequently, purity of rare earth chlorides in the higher temperature region was about 95 %.

Rare earth chlorides and other metal chlorides were separated well, based on the difference in their volatility and reactivity with Al_2Cl_6 to form gaseous complexes. On the other hand, when KCl was used as a complex former, rare earth chlorides deposited at nearly the same temperature region as in the case of $AlCl_3$. However, KCl and $CaCl_2$ were also deposited together with the deposit of the rare earth chlorides, and the purity of the rare earth chlorides was significantly reduced by their contamination. $AlCl_3$ was found to have advantages as a complex former in that, rare earth chlo-

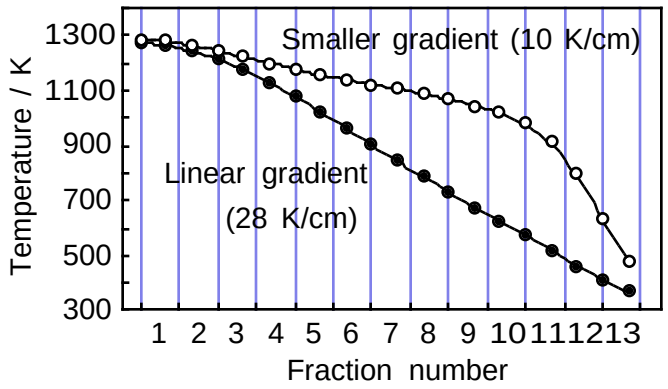

Figure 2.7 Temperature gradients employed for the recovery process of the used polishes

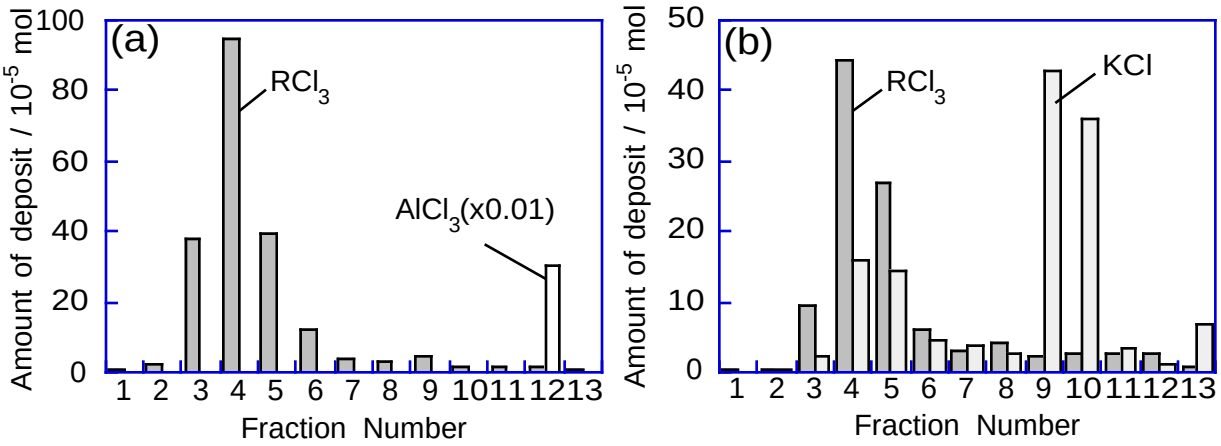

Figure 2.8 Distribution of metal chloride deposits under the linear gradient. Complex former was (a) $AlCl_3$ and (b) KCl

rides were almost completely transported and separated from other metal chlorides by using it, and that recycling of $AlCl_3$ was also possible.

2.3.4 Mutual Separation Charecteristics of Rare Earths

Mutual separation characteristics of rare earths were investigated for the CVT processes using $AlCl_3$, which had been found to be more appropriate as a complex former. The most deposits of rare earth chlorides were at the temperature region 1213 K to 733 K in the CVT experiment under the linear temperature gradient. To improve mutual separation efficiency between the rare earth chlorides, the smaller temperature gradient in the higher temperature region was adopted. Figure 2.9 shows distribution of the deposits of $LaCl_3$ and $CeCl_3$ for the experiment using sample B, whose reaction time was 82 h. In both samples, La and Ce occupied more than two thirds of the whole polishes. Therefore, mutual separation between La and Ce is especially important in the separation

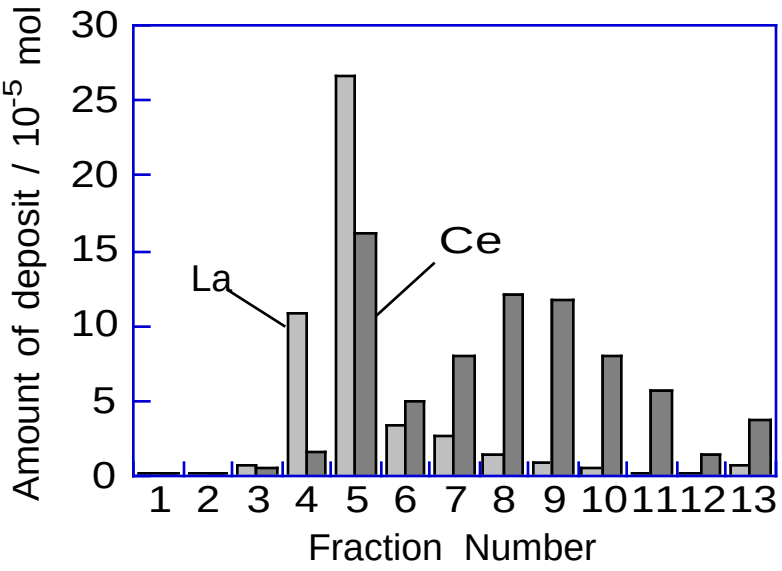

Figure 2.9 Distrubution of $LaCl_3$ and $CeCl_3$ for the CVT experiment using sample B as raw material under small gradient

process of rare earths from used polishes. Relationship between the separation factors and reaction time with % yield of $LaCl_3$ and $CeCl_3$ for the experiments using sample B as raw material is shown in Figure 2.10. The separation factor in the higher temperature side, $\beta_{La/Ce}$, increased gradually with increasing reaction time from 24 h to 82 h, while the separation factor in the lower temperature side, $\beta_{Ce/La}$, rapidly increased from 24 h to 48 h, and remained constant from 48 h to 82 h. The different behavior of the separation factors is due to the difference in the amount of $LaCl_3$ and $CeCl_3$ transported. Generally in the CVT process, $CeCl_3$ is transported to lower temperature region more rapidly than $LaCl_3$ is because of the higher stability of its gaseous complex with $AlCl_3$. For the CVT experiment with relatively short reaction time less than 48 h, $CeCl_3$ was concentrated in the low-temperature side. After 48 hours of CVT reaction, transported amount of $LaCl_3$ relatively increased and $LaCl_3$ was concentrated in the high-temperature side gradually. The separation efficiency between La and Ce improved with increasing the overall yield of $LaCl_3$ and $CeCl_3$. The separation factor values $\beta_{La/Ce}$ and $\beta_{Ce/La}$ after 82 hours reaction were 2.56 and 4.47, respectively. The highest purity of $LaCl_3$ and $CeCl_3$ were 80.0 % at FN = 4 and 81.9 % at FN = 11, respectively. $LaCl_3$ and $CeCl_3$ were expected to be separated almost completely by repeating this process more than four times.

Table 2.3. Separation factors between rare earth elements of sample A and B

Sample	$\beta_{La/Ce}$	$\beta_{La/Pr}$	$\beta_{La/Nd}$	$\beta_{Ce/Pr}$	$\beta_{Ce/Nd}$	$\beta_{Pr/Nd}$
A	2.43	2.92	2.66	1.06	1.13	1.03
B	2.56	2.07	2.22	1.31	1.32	1.01

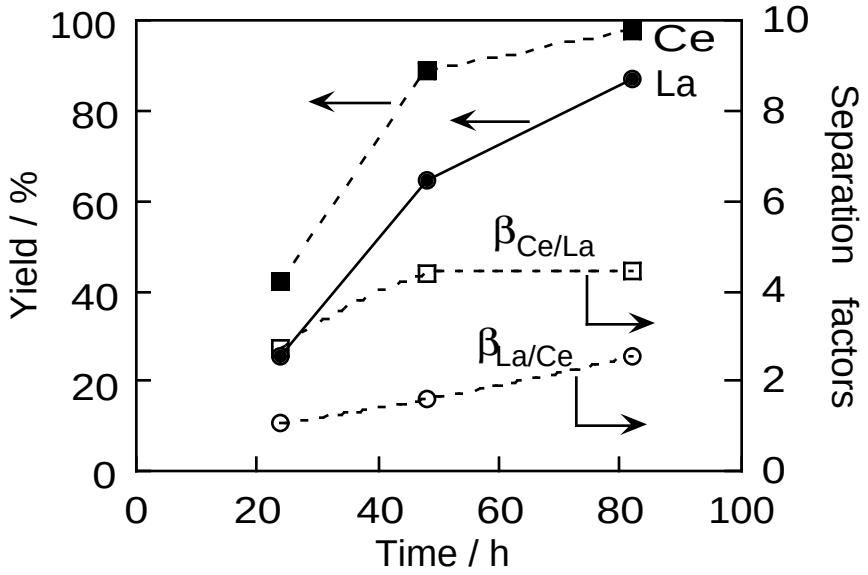

Figure 2.10 Separation factors between La and Ce and yields of $LaCl_3$ and $CeCl_3$ as a function of reaction time

Separation factors between the two elements obtained from the CVT experiment using sample A and B as raw materials are summarized in Table 2.3. Between sample A and B, separation factor values obtained differed slightly and this is because of the difference in their composition, but the overall separation characteristics for both samples were similar. It was also possible to separate $LaCl_3$ and $CeCl_3$ from mixture of $PrCl_3$ and $NdCl_3$, respectively, but not $PrCl_3$ from $NdCl_3$. However, Murase et al. has presented that mutual separation efficiency as high as solvent extraction process was obtained for Pr–Nd binary system in the CVT process by introducing temperature gradients at the constant-temperature plateau zone. Therefore, it is proposed that each rare earths in the polishes can be separated individually by repeated CVT process with optimized of temperature gradient.

2.4 Conclusions

Rare earth chlorides formed by chlorination of the used polish are transported chemically along a temperature gradient via gaseous complex with aluminum chloride. Using $AlCl_3$ as the forming complex, deposits of rare earth chlorides are obtained free of the other metal chlorides. It has been found that it was possible to extract of the rare earths from the used polish by the chemical vapor transport process.

Mutual separation between rare earth chlorides based on the difference between their formation-dissociation equilibrium of vapor complexes was possible. Satisfactory separation characteristics were obtained especially between La and Ce.

Chapter 3

Surface modification of mixed oxides using chemical vapor transport

3.1. Introduction

In chlorination of physical mixture of oxides, each component oxide is chlorinated separately and its chlorination rate depends on chlorination rate of pure oxides and its molar fraction. However, chlorination of mixed oxides is more complicated, and different phase from starting material often forms through chlorination. In chlorination of pyrochlore mineral $CaNaNb_2O_6F$ at 1273 K, orthorhombic $CaNb_2O_6$ forms as well as NaCl, $CaCl_2$, $NbOCl_3$, and $NbOF_3$ [83].

$$CaNaNb_2OF_6\,(s) \rightarrow x\,NaCl\,(s, l) + (x/2)CaCl_2\,(s, l) + (1-x)CaNaNb_2O_6F\,(s) + (x/3)NbOF_3\,(g) + (2x/3)NbOCl_3\,(g) + (x/2)CaNb_2O_6\,(s) + x\,O_2\,(g) \quad (3.1)$$

This phase saparation by chlorination is applicable to synthesize metastable phase. In chemical vapor transport, metal chlorides are eliminated as gaseous complexes by complex formation with $AlCl_3$. This makes it possible to carry out materials processing by dry process.

Automotive three-way catalysts (TWCs) convert three main pollutants such as CO, hydrocarbon (HC), and NO_x to CO_2, H_2O, and N_2 simultaneously[29]. However, the air-to-fuel ratio in the catalytic converters needs to be kept near the stoichiometric value (about 14.6) to attain the simultaneous conversion. Cerium oxide (ceria) is an important component of promoters for the TWCs [30, 31] because of its oxygen storage capacity (OSC), based on the redox behavior between Ce^{3+} and Ce^{4+}: ceria plays a role in widening the apparent air/fuel ratio where the catalysts act effectively, by releasing oxygen in “reducing conditions” and storing oxygen in “oxidizing conditions”. In recent years, the incorporation of Zr into CeO_2 lattices has been reported to improve thermal stability as well as oxygen storage capacity[32, 33]. The subject in the promoters of the TWCs is improvement in the oxygen release property at lower temperatures and in thermostability at high temperatures. Whereas oxidation of the present promotor readily proceeds even at room temperature, its reduction requires relatively higher temperatures above 600 K. As restrictions for automotive exhaust gas become stricter, the need to remove these exhaust gas, especially in low temperatures, increase year by year. Many attempts have been made for lowering the oxygen re-

lease temperature of CeO_2–ZrO_2 solid solutions[34–46]. One of the important factors, which has an effect on the oxygen release property, is the textural property of the solid solution. It was shown that $Ce_{0.5}Zr_{0.5}O_2$ solid solution with high surface area, which was derived by sol–gel route, released oxygen at much lower temperature than that with low surface area prepared by the solid-state reaction[37, 38]. Doping of trivalent ions such as Y, La, and Ga into CeO_2–ZrO_2 solid solutions facilitates the diffusion of oxygen in the lattice by formation of anion defects and decreases the reduction temperature of the solid solutions[39, 40]. Loading of noble metals on the solid solutions also improves the oxygen release property by a synergetic effect between the novel metals and the supports[41]. In addition to these modification, it has been reported that the reduction at high temperatures (1273–1323 K) and the subsequent reoxidation at mild temperatures (700–873 K) reduce the oxygen release temperature of the CeO_2-ZrO_2 solid solutions [37–39, 43–46, 84]. Otsuka-Yao-Matuso et al. found that the pyrochlore-like phase denoted to κ-phase formed as a result of the reduction/reoxidation cycle [44–46,84]. In our laboratory, pyrochlore $Ce_2Zr_2O_7$ formed by thermal decomposition of an oxalate precursor in inert gas, and the similar pyrochlore-like mixed oxides with excellent oxygen storage capacity was obtained by reoxidation of it [48]. Although the oxygen release property depends on both the properties of bulk and surface, there have been few studies on the surface modification of CeO_2-ZrO_2 solid solutions.

As described above, in the chemical vapor transport process, metal components in the oxides are volatilized through the chlorination and the subsequent formation of the vapor complexes. It seems that chlorination of mixed oxides heterogeneously occurs because of the difference of each component in reactivity with chlorine. If the condition of chlorination could be controlled so that only the surface of samples is chlorinated, this heterogeneity in chlorination induces formation of a rough and defective surface phase with a composition and structure different from those of bulk. This surface treatment process, which we named “chemical filing”, is promising for the surface modification of catalytic materials. In addition to the reduction behavior at low temperatures, improvement in thermostability is also expected for long-term, high-temperature chemical filing treatment.

In this chapter, the effects of the chemical filing treatment on surface and bulk structures of CeO_2-ZrO_2 solid solutions was investigated and the elucidation of the mechanism of the modification on oxygen release ability was attempted. Two kinds of the chlorination treatments were attempted. First method is the gas-solid chlorination process, which consists of the chlorination with Cl_2 gas and the subsequent formation of the gaseous complexes. Second method is the solid-state chlorination process using NH_4Cl as a chlorinating agent.

3.2. Experimental Details

3.2.1 Starting materials

Aqueous solutions of cerium nitrate $Ce(NO_3)_3$ and zirconyl nitrate $ZrO(NO_3)_2$ (>99.9% in purity) were obtained from Shin-Nippon Kinzoku Kagaku Co., Ltd. Aluminum chloride (99.99%) and active carbon were purchased from Aldrich and Nacalai Tesque Inc., respectively, and used as received.

Three methods were used to prepare the starting CeO_2–ZrO_2 powders. The first method was thermal decomposition of a Ce–Zr mixed oxalate according to a procedure published previously.[48] Briefly, the precipitate of cerium zirconyl oxalate $Ce_2(ZrO)_2(C_2O_4)_5 \cdot n\ H_2O$ was formed by adding a mixture of 1.0 M aqueous solutions of cerium nitrate and zirconyl nitrate with a Ce / Zr ratio of 1/ 1 to 0.5 M oxalic acid solution and subsequently adjusting the pH value of the solution to 2 with ammonium hydroxide. The precipitate was washed with deionized water several times, dried at 353 K overnight, and heated in an Ar flow at 1273 K for 5 h to be converted into black powder. The sample obtained by this method is denoted "oxa-CeO_2–ZrO_2." The second method of the preparation was coprecipitation of Ce and Zr hydroxides. First, the equimolar mixture of aqueous solutions of cerium and zirconyl nitrates was added to excess ammonium hydroxide. After being washed and dried in a manner similar to the first method, the precipitate was heated in air at 1173 K for 5 h. This sample is denoted "cp-CeO_2–ZrO_2." The third method is reduction of the cp-CeO_2–ZrO_2 in an H_2 flow at 1323 K for 5 h, with subsequent reoxidation in air at 873 K for 5 h. The obtained sample is denoted as "reduced/reoxidized CeO_2–ZrO_2."

3.2.1 Chemical filing treatment by gas-solid reaction

These starting CeO_2-ZrO_2 powders were subjected to the chemical filing processes. The chemical filing process consists of two steps: chlorination and formation of the vapor complexes. The CeO_2-ZrO_2 solid solutions are chlorinated in the presence of carbon. The resulting chlorides react with aluminum chloride to form the vapor complexes, and are removed from the samples.

The apparatus used for the chemical filing process is a similar to that used in the rare earth separation process (Chapter 1). The CeO_2-ZrO_2 solid solutions of 0.30 g were mixed with active carbon of 0–0.30 g as a deoxidant, and the mixture was loaded on an alumina boat and introduced into the furnace B. The anhydrous $AlCl_3$ (8.0×10^{-3} mol) powder in a glass ampoule with a small hole was put into the furnace A. After the temperature of the furnace B was raised to 1273 K in a N_2 flow, N_2-Cl_2 mixed gas (flow rate: N_2 = 30–600 cm^3min^{-1}, Cl_2 = 5 cm^3min^{-1}) was introduced into the reactor for 1-60 min. Then N_2 gas with a flow rate of 300 ml/min was introduced for 1 h, and $AlCl_3$ was heated in the furnace A at 363 K. The samples after the chemical filing were calcined in air at

673 K for 5 h for complete reoxidation and removal of excess carbon.

Three kinds of additional samples were prepared to confirm effects of chemical filing: The sample prepared by reoxidation of the oxa-CeO_2-ZrO_2 in air at 673 K for 5 h (reoxidized sample) and those prepared by heating of the oxa-CeO_2-ZrO_2 and the cp-CeO_2-ZrO_2 with active carbon in a N_2 flow at 1273 K for 1 h, followed by calcination in air at 673 K for 5 h.

3.2.2 Chemical filing treatment by solid-state reaction

The CeO_2-ZrO_2 powders or the cerium zirconyl oxalate were mixed with NH_4Cl in alumina mortar for 15 minutes. The proportion of the raw materials to NH_4Cl was from 1/1 to 1/5. The mixtures were loaded on the alumina cruicible and set at an electric furnace. The samples were heated in air at a heating rate of 3.25 K min^{-1} to 1273 K and held at this temperature for 60 min.

3.2.3 Characterization

Hydrogen consumption was evaluated by temperature-programmed reduction (TPR) experiments using a thermal conductivity detector of a gas chromatograph (Shimazu, GC-8A). To minimize the effects of adsorbed species on TPR, all the samples were pretreated in He (80 cm^3 min^{-1}) at 473 K for 2 h before the initial TPR experiment. The TPR characterization was performed on 0.03 g of catalyst under a H_2 flow with a flow rate of 80 $cm^3 min^{-1}$ from room temperature to 1273 K(heating rate 10 K min^{-1}). The amount of hydrogen consumption was estimated from the integrated peak areas using CuO as a standard.

Ammonia TPD (Temperature-programmed desorption) experiments were carried out to estimate the amount of acid sites on the samples by using the same thermal conductivity detector in the TPR experiment. Prior to TPD, 0.09 g of the samples was heated at 973 K for 1 h in a flow of He with a flow rate of 30 $cm^3 min^{-1}$, then NH_3 (flow rate: 30 ml/min) was adsorbed on the samples at 973 K for 1 h, and the samples were treated again with He for 1 h at the same temperature. The TPD was performed under an He flow with a flow rate of 30 cm^3 min^{-1} from room temperature to 973 K (heating rate 10 K min^{-1}).

The X-ray powder diffraction patterns were measured using a MAC Science M18XHF-SHA diffractometer using Cu–Ka radiation. FT-Raman spectra were obtained on the Ultimate Raman System (Jobin Yvon T64000). The spectra were excited with an Ar ion laser operating at 488.0 nm wavelength, and the laser power was 150 mW. BET surface area of the samples was measured with a Mircometrics FlowSorb II 2300 instrument. Bulk composition of the samples was determined by a X-ray fluorescent spectrometer (Rigaku System 3270A). The composition and electronic state of the surface of the samples were investigated by an X-ray photoelectron spectroscopy apparatus

(Physical Electronics, Model-5500MT). Microstructure of the powders was observed with a Hitachi H-800 transmission electron microscope operating at 200 kV.

3.3 Results and Discussions

3.3.1 Chemical filing treatment by gas-solid reaction

(1) Optimization of chemical filing condition

In the chemical filing process, degree of chlorination determines surface and bulk properties of the samples. Desirable chemical filing condition can be obtained when surface chlorination is completed, and modification on bulk structure is minimized. Main factors that effect the chemical filing conditions are the amount of carbon and the N_2/Cl_2 ratio of the introduced gas.

Effects of the amount of active carbon were investigated by chlorination in a N_2–Cl_2 flow with the N_2/Cl_2 ratio of 6/1 for 1 h using 0, 0.06, 0.15, and 0.30 g of active carbon. When the amount of active carbon was 0 or 0.06 g, chlorination did not proceed. On the other hand, with 0.30 g of active carbon, it was found that the excess carbon inhibited the chlorination reaction. The same results have been reported for the chlorination of bastnaesite concentrate. The optimal amount of active carbon is 0.15 g, which is half the mass of the starting material.

The effect of the N_2/Cl_2 ratio was investigated in the range of 6/1 to 120/1 by using the optimized amount of carbon. With the high Cl_2 content, the phase decomposition into CeO_2 and ZrO_2 occurred in a very short chlorination time less than 5 min. This phase decomposition is rationalized as oxidation of Ce(III) in pyrochlore type $Ce_2Zr_2O_7$, where chlorine acts on as a oxidizing agent. In the presence of carbon, Ce(III) is oxidized to form CeO_2, and a part of zirconium is chlorinated to form $ZrCl_4$.

$$Ce_2Zr_2O_7 + (3/2 - x)\,C + 2(2 - x)\,Cl_2 \rightarrow 2\,CeO_2 + x\,ZrO_2 + (2 - x)\,ZrCl_4 + (3/2 - x)CO_2 \quad (3.2)$$

On the contrary, in the chemical filing condition with extremely low Cl_2 content, surface chlorination was not completed even after a long reaction time more than 1 h. The N_2/Cl_2 ratio of 60/1 was found to be the most appropriate for complete chlorination of the surface.

(2) Structural modification by chemical filing

Table 3.1 summarizes the surface and bulk composition of oxa-CeO_2–ZrO_2 powders after the

surface treatment, which were determined by X-ray photoelectron spectroscopy (XPS) and X-ray fluorometry, respectively. The chlorination was carried out for 5, 10, and 50 min at N_2/Cl_2 = 60/1. X-ray fluorescence analysis showed that the CeO_2–ZrO_2 solutions contain only Ce and Zr. Because no trace of aluminum was detected, the possibility of the formation of Al_2O_3 by the reaction of samples with aluminum chloride can be excluded. It also should be mentioned that no peaks related to chlorine were observed in the XPS spectra, suggesting that no chloride or oxychloride species remained on the surface of the CeO_2–ZrO_2 solid solutions. Surface enrichment of cerium proceeded with increasing chlorination time, and the bulk composition of the samples was unchanged by the chemical filing treatment,.

Table 3.1 The bulk and surface composition of oxa-CeO_2-ZrO_2 powders after the surface treatment for various reaction time

Chlorination time / min	Composition in bulk	Composition in surface
0*	$Ce_{0.4}Zr_{0.6}O_2$	$Ce_{0.45}Zr_{0.55}O_2$
5	$Ce_{0.4}Zr_{0.6}O_2$	$Ce_{0.47}Zr_{0.53}O_2$
10	$Ce_{0.4}Zr_{0.6}O_2$	$Ce_{0.53}Zr_{0.47}O_2$
50	$Ce_{0.7}Zr_{0.3}O_2$	$Ce_{0.74}Zr_{0.26}O_2$

Figure 3.1 compares X-ray diffraction patterns of the oxa-CeO_2–ZrO_2 powders after the chemical filing treatment for various reaction times. As previously reported, the CeO_2–ZrO_2 mixed oxide prepared from thermal decomposition of a cerium zirconyl oxalate had the cubic pyrochlore struc-

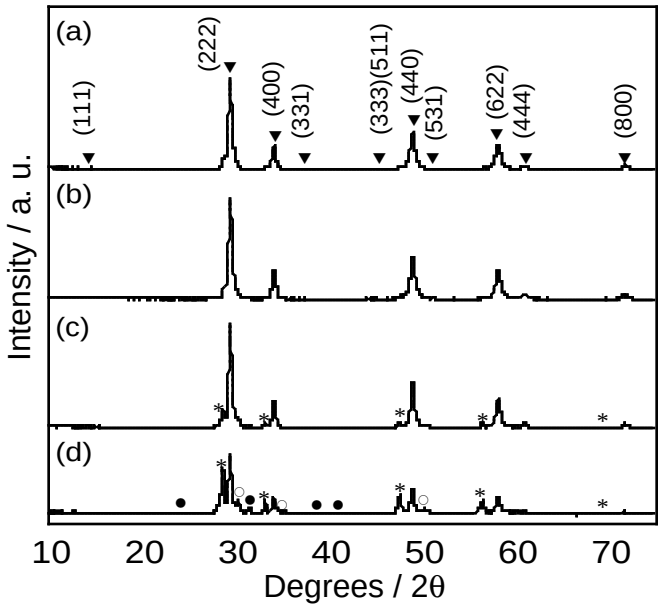

Figure 3.1 X-ray diffraction patterns of CeO_2-ZrO_2 solid solutions prepared from the oxalate, which are calcined (a) and chemical-filed for 5 min (b), 10 min (c), 50 min (d):(▼) pyrochlore-like phase: (*) CeO_2; (●) monoclinic -ZrO_2; (○) tetragonal-ZrO_2

ture [48]. Lattice contraction and formation of pyrochlore-like structure were observed after oxidation of the pyrochlore sample (Figure 3.1 (a)). Calculation of unit cell parameter was carried out assuming fluorite structure by using line (111) of fluorite and the cubic relationship of d_{hkl} and the cell parameter: $1/d_{hkl}^2 = h^2 + k^2 + l^2 / a^2$. The calculated unit cell parameter was 5.3429 (Å). The composition estimated by using the empirical equation by Kim[87] for the lattice parameter change of fluorite solid solutions was $Ce_{0.432}Zr_{0.568}O_2$. This is comparable to that obtained by X-ray fluorometry. No apparent change of intensities or positions of the peaks was observed by the surface treatment with chlorine within 5 min (Figure 3.1 (b)). After chlorination treatment for longer time, however, the XRD pattern indicated the phase decomposition. The intensity of the peaks of the

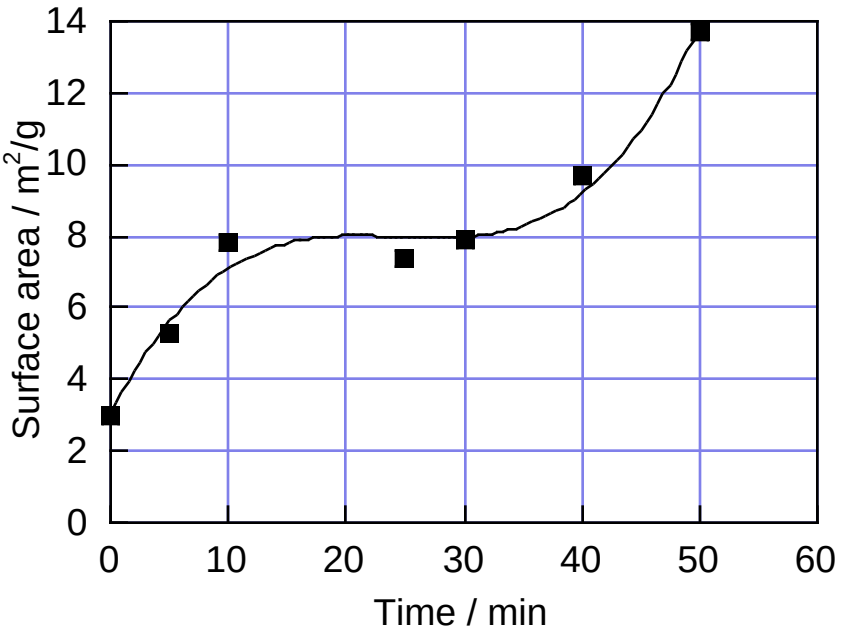

Figure 3.2 Relationship between the surface area of CeO_2-ZrO_2 solid solutions prepared from the oxalate and chlorination time in the chemical filing.

pyrochlore-like phase decreased, and new peaks of the cubic CeO_2 phase and the monoclinic and tetragonal ZrO_2 phases appeared (Figure 3.1 (c), (d)).

The relationship between chlorination times and the surface areas of the samples in the chemical filing is shown in Figure 3.2. The surface area of the only reoxidized sample was 3.0 m^2/g, which was comparable to the value previously reported for the CeO_2–ZrO_2 powders prepared from a oxalate[48]. After the 5 and 10 min chlorination, the surface area increased to 5.3 and 7.8 m^2/g, respectively. After chlorination for 50 min, the surface area remarkably increased. From the results of the XRD investigations, the small and the large increases in the surface area are attributed to the modification on the surface and in the bulk structures of the samples, respectively.

Raman scattering is generally detectable within a depth of 10–100 nm from the surface of samples, whereas X-rays reach a depth of more than 1 mm from the surface. Therefore, Raman

spectroscopy is more appropriate than X-ray diffraction for structural analysis of the surface of solids. Figure 3.3 shows Raman spectra of oxa-CeO_2–ZrO_2 solid solutions collected in the region 100–800 cm^{-1} with and without the chemical filing. For CeO_2–ZrO_2 solid solutions with a Ce/Zr ratio of about 1/1, there are three possible structures: tetragonal, fluorite, and pyrochlore-related structures [49]. The Raman spectrum of the reoxidized sample features six strong bands centered at 272, 304, 446, 470, 578, and 611 cm^{-1} and a shoulder band at about 640 cm^{-1}. This spectrum is similar to that of κ-phase, which is newly apparent because of the reduction and reoxidation of a

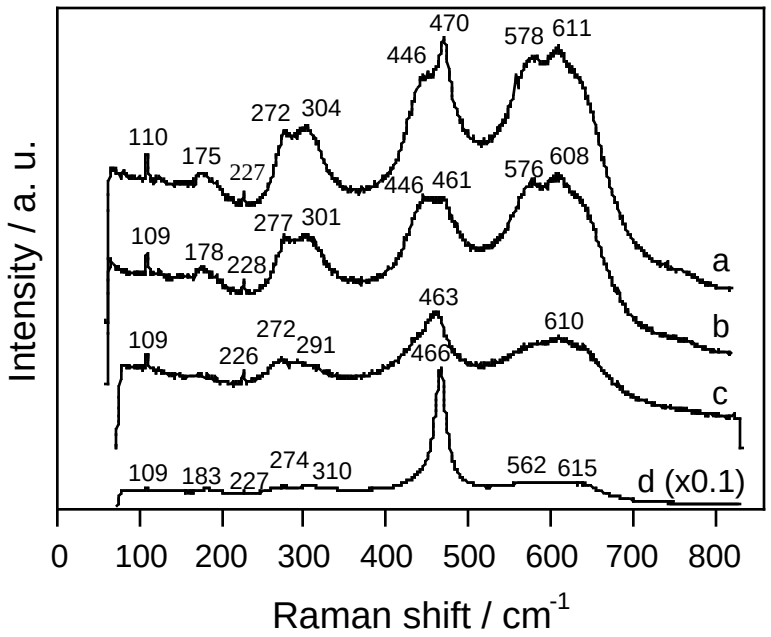

Figure 3.3 Raman sepctra of CeO_2-ZrO_2 solid solutions prepared from oxalate, which are calcined (a) and chemical-filed for 5 min (b), 10 min (c), and 50 min (d).

solid-state synthesized CeO_2–ZrO_2 (Ce/Zr = 1/1) solid solution [45,46]. In the pyrochlore structure $A_2B_2O_7$ (space group $Fd3m$), six Raman active modes $A_{1g} + E_g + 4\ T_{2g}$ have been predicted [50]. However, only four T_{2g} bands centered at 300–320, 395–400, 495–538, and 516–596 have been observed in the Raman spectra of $Ln_2Zr_2O_7$ (Ln = La, Nd, Sm, Gd) pyrochlore-type compounds [50]. Therefore, the peaks centered at 304, 470, and 578 in the Raman spectra of the reoxidized sample indicate the presence of the pyrochlore-like structure. The other three bands centered at 272, 446, and 611 are attributable to E_g bands of tetragonal solid solution. It seems that the structure of κ-phase is intermediate between tetragonal and pyrochlore by lowering of symmetry as a result of the displacement of oxygen from ideal positions.

After the chlorination for 5 min, the T_{2g} band at 470 cm^{-1} relatively decreases compared with the reoxidized sample. Although the intensity of the other peaks remained unaltered, the broadening was observed. These finding suggests that oxygen displacement was occurred and the surface structure was distorted by the formation of the defect.

After chlorination for a longer time, the intensity of the bands attributed to the pyrochlore and tetragonal structures decreased, and a new band appeared at 463 cm^{-1}, which belongs to T_{2g} Raman active mode of fluorite structure. This suggests the high content of fluorite CeO_2 on the surface of the samples chlorinated for a long time as a result of the phase decomposition.

(3) Effect of chemical filing on oxygen release property

TPR profiles of the reoxidized and the chemical filed oxa-CeO_2-ZrO_2 powders are reported in Figure 3.4. Fornasiero et al. reported that TPR profiles could be deconvoluted into several Gaussian

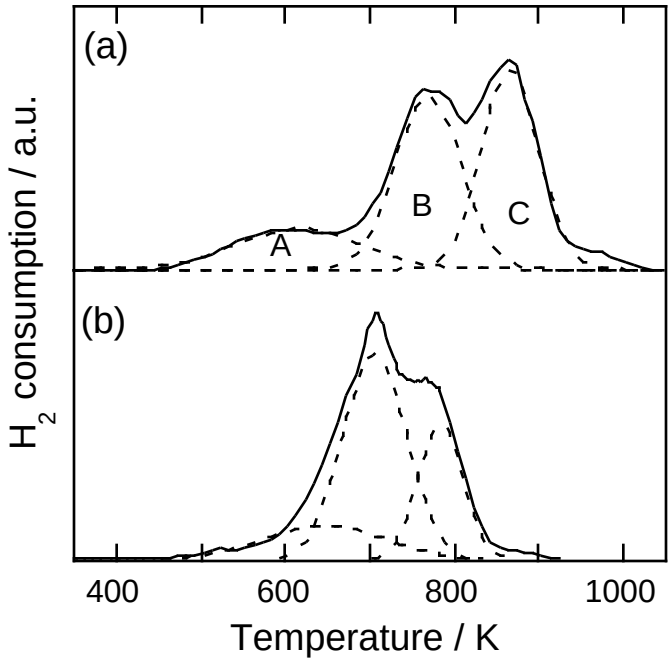

Figure 3.4 TPR profile of oxa-CeO_2-ZrO_2 solid solutions calcined (a) and chemical-filed for 5 min (b).

Table 3.2. The peak temperatures and H_2 consumption in the TPR of oxa -CeO_2–ZrO_2 powders after the chemical filing for various reaction time

Chlorination	Peak temperature / K			H_2 consumption / ml g^{-1}			
time / min	A	B	C	A	B	C	total
0	615	768	865	7.9	14.3	15.4	37.6
5	645	706	784	8.9	17.1	8.7	34.7
10	622	715	795	8.0	17.9	4.6	30.5
30	622	703	781	6.9	11.3	6.9	25.1
50	669	725	816	10.8	6.8	4.8	22.4

type profiles [38]. The TPR profiles of the reoxidized and chemical-filed samples were deconvoluted into three Gaussians. Peak temperatures and hydrogen consumption of the deconvoluted peaks are described in Table 3.2. According to Fornasiero et al. [51], the lowest-temperature peak is due to

reduction both at the surface and in the bulk, because the amount of H_2 consumption calculated from the linear relationship with surface area [52] is much lower than that estimated experimentally for the lowest-temperature peak. Therefore, the first peak in the TPR profiles corresponds to the reduction of the surface and bulk, and both of the second and the third peaks are attributed to reduction processes in the bulk. This splitting of the reduction process in the bulk into the three peaks is a characteristic of a CeO_2-ZrO_2 solid solution prepared using an oxalate precursor [48] and it suggests the existence of three kinds of environments around oxygen atoms in the lattice. Although the peak temperature for the first peak was not largely altered by the chemical filing process, those of the second and the third peaks were lowered by more than 50 K. The correlation between the low temperature reduction peaks in the TPR profiles and three-way activity has been established for the CeO_2-based catalysts. The disappearance of low temperature peaks in TPR spectra causes a significant deactivation of the catalysis. For example, the conversions of carbon monoxide and nitrogen monoxide at the stoichiometric A/F ratio extremely decreased together from ca. 80% to ca. 60%[53,54]. In addition, the oxygen release property in low temperatures also plays an important role in the reduction of hydrocarbon emission after cold start. Recently, Zamar et al. measured activity of CeO_2-based solid solutions for methane combustion. In their work, the TPR peak temperatures of $Ce_{0.8}Zr_{0.2}O_2$ and $Ce_{0.8}Hf_{0.2}O_2$ with similar surface areas were about 820 K and 870 K, respectively, and methane conversion in 820 K over the former was about 8% higher than that over the latter [55], suggesting that the lowering in oxygen release temperature by 50 K improves the activity of hydrocarbon combustion. The H_2 consumption for the third peak decreased, suggesting that the release of relatively stable oxygen became difficult by the annealing at high temperatures during the chemical filing treatment.

Total H_2 consumption gradually decreased with increasing chlorination time from 5 to 50 min. This decrease is partially correlated to the decrease in the component of pyrochlore-like structure by the phase separation to CeO_2 and ZrO_2. Another reason is the surface Ce enrichment shown by the XPS measurements. Dissociation of H_2 over ZrO_2 surface occurred at lower temperatures compared to that over CeO_2 surface, and also, surface sites of strong Lewis acidity which may play a role in H2 activation are generated by heat treatment of ZrO_2. Consequently, the lower the zirconium content in the surface of CeO_2-ZrO_2 solid solution, the lower the Lewis acidity and the surface activity against H_2 dissociation. Actually, the amount of desorbed NH_3 of the chemical-filed sample in the NH_3 TPD experiments was smaller than that of the reoxidized sample, indicating the decrease in Lewis acidity.

The chemical filing treatment was most successful with chlorination for 5 min because of the largest H_2 consumption in low temperatures. The reproducibility of this result was confirmed by the profiles of the three TPR runs of the samples independently treated with the same optimized condition.

(4) Mechanism of the chemical filing process

The oxygen release property was also investigated for the reduced/reoxidized-CeO_2-ZrO_2 powders with and without the chemical filing treatment by means of the TPR techniques. Only a single peak was observed for the both TPR profiles in contrast to those of the oxa-CeO_2-ZrO_2 powders. The H_2 consumption of the sample increased from 24.2 ml g^{-1} to 29.3 ml g^{-1} by the chemical filing treatment. However, the peak temperature of the sample did not change from 750 K after the chemical filing. The similar result was also obtained in the case of the cp-CeO_2-ZrO_2 powders. These minor improvements in the reduction behavior of the reduced/reoxidized and the cp-CeO_2-ZrO_2 powders by the chemical filing process indicate that the process gives a significant effect on the oxygen release property only to the oxa-CeO_2-ZrO_2 powder.

There still remains the possibility that the improvement of the oxa-CeO_2-ZrO_2 powder in oxygen release property by the chemical filing is simply ascribed to reducing action of carbon, because the reduction/reoxidation cycle generally lowers oxygen release temperature of CeO_2-

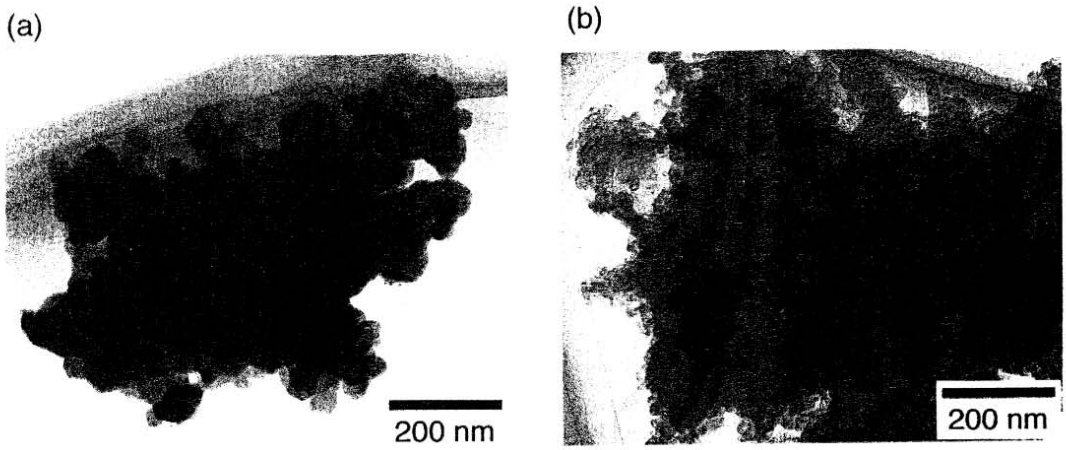

Figure 3.5 Transmission electron micrograph of CeO_2-ZrO_2 solid solutions, which are calcined (a) and chemical filed for 5 min (b).

ZrO_2 solid solutions. Then the reduction behavior of the oxa-CeO_2-ZrO_2 powder prepared by heating with active carbon and subsequent reoxidization was investigated and compared with those of the reoxidized and the chemical-filed samples for confirmation of the chemical filing effect. The peak temperatures and H_2 consumption in TPR profiles for these samples are summarized in Table 3.3. Peak temperature for the carbon treated sample was lower only by 20 K than that for the calcined one, and the H_2 consumption was significantly lowered by carbon treatment to 26.3 ml g^{-1}. This indicates that the effect of carbon reduction on the oxygen release property of the oxa-CeO_2-ZrO_2 sample is smaller than that of the chemical filing.

Figure 3.5 shows transmission electron micrographs of the reoxidized and the chemical-filed

oxa-CeO_2-ZrO_2 powders. Surface morphology of the chemical filed powder was considerably different from that of the calcined one: whereas the surface of the reoxidized sample was almost smooth, that of the chemical-filed sample was very rough. These TEM observations are consistent with the surface structural modification suggested by the Raman spectra and the XPS measurements. This modification is induced by oxidative chlorination with Cl_2. By chlorination, Ce^{3+} is oxidized to Ce^{4+}, zirconium is partially removed to form volatile $ZrCl_4$. As a result, defective structure formed on the surface. This defective surface phase facilitates the diffusion of the bulk oxygen into the surface, resulting in the improvement in the oxygen release properties. Since the existence of Ce^{3+} in the lattice is important to proceed the chlorination, the cp-CeO_2-ZrO_2 powder in which only Ce^{4+} exists is hard to undergo the chemical filing. The proposed mechanism of the chemical filing is illustrated in Figure 3.6.

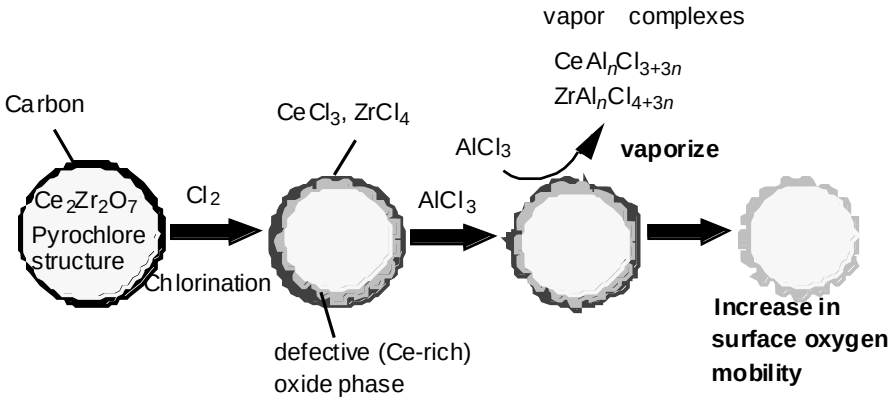

Figure 3.6 Schematic mechanism proposed for surface modification by the chemical filing process

(5) Reduction-oxidation behavior and thermostability of CeO_2-ZrO_2 powders

The effect of continuous reduction and reoxidation cycles on the structure and reduction behavior was investigated for the CeO_2-ZrO_2 powders. The reduction was carried out in a flow of H_2 at a heating rate of 10 K min^{-1} up to 1273 K and then the sample was held at this temperature for 10 min. After the atmosphere was replaced with He for 15 min, the sample was reoxidized in a flow of air for 10 min at 1273 K. The TPR profiles of the chemical-filed oxa-CeO_2-ZrO_2 powders after the reduction and reoxidation cycles for 1 and 10 times are compared in Figure 3.7. The H_2 consumption and peak temperatures in the TPR of the cycled and fresh samples for the chemical-filed and the carbon-treated oxa-CeO_2-ZrO_2 and the reduced/reoxidized-CeO_2-ZrO_2 are summarized in Table 3.3. The peak temperature in the TPR of the chemical-filed sample was further lowered by the one reduction/reoxidation cycle by more than 50 K, and the amount of H_2 consumption slightly decreased. After 10 reduction/reoxidation cycles, the peak temperature remain unaltered, although

the H_2 consumption decreased. The TPR profiles after 20 and 30 cycles were comparable to that after 10 cycles. This decrease in H2 consumption is mainly due to the disappearance of the higher temperature peak and H_2 consumption at the lower temperature peak was almost unaltered even after 30 times. The similar tendency was observed in the case of the carbon treated sample. After 6 cycles, the peak at high temperature disappeared, and the peak temperature decreased from 751 K to 715 K. However, this temperature is still more than 50 K higher than that of the 30 cycled

Table 3.3 The peak temperatures and H_2 consumption of the recycled and fresh samples in the TPR for oxa-CeO_2-ZrO_2 and reduced/reoxidized CeO_2-ZrO_2.

Sample	No. of recycles	Peak temperature / K	H_2 consumption /ml g^{-1}
calcined	0	768	37.6
chemical-filed	0	707	34.7
	10	659	25.8
carbon-treated	0	751	26.3
	6	715	17.3
reduced/reoxidized	0	756	24.2
	10	784	23.4

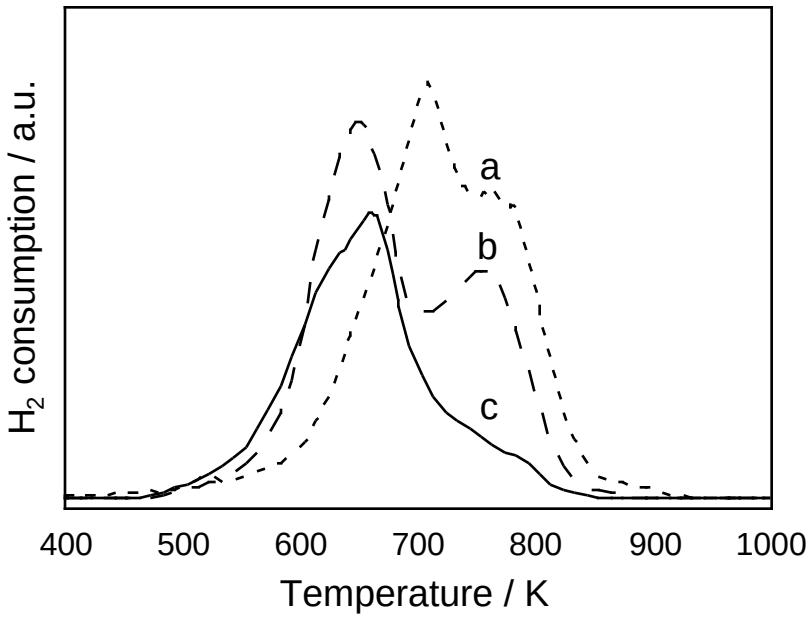

Figure 3.7 TPR profile of the CeO_2-ZrO_2 powders prepared from the oxalate, which are chemical-filed (a) and recycled 1 (b) and 10 (c) times after the chemical filing

chemical-filed sample, suggesting that the chemical-filed sample shows higher oxygen release property than the carbon-treated sample even after the redox cycles at high temperatures. The improvement in the oxygen release property by the reduction/reoxidation cycles was explained on the basis of formation of mesoporosity, which should be attributed to stress and to coalescence of dislocations induced by the large expansion/shrinkage of the lattice [38]. By extensive sintering

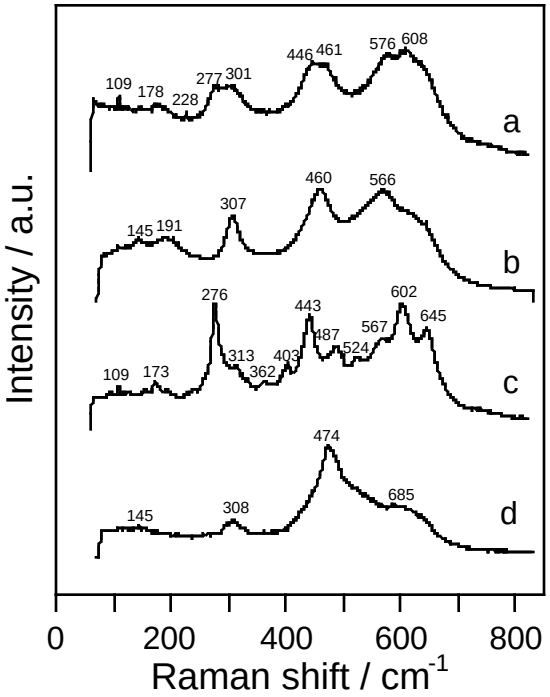

Figure 3.8 Raman spectra of chemical-filed CeO_2-ZrO_2 solid solutions, which are fresh (a) and recycled 10 times (b), and reduced/reoxidized CeO_2-ZrO_2 solid solutions, which are fresh (c) and recycled 6 times (d).

during this treatment, however, surface area of the sample decreased. The TPR profile of the cycled reduced/reoxidized sample features the shift of peak temperature to about 50 K higher compared to the fresh one. Sintering and phase transition by high temperature redox process are the main possible causes of the increase in oxygen release temperature.

The Raman spectra of the chemical-filed sample and the reduced/reoxidized-CeO_2-ZrO_2 sample after the reduction/reoxidation cycles are shown in Figure 3.8. The feature of the Raman spectra of the recycled chemical-filed sample is somewhat different from that of the fresh sample. The three E_g bands of tetragonal structure at 272, 446, 640 cm^{-1} disappeared, and only the bands attributed to pyrochlore-like structure remained. This agrees with the decrease in the number of peaks in the TPR profile, suggesting that the high temperature redox cycles induce the homogenization of the solid solution. This phenomenon seems to be common for the CeO_2-ZrO_2 powders derived from oxalate, since the similar behavior was also observed for the carbon-treated sample. On the other hand, the Raman spectra of the reduced/reoxidized sample was greatly changed by the reduction/reoxidation cycles. Many bands related to the pyrochlore-like structure in the fresh sample disappeared and strong broad band centered at 474 cm^{-1} with a shoulder at 685 cm^{-1} and two weak bands at 145 and 308 cm^{-1} appeared. The peak at 474 cm^{-1} suggests the presence of fluorite phase, and the other peaks are attributed to the tetragonal phase. These results show that large structural modification with phase transition occurred during the redox cycles.

Durability of the samples was also investigated in oxidizing atmosphere at high temperature. The reduction behavior of the chemical-filed CeO_2-ZrO_2 powders calcined in a flow of air at 1323 K for 5 h was also evaluated by the TPR. Although the amount of H_2 consumed in the TPR was comparable to that for the 30 cycled sample, the peak temperature was lower by about 20 K than the fresh sample. In contrast, the peak temperature of the reduced/reoxidized-CeO_2-ZrO_2 increased by about 30 K after the oxidation, and the H_2 consumption also decreased. This indicates the thermostability of the chemical filed sample is superior to those of the samples prepared by the conventional methods. The oxygen release temperature of the chemical-filed sample after high temperature oxidation is still lower than that of the fresh reduced/reoxidized sample.

3.3.2 Chemical filing treatment by solid-state reaction

In previous section, it was found that a surface treatment, which consists of surface chlorination using chlorine gas and elimination of the formed metal chlorides by chemical vapor transport, lowered oxygen release temperature of the CeO_2-ZrO_2 mixed oxides prepared by the thermal decomposition of cerium zirconyl oxalate. Surface selective reaction is expected for solid-state reactions compared to gas-solid reaction. Ammonium chloride (NH_4Cl) has been used for synthesis of rare earth chlorides from the corresponding oxides[85,86], and have the advantage over the other solid chlorinating agents in that no metal component remains after the chlorination reaction.

The X-ray diffraction patterns of the samples treated with NH_4Cl are compared in Figure 3.9.

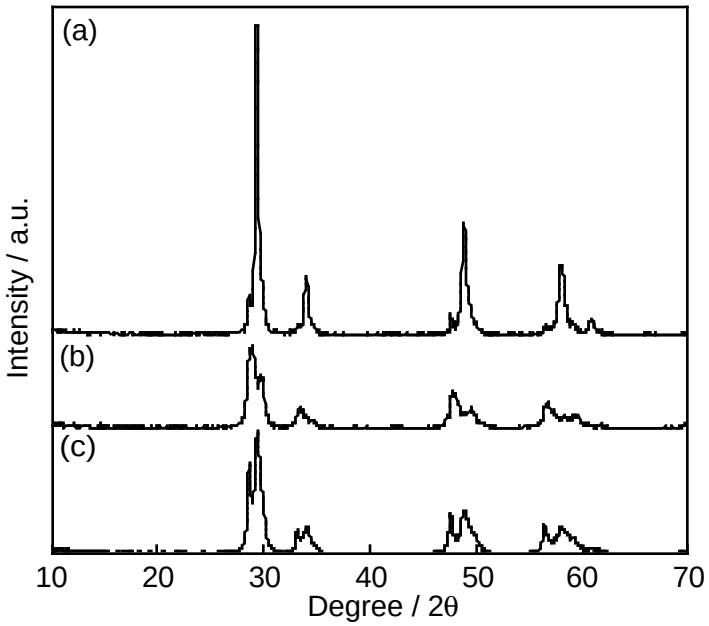

Figure 3.9. XRD patterns for samples treated with NH_4Cl: raw material were (a) oxa-CeO_2-ZrO_2, (b) cp-CeO_2-ZrO_2, and (c) cerium zirconyl oxalate.

No peaks assigned to NH_4Cl was observed, suggesting that no NH_4Cl remained in the samples after the treatment. The results of the X-ray diffraction also indicated that no chloride and oxychloride species existed on the samples. For the samples obtained by the NH_4Cl treatment of cerium zirconyl oxalate and the cp-CeO_2–ZrO_2, remarkable phase separation to the Ce-rich phase and the Zr-rich phase was observed. The peaks of the pyrochlore-like phase was substantially maintained for the oxa-CeO_2–ZrO_2 treated with NH_4Cl, although weak peaks assigned to CeO_2 appeared. The chlorination reaction occurred at the surface of the starting material in contact with NH_4Cl. In the case of the rare earth oxides, the following equation is assumed for the chlorination with NH_4Cl [85]

$$12\ NH_4Cl + R_2O_3 \rightarrow 2\ (NH_4)[RCl_6] + 6\ NH_3 + 3\ H_2O \quad (3.3)$$

$$2\ (NH_4)_3[RCl_6] \rightarrow \{(NH_4)[R_2Cl_7] + 5\ NH_4Cl\} \quad (3.4)$$

$$\{(NH_4)[R_2Cl_7] \rightarrow 5\ NH_4Cl\} \quad 2\ RCl_3 + 6\ NH_4Cl \quad (3.5)$$

The similar reaction is predicted in the chlorination of the CeO_2–ZrO_2 mixed oxides. The chlorination reaction proceeds in the temperature range from 500 K to 700 K as in the case of binary rare earth oxides[85], and NH_4Cl decomposes into NH_3 and HCl and vaporizes at higher temperature.

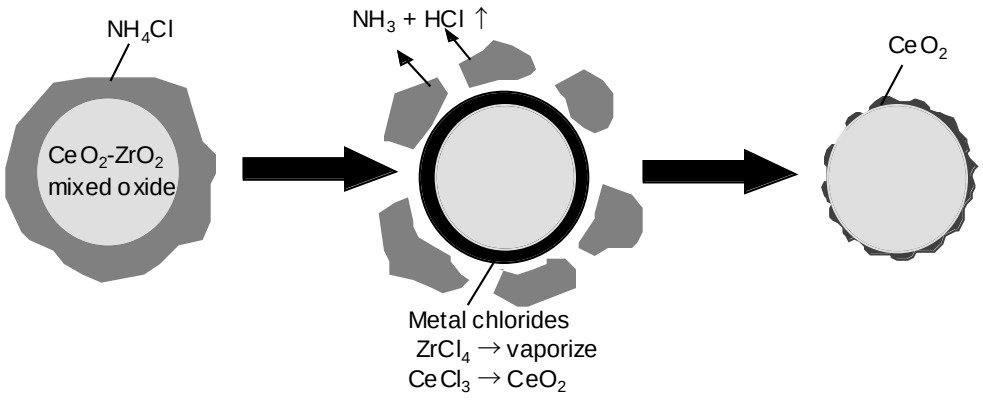

Figure 3.10. Schematic mechanism proposed for surface modification with NH_4Cl.

While $ZrCl_4$ formed by the chlorination has extremely high vapor pressure at about 600 K and is removed from the reaction zone by immediate volatilization, $CeCl_3$ has very low vapor pressure at the same temperature and is oxidized in air to form CeO_2. Since the surface area of the oxa-CeO_2–ZrO_2 was $3 m^2 g^{-1}$ and was much smaller than those of the cerium zirconyl oxalate and the cp-CeO_2-ZrO_2, progress of the chlorination in the inner part is prevented only for the oxa-CeO_2–ZrO_2. The proposed mechanism of the surface modification with NH_4Cl is illustrated in Figure 3.10.

Figure 3.11 shows the TPR profiles of the oxidized and the NH_4Cl-treated oxa-CeO_2-ZrO_2 powders. Peak temperature and H_2 consumption in the TPR experiments of the oxidized sample and the chemically filed sample with NH_4OH or chlorine gas are summarized in Table 3.4. As described in section 3.3.1, the TPR profile of the calcined oxa-CeO_2–ZrO_2 showed two distinct

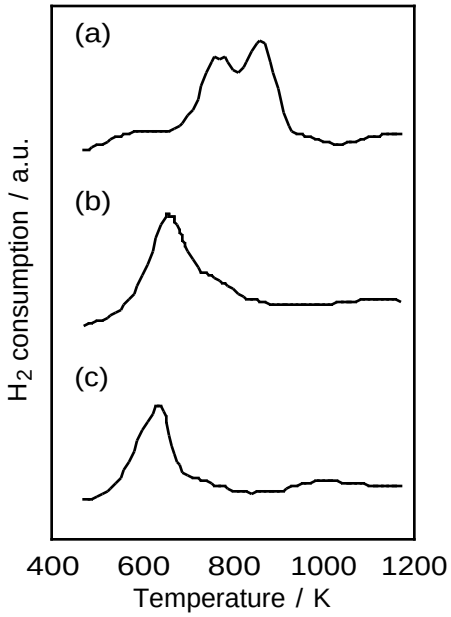

Figure 3.11 TPR profile of the oxa-CeO_2–ZrO_2 powders, which are calcined (a), NH_4Cl-treated (b), and recycled 5 times after the chemical filing (c).

peaks assigned to bulk reduction centered at 768 K and 865 K, respectively. The peak temperature shifted to the lower temperature side by more than 100 K after the chemical filing treatment with NH_4Cl. This oxygen release temperature was also about 100 K lower than that of the reduced/ reoxidized one. The H_2 consumption slightly decreased compared to the calcined sample. It means that the release of relatively stable oxygen became difficult by annealing at high temperature during the chemical filing treatment.

Effect of the high temperature reduction-oxidation cycle (section 3.3.1 (5)) on oxygen release property of the NH_4Cl-treated oxa-CeO_2-ZrO_2 was studied. The TPR profile of the sample after 5 reduction/oxidation cycles is shown in Figure 3.11 (c). The peak temperature and the H_2 consumption in the TPR of the recycled sample is shown in Table 1. After 5 cycles, the peak temperature of the oxygen release is further lowered by about 20 K, and the H_2 consumption is still higher than the reduced/reoxidized sample. Since the cycled reduced/reoxidized sample featured

Table 3.4 Peak temperature and H_2 consumption in the TPR for the NH_4Cl -treated CeO_2-ZrO_2 powders

raw material	No of recycles	Peak temperature / K	H_2 consumption / ml g^{-1}
oxa-CeO_2-ZrO_2	0	658	35.0
	1	639	27.2
	5	638	25.9
cp-CeO_2-ZrO_2	0	731	20.2
Ce-Zr oxalate	0	663	17.0

the shift of peak temperature to about 50 K higher compared to the fresh one (See section 3.3.1 (5)), It can be concluded that the thermostability of the sample, which is chemically filed with NH_4Cl, is superior to those of the samples prepared by the conventional methods.

The sample obtained by the direct chlorination of cerium zirconyl oxalate with NH_4Cl exhibited poor oxygen release properties. Its oxygen release temperature and the amount of O_2 release of the former sample were 731 K and 10.1 mlg^{-1}, respectively. On the other hand, the oxygen release temperature of the cp-CeO_2–ZrO_2 was lowered by the NH_4Cl treatment to 663 K, which is comparable with that of the NH_4Cl-treated oxa-CeO_2–ZrO_2, the amount of oxygen release greatly decreased to 8.5 mlg^{-1}. Both the samples release oxygen at relatively low temperature because of their high surface area. However their oxygen release property of the bulk is inactivated by the phase separation.

The oxygen release peak temperature of the chemically filed oxa-CeO_2-ZrO_2 sample with NH_4Cl was about 50 K lower than that of the chemically filed sample with chlorine gas. This is due to the difference of the two kinds of the chemical filing treatment in mechanism. In the chemical filing treatment with chlorine gas, chlorination proceeds not only in the surface but only in the inner part of the sample by diffusion of Cl_2. In solid-state chemical filing, on the other hand, the sample is surrounded by NH_4Cl, and the surface chlorination proceeds more homogeneously. Surface area of the chemically filed CeO_2-ZrO_2 mixed oxides with NH4Cl (6.8 m^2g^{-1}) was larger than that of the chemically filed sample with chlorine gas (5.3 m^2g^{-1}), despite their similar X-ray diffraction patterns and heating of the former sample in more severe condition than the latter sample.

3.4 Conclusions

Chemical filing process is a promising method for preparation of CeO_2-ZrO_2 mixed oxide catalysts with improved oxygen release property and durability. This process was only effective for the CeO_2-ZrO_2 powder prepared by thermal decomposition of oxalate, because the filing proceeded by oxidative chlorination with chlorine which accompanied oxidation of Ce^{3+} and removal of Zr. The results of TEM observation and Raman spectra showed the surface modification of the solid solution by the filing process. The oxygen release temperature of the chemical-filed sample was more than 50 K lower than that of the sample without filing. The amount of the released oxygen was nevertheless unchanged by the treatment. It was confirmed by the experiments using the blank sample that the improvement in oxygen release property was not attributed to the reduction with carbon but to the chemical filing effect. The repetitive reduction/reoxidation cycles further lowered the reduction temperature of the chemical-filed solid solution, and the reduction temperature was maintained after 30 redox cycles. The oxygen release property of the sample after oxidation at 1323

K for 5 h was superior to that of the solid solution prepared by several conventional methods, suggesting that the chemical filing improves not only reduction behavior but also durability of CeO_2-ZrO_2 solid solutions. The solid-state chlorination with NH_4Cl also improved the oxygen release property and thermostability of the oxalate-derived CeO_2–ZrO_2 powder.

Chapter 4

Thermodynamic studies on dissociation of metal iodides at high temperatures in metal halide lamps

4.1 Introduction

Metal halide lamps are a kind of high-intensity discharge (HID) system, which contains rare gas, mercury, and metal halides, and have a good color-rendering quality and high energy efficiencies compared to conventional high-pressure mercury lamps by addition of metal halides [56, 57]. Although they have been practically used since thirty years ago, recent improvement of their color-rendering properties by use of a rare earth halide as an additive and development of lamps with smaller size extends its use into indoor lighting and head lights of cars. The principle of emission in the lamps is as follows: First, the temperature of mercury arc discharge goes up to about 5000 K in the center of a lamp. Accordingly, metal halides are heated at about 1300 K on the tube wall and evaporate. The metal halides diffuse and decompose at the high temperature arc core to form corresponding metal and halogen atoms.

$$MX_n(g) \rightarrow M(g) + n\,X(g) \qquad \text{(X: halogen)} \qquad (4.1)$$

The resulting metal atoms are then available for ionization and excitation and modify the spectrum and electrical characteristics. The emission occurs when a part of the metal atoms in excited states return to a ground state. Then all the metal atoms diffuse into the tube wall and recombine with halogen atoms to form the corresponding halides at the wall. Therefore, in a metal halide lamp, dissociation of metal halides in the high temperature arcs and their recombination at the wall are repeated reversibly. Among metal halides, metal iodides are used most frequently, because they have higher vapor pressures and decompose at lower temperatures than the corresponding chlorides or bromides. Representative metal halide lamp systems of iodides are NaI/TlI/InI/Hg, ScI_3/NaI/Hg, DyI_3/TlI/Hg, and SnI_2/Hg systems.

For prediction of the emission efficiency, it is important to learn the partial pressure distribution of metal vapors in the metal halide lamps, where the temperature varies from 4000–6000 K at the axis to 1000–1300 K at the wall. There have been two major methods of investigating vapor phase species in the lamps. The first method is a spectroscopic measurement [58–61]. In this method, emission and absorption of the intrinsic spectral lines of atoms and ions were measured, and the temperature distribution and the pressure distributions of the atoms and ions were estimated from

the intensities of the spectral lines. Densities of dominant molecular species in the discharge were calculated with thermodynamic constants assuming Local thermodynamic equilibrium (LTE). van den Hoek and Visser estimated the vapor densities of the atomic and molecular species occurred in DyI_3/Hg-arc by this technique [58].

The second method is a model calculation, whose general procedure of calculation has been reviewed in some literatures [62, 63]. In this method, with the balance equations for mass, energy, charge, and radiation, radial distribution of temperature in the lamp is estimated, and then, based on LTE, the plasma composition is calculated. However, it requires complicated calculation for estimating distribution of vapor species in multi component systems.

These conventional methods have disadvantage of the lack of adaptability to the other systems. It is difficult to predict partial pressure distribution for an unknown lamp system. In this chapter, the distribution of metal vapors in the metal halide lamp systems of iodides was related to the Gibb's energy change corresponding to the dissociation reaction of the iodides, and the elucidation of the dissociation behavior from a thermodynamic point of view was attempted.

4.2 Experimental Details

4.2.1 Experimental data

In Figure 4.1, relationships between the vapor densities of the various molecular and atomic species and temperature in the metal halide lamp systems, DyI_3/Hg, CsI/Hg, ScI_3/NaI/Hg, and TlI/NaI/Hg, derived from the radial distributions of the densities and temperature in the literatures [58–60], are given. The distributions have been estimated by using emission spectroscopy techniques (DyI_3/Hg, CsI/Hg) or model calculations (ScI_3/NaI/Hg, TlI/NaI/Hg) for the arc lamps, in which 32–36 mg of mercury and 20–25 Torr of argon gas were filled. The vapor density is defined here as the number of atoms or molecules, which exist in a unit volume. From the curves it can be seen that a large portion of TlI and CsI dissociates into the atoms more than 2500 K, while NaI is more stable and starts to dissociate at about 3000 K. The rare earth iodides possess higher stability than the monoiodides. Scandium iodide especially is so stable that the proportion of the metal vapor is small even more than 3000 K. This indicates that the iodides with smaller molecular weights have higher stabilities among the same kind of iodides.

4.3.2 Thermodynamic data

It is possible to calculate the vapor density distribution in the metal halide lamps at equilibrium with the Gibb's energy changes of Eq. (4.2) for each iodide

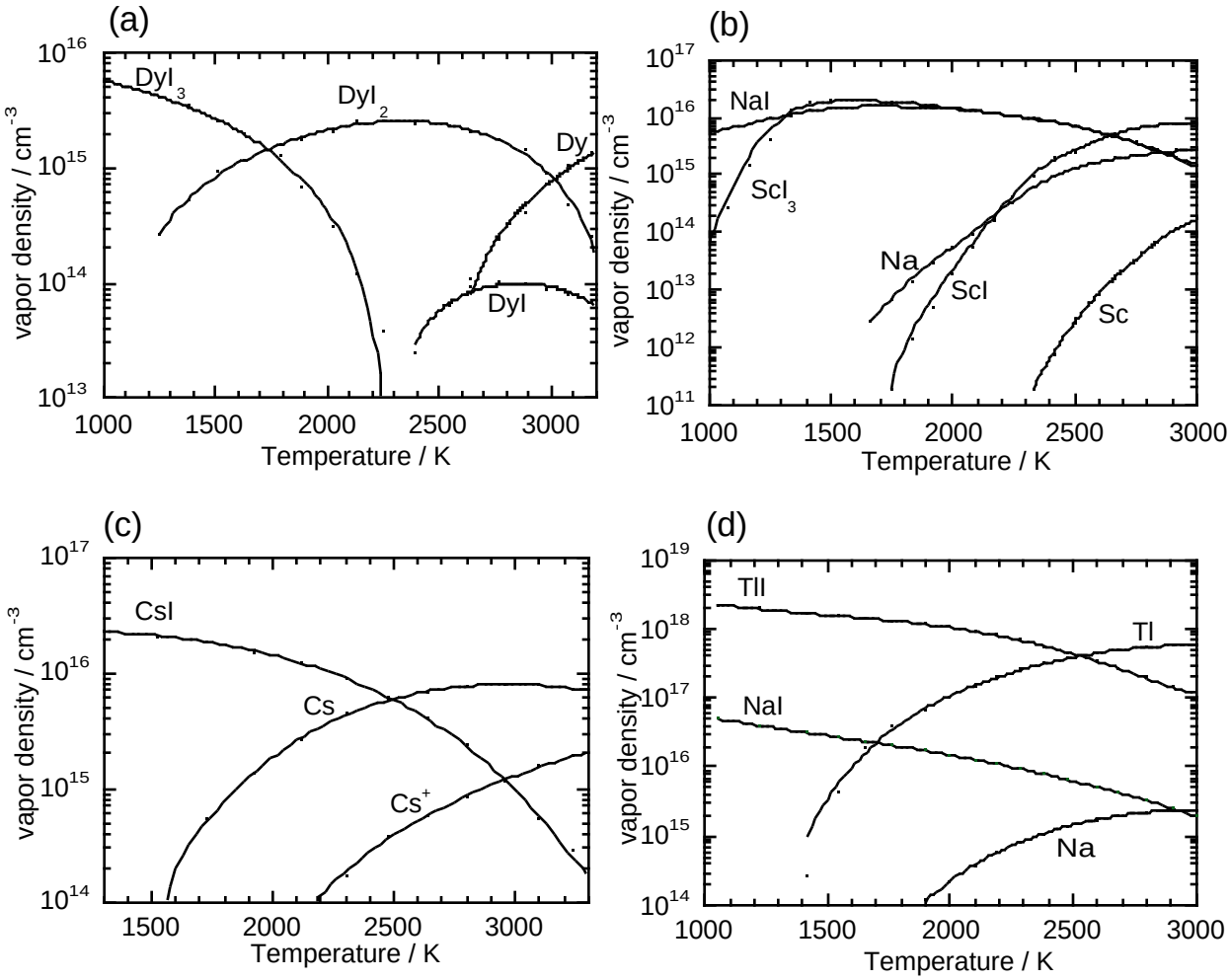

Figure 4.1 Relationship between the vapor densities of the various molecular and atomic species and temperature in (a) DyI_3/Hg, (b) ScI_3/NaI/Hg, (c) CsI/Hg, and (d) TlI/NaI/Hg arc discharge lamps in the literatures

Table 4.1 Enthalpy changes calculated from Ritter energy values, and entropies and heat capacities respectively calculated according to Eq. (4.3) and Eq. (4.4) for rare earth monoiodides and diiodides

Iodides	$\Delta H^\circ_{m,f,298}$ (kJ mol^{-1})	S°_m (JK^{-1}mol^{-1})	$C^\circ_{m,p}$ (JK^{-1}mol^{-1})
ScI	191.21	254.89	39.50
DyI	96.65	270.64	36.50
ScI_2	–54.81	304.72	53.11
DyI_2	–154.4	319.22	53.58

$$MI_n\,(g) \rightarrow M\,(g) + n\,I\,(g) \qquad (4.2)$$

The Gibb's energy changes for sodium, cesium, thallium, scandium, and dysprosium iodides were calculated by using the formation enthalpies and entropies of NaI, CsI, TlI, ScI_3, DyI_3, Na, Cs, Tl, Sc, Dy, and iodine in vapor phase[25, 26, 64–69].

On the other hand, many difficulties arise in the calculation of the Gibb's energy changes for the reduced iodides (ScI, DyI, ScI_2, and DyI_2), because their thermodynamic quantities in vapor phases have been scarcely estimated. We adopted the formation enthalpies of the gaseous rare earth monoiodides [70] and diiodides [71],which had been estimated by Struck and Baglio through the formation energy of the molecule from its ions (Ritter energy). Their entropies and heat capacities were calculated by considering the contribution of the translation, vibrational, and rotational components:

$$S_m = S_{m,\,trans} + S_{m,\,rot} + S_{m,\,vib}, \qquad (4.3)$$

$$C_{m,\,P} = C_{m,V} + R = (C_{m,\,trans} + C_{m,\,rot} + C_{m,\,vib}) + R\ . \qquad (4.4)$$

For the estimation of the rotational entropies and heat capacities of scandium and dysprosium diiodides, it was assumed that they were linear molecules. The obtained enthalpy changes of formation, entropies, and heat capacities of the gaseous monoiodides and diiodides are shown in Table 4.1. By using these thermodynamic quantities, the Gibb's energy changes of the monoiodides and diiodides were calculated.

The least-squares method was carried out for a plot of the Gibb's energy change against temperature at the temperature range of 1000 to 3000 K to obtain the following first-order equation:

$$\Delta G = a - b\,T \qquad (a, b : \text{constant}). \qquad (4.5)$$

The parameters a and b are given in Table 4.2. The relationship of $\Delta G = \Delta H - T\Delta S$ holds between ΔG, ΔH, and ΔS. Accordingly, a and b are expressed as

$$a = \Delta H_{av}, \qquad b = \Delta S_{av}. \qquad (4.6)$$

Where, ΔH_{av} and ΔS_{av} are the average enthalpy and entropy changes of Eq. (4.2) at the temperature range of 1000 to 3000 K, respectively. From the value of the Gibb's energy change obtained by Eq. (4.5), the equilibrium constant of Eq. (4.2), K_p ($= P_M \cdot (P_I)^n / P_{MIn}$), is calculated as follows:

$$K_p = \exp\,(-\Delta G / RT). \qquad (4.7)$$

Meanwhile, the equilibrium constant is expressed using the fraction x of the metal atoms in vapor phase and the total vapor pressure p of the metal iodides at the wall temperature:

$$K_P = \frac{\left(p \cdot \frac{x}{1+nx}\right)\left(p \cdot \frac{nx}{1+nx}\right)^n}{\left(p \cdot \frac{1-x}{1+nx}\right)} = \frac{n^n p^n x^{n+1}}{(1-x)(1+nx)^n}. \quad (4.8)$$

When K_p is given, x is acquired by solving this equation. The density of the metal vapors formed by the dissociation in each temperature is calculated with x:

$$n(\mathrm{M}) = x\, \Sigma n(\mathrm{M}). \quad (4.9)$$

Where $\Sigma n(\mathrm{M})$ denotes the total vapor density of the metal species in a temperature T, which is given by

$$\Sigma n(\mathrm{M}) = p\, N_A / RT \qquad (N_A : \text{Avogadro's number}). \quad (4.10)$$

The densities of the other vapor species (MI, MI_2, MI_3) are calculated with the following equations:

$$n(\mathrm{MI}) = x'(1-x)\Sigma n(\mathrm{M}), \quad (4.11)$$

$$n(\mathrm{MI_2}) = x''(1-x')(1-x)\Sigma n(\mathrm{M}), \quad (4.12)$$

$$n(\mathrm{MI_3}) = (1-x'')(1-x')(1-x)\Sigma n(\mathrm{M}). \quad (4.13)$$

where x' and x'' are the solutions of Eqs. (4.8') and (4.8'') when $p' = (1-x)/(1+3x)p$ and $p'' = (1-x')/(1+2x')p'$ are substituted.

$$K_P' = \frac{n^n p'^n x'^{n+1}}{(1-x')(1+nx')^n} \quad (4.8') \qquad K_P'' = \frac{n^n p''^n x''^{n+1}}{(1-x'')(1+nx'')^n} \quad (4.8'')$$

Table 4.2 Parameter a, a', b, and b' for the approximation equations of Gibb's energy changes $\Delta G = a - bT$ (based on thermodynamic data) and $\Delta G' = a' - b'T$ (based on spectroscopic measurement or model calculation) in the dissociation reaction $MI_n(g) \rightarrow M(g) + n\, I(g)$

Iodides	a	b(x10³)	a'	b'(x10³)	a–a'	b–b'(x10³)
NaI	536.2	179.8	290.7	165.6	245.5	14.2
ScI	602.7	101.3	–83.8	104.8	686.5	–3.5
CsI	279.8	58.0	267.8	49.6	12.0	8.4
TlI	286.0	94.3	277.2	91.9	8.8	2.4
DyI	410.5	88.3	16.3	116.3	394.2	–28.0
ScI_2			280.3	249.3		
DyI_2	1379.8	33.4	380.0	255.5	999.8	78.2
ScI_3	1676.2	32.5	435.1	280.8	1241.1	43.9
DyI_3	1558.7	36.9	611.1	287.3	947.6	82.1

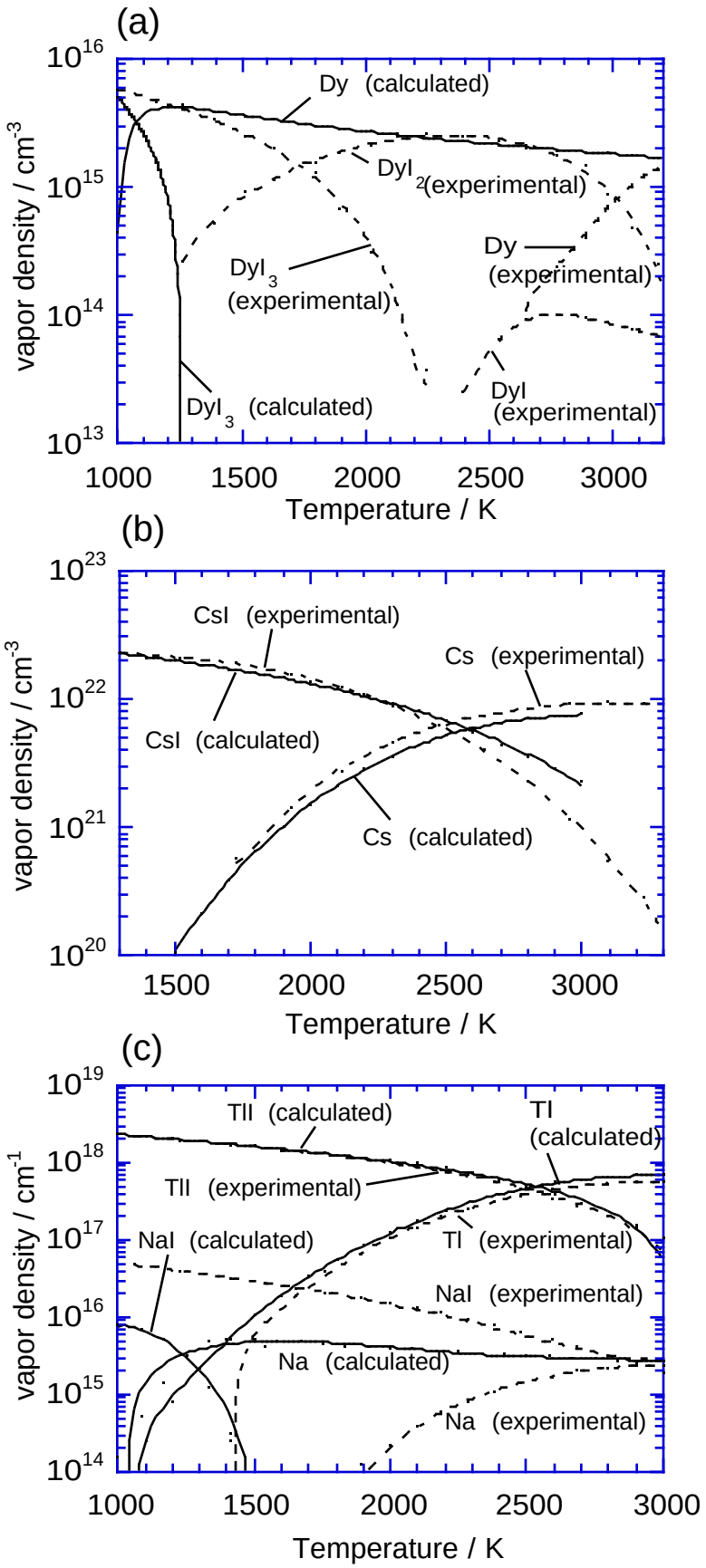

Figure 4.2 Vapor densities of the metal and iodides in (a) DyI_3/Hg, (b) CsI/Hg, and (c) TlI/NaI/Hg arc discharge lamps as a function of temperature. The solid and dashed lines denote the

4.3 Results and Discussion

4.3.1 Comparison with the experimental data

Figure 4.2 shows the comparison of the densities calculated by the known thermodynamic functions with those experimentally determined [58, 59, 63]. While the difference between the experimental and calculated values was small for the cesium and thallium iodides, the great difference was observed for the sodium and rare earth iodides. The experimental density values of the metal vapors formed by these iodides at high temperatures were smaller than the calculated one.

We tried to estimate apparent Gibb's energy changes of the dissociation of the metal iodides (Eq. (4.2)) from the experimental data [58–63] to elucidate their dissociation and stabilization behavior in the metal halide arc discharge from a thermodynamical point of view. In the dissociation reaction, the fraction x of the metal vapor in the vapor phase is calculated by

$$x = n(\mathrm{M}) / \Sigma n(\mathrm{M})$$
$$= n(\mathrm{M}) / (n(\mathrm{MI}_n) + n(\mathrm{MI}_{n-1}) + \cdots + n(\mathrm{MI}) + n(\mathrm{M})). \quad (4.14)$$

where $n(\mathrm{MI}_n)$ are the densities of the vapor species MI_n (n = 1–3). The pressure equilibrium constant K_p of Eq. (4.2) is obtained by Eq. (4.8), and the apparent ΔG values in the dissociation reaction are calculated from the obtained equilibrium constants by

$$\Delta G = -RT \ln K_\mathrm{p}. \quad (4.15)$$

The first-order equation $\Delta G' = a' - b' T$ was obtained by the least-squares method in a similar manner as above. Table 4.2 summarizes the parameters a' and b' of the equation.

For CsI and TlI, the values of the parameters a' and b' were fairly close to those of a and b, respectively. On the other hand, the value of a' was much larger than that of a for NaI. Since the parameters a and a' represent the average enthalpy changes of the dissociation of a iodide as described above, it is concluded that the apparent stability of NaI is enhanced in the metal halide arc discharge. The difference of the parameter Δb ($= b - b'$), in the monoiodides increases with decreasing the molecular weight. Then, the equation was derived for Δb in the monoiodides as follows:

$$\Delta b = 0.0242 - 0.06426\, M. \quad (4.16)$$

Where M is molecular weight. The difference of the parameter Δa ($= a - a'$) for the monoiodides except NaI follows the relationship of

$$\Delta a = 23.466 - 44.209\, M. \quad (4.17)$$

For the rare earth iodides, the relationship between their molecular weight and the difference Δa and Δb was obtained according to the following schemes:

$$\Delta a = 1670.2 - 2486.9\, M, \tag{4.18}$$

$$\Delta b = -0.011804 + 0.32436\, M. \tag{4.19}$$

As in the case of NaI, the value of a was much larger than that of a' in both rare earth iodides. In order to determine the magnitude of their apparent stabilization, the Gibb's energy changes for the following three steps of the dissociation were calculated

$$RI_3\,(g) \rightarrow RI_2\,(g) + I\,(g) \tag{4.20}$$

$$RI_2\,(g) \rightarrow RI\,(g) + I\,(g) \tag{4.21}$$

$$RI\,(g) \rightarrow R\,(g) + I\,(g) \tag{4.22}$$

The resulting Gibb's energy changes are listed in Table 4.3. Among the three reactions, the smallest and largest Gibb's energy changes of the dissociation were obtained for Eq. (4.20) and Eq. (4.21), respectively. The difference in the parameter Da is especially large for Eq. (4.21) and Eq. (4.22). This suggests that the rare earth diiodide is readily formed, while the dissociation of the diiodide is relatively hard to proceed because of the increase in the Gibb's energy changes of Eq. (4.21) and Eq. (4.22).

Table 4.3 Gibb's energy change for the dissociation reactions of rare-earth iodides derived from sepectroscopic data or model calculations and the thermodynamic data listed in Table 4.2

	ΔG_T (kJ mol^{-1})	
	from spectroscopic measurement	
Reaction	or model calculation	from thermodynamic data
ScI_3		
$ScI_3\,(g) \rightarrow ScI_2\,(g) + I$	$86.48–33.6\times10^3\,T$	$154.82–31.53\times10^3\,T$
$ScI_2\,(g) \rightarrow ScI\,(g) + I$	$987.01–189.85\times10^3\,T$	$364.03–144.48\times10^3\,T$
$ScI\,(g) \rightarrow Sc\,(g) + I$	$602.71–101.3\times10^3\,T$	$–83.75–104.79\times10^3\,T$
DyI_3		
$DyI_3\,(g) \rightarrow DyI_2\,(g) + I$	$178.89–35.62\times10^3\,T$	$231.07–31.77\times10^3\,T$
$DyI_2\,(g) \rightarrow DyI\,(g) + I$	$969.26–245.41\times10^3\,T$	$363.68–139.22\times10^3\,T$
$DyI\,(g) \rightarrow Dy\,(g) + I$	$410.54-88.33\times10^3\,T$	$16.34–116.3\times10^3\,T$

The apparent Gibb's energy change of the dissociation of the metal iodides in the metal halide lamps is generally expressed as

$$\Delta G = \Delta H_{av} + \Delta a + (\Delta S_{av} + \Delta b)\, T. \qquad (4.23)$$

If the thermodynamic quantities are known, Eq. (4.23) is applicable to the other iodides whose partial pressure distribution have never been experimentally estimated. Among the same kind of the iodide (monoiodide or triiodide), the smaller the molecular weight of the iodide is, the larger the increment of the average enthalpy change (Δa) becomes. The increase in the enthalpy change is explained on the basis of the diffusion of the iodides into the arc. The diffusion rate of the iodide in the lamps is faster than its dissociation rate into the metal. Therefore the diffusion precedes the dissociation, and the dissociation temperature is apparently shifted to the high temperature side. That is the iodide is apparently stabilized. There are two possible diffusion mechanisms in the metal-halide lamp systems: chemical transport and convection. The deviation from equilibrium mainly results from the latter effect. Larger the amount of mercury sealed in the lamps, larger the effect of convection on diffusion of the iodides. In all the lamp systems under consideration, however, filled amount of mercury was almost the same (32–36 mg). It was also observed that effect of convection is especially large for NaI compared to TlI [79]. Therefore, the iodide with smaller molecular weight is subject to diffuse faster, and the deviation becomes larger.

4.3.2 The reliability of equations

For CsI, TlI, and DyI_3, the vapor density values derived from Eq. (4.23) fairly agreed with the original values obtained experimentally at a temperature range of 1000 to 3000 K. Especially in the case of DyI_3, the derived vapor density profile was much closer to the experimental one (Figure 4.3) than that estimated only with the known thermodynamic data (Figure 4.2 (a)). This indicate that it is possible to predict the vapor density distribution for these iodides in the metal halide arc discharge with the obtained Gibb's energy equation.

On the other hand, an apparent deviation was observed for NaI and ScI_3. While the obtained vapor density values in these cases almost agreed with those experimentally estimated in high temperatures more than 2500 K, the deviation increased with decreasing temperature. It seems that this deviation is attribute to the formation of vapor complexes, which are the volatile compounds formed by the reaction of rare earth iodides with alkaline metal iodides at high temperatures [72–78]

$$RI_3\,(g) + AI\,(g) = ARI_4\,(g) \qquad \text{(A: Alkaline metal, R: Rare earths)} \qquad (4.24)$$

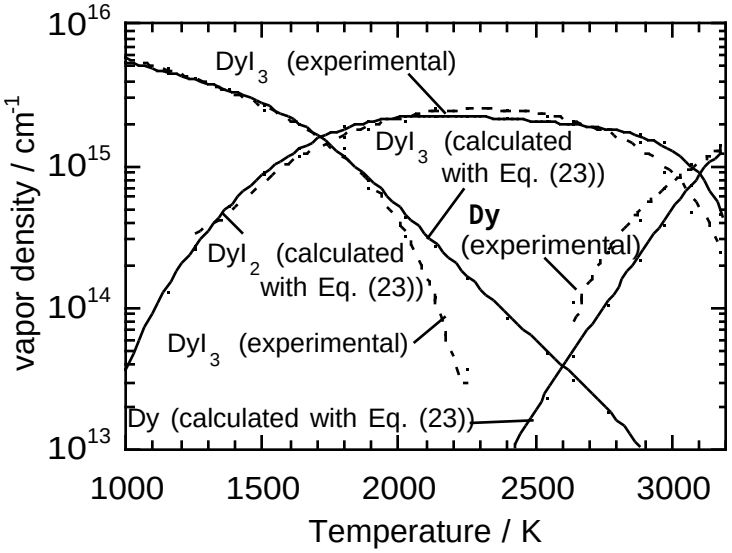

Figure 4.3 Vapor density of dysprosium metal and iodides in DyI_3/Hg arc discharge lamps as a funcion of temperature. The solid and dashed lines denote those calculated with Eq. (4.23) and experimental ones, respectively.

The apparent vapor pressure of rare earth iodides largely increases by the formation of the vapor complexes. The correction of the vapor density values of ScI_3 and NaI was tried by assuming the formation of vapor complexes. In the ScI_3-NaI system, a vapor complex $NaScI_4$ evaporates at the wall temperature, diffuses into the center of the arc, and decomposes into the rare earth iodide and sodium iodide

$$NaScI_4\,(g) \rightarrow ScI_3\,(g) + NaI\,(g) \qquad (4.25)$$

The resulting ScI_3 dissociates according to Eq. (4.2). When $\Sigma n(ScI_3)$ denotes the total number density of all the scandium species except $NaScI_4$, $\Sigma n(ScI_3)$ is calculated using the density of scandium metal n(Sc) in the literature data and the calculated value of x as follows:

$$\Sigma n(ScI_3) = n(Sc) / x. \qquad (4.26)$$

The fraction of the scandium species, X, formed by the decomposition of $NaScI_4$ in the total scandium species is given by $X = \Sigma n(ScI_3) / \Sigma n(Sc)$, and the equilibrium constant of Eq. (4.25) is obtained from

$$K_{\text{P, Eq. (4.25)}} = p \cdot X^2 / (1 - X^2). \qquad (4.27)$$

The Gibb's energy change of the decomposition was calculated with $K_{\text{P, Eq. (4.25)}}$. The least-squares method was carried out for the plot of the Gibb's energy changes for Eq. (4.25) against temperatures. The obtained equation is

$$\Delta G_{\text{Eq. (4.25)}} = 645.08 - 0.21402\,T. \qquad (4.28)$$

The average enthalpy and entropy changes for Eq. (4.25) are ΔH_{av} = 645.08 kJ mol^{-1} and ΔS_{av} = – 0.21402 kJ K^{-1} mol^{-1}, respectively . This ΔH value is much larger than the literature value at 731 K (223 kJ mol^{-1}). The great difference between the two ΔH values is ascribed to the apparent stabilization of $NaScI_4$ as a result of its faster diffusion rate by convection compared to the dissociation reaction rate as in the case of the binary metal iodides. The corrected density of the scandium vapor is given by

$$n(\mathrm{Sc}) = x \cdot \Sigma n(\mathrm{ScI_3}) = x \cdot X \cdot \Sigma n(\mathrm{Sc}). \qquad (4.29)$$

The density of the other vapor species were also corrected with X. In this case, the density of ScI_3 is the sum of those of ScI_3 and $NaScI_4$.

$$n(\mathrm{ScI_3}) = \{(1 - x'') \cdot (1 - x') \cdot (1 - x) \cdot X + (1 - X)\} \Sigma n(\mathrm{Sc}) \qquad (4.30)$$

The similar correction was also carried out for NaI. The almost same distribution of the vapor density as the experimental one was obtained as a result of the correction. Figure 4.4 shows the vapor density profile of the Sc metal and iodides estimated with Eq. (4.23) before and after the correction. One can see that the difference between the vapor profiles, which is due to the existence of the vapor complex, is gradually reduced with increasing temperature. It is reasonable to assume that the vapor complex formed at the tube wall decomposes successively, as it diffuses into the arc and the temperature increases.

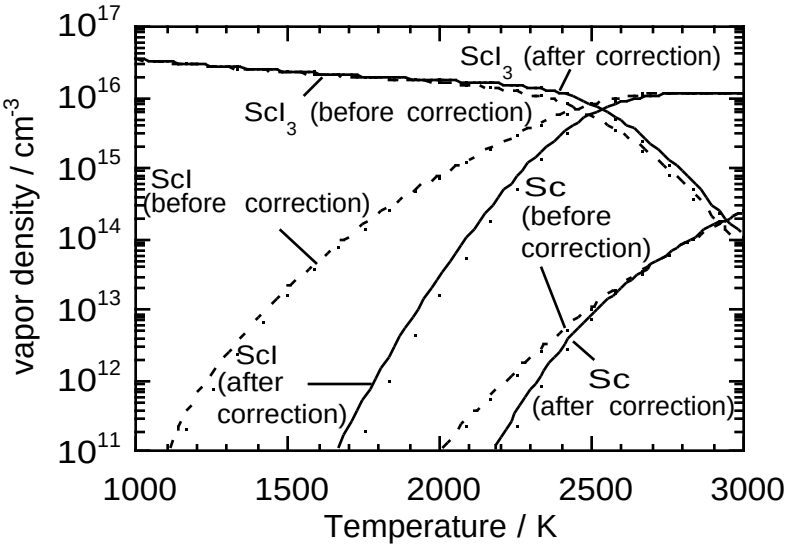

Figure 4.4 Vapor density of the scandium metal and iodides in ScI_3/NaI/Hg arc discharge lamps as a function of temperature. The solid and dashed lines denote the calculated ones before and after correction, respectively.

4.4 Conclusion

The vapor density of the metal vapors occurred in the metal halide arc discharge can be estimated approximately with the first-order equation of Gibb's energy change of the metal iodide dissociation derived from the thermodynamic data and the increments of the enthalpy and entropy changes which are due to the stabilization of the iodide and dependent on the molecular weight of the iodides. It is possible to calculate the increments, and subsequently to estimate the vapor densities for the other metal iodides whose partial pressure distribution have never been experimentally estimated. The calculated vapor density distribution agree with that experimentally estimated for CsI, TlI, and DyI_3. Though the density values calculated with the equation are larger than the experimental ones in the ScI_3-NaI system, they are corrected by considering the enhancement of volatility of the iodide by vapor complex formation. The apparent stabilization of both of the metal iodides and vapor complexes, which results from their faster diffusion rate compared to the dissociation rate, is suggested, and the metal iodides with a smaller molecular weight are inclined to be more stabilized.

Summary

In the work of this thesis, chemical vapor transport reaction mediated by metal halide gaseous complexes has been investigated and applications of the reaction to metal extraction process and materials processing process were attempted. The results obtained through this work are summarized as follows:

Chapter 1. The chemical vapor transport efficiency for pure yttrium chloride YCl_3 mediated via RAl_nCl_{3+3n} vapor complex was measured and compared with those of lanthanoid chloride $LnCl_3$ (Ln=Dy, Ho, Er), in which these four kinds of rare earth ion R(III), especially Ho, Y and Er, have very similar ionic radius values. Mutual separation of the binary systems YCl_3-$LnCl_3$ and Y_2O_3-Ln_2O_3 (Ln=Dy, Ho, Er) was conducted by the CVT process via the gaseous complexes $RKCl_4$. The "unexpected" CVT experimental results, both expressed as the lowest CVT efficiency and the lowest gaseous complex stability for YCl_3 with respect to the ionic radius of Y (III) compared with those of $LnCl_3$ (Ln=Dy, Ho, Er), were observed and discussed on the basis of the difference in the ionic structure and electronic configuration of Y (III) with those of Ln(III) (Ln=Dy, Ho, Er). Further, the improved separation factor of bEr/Y (1.52) and bDy/Y (1.35) were obtained by optimizing both of the temperature gradient and the flow rate of the carrier gases for these systems.

Chapter 2. A dry recovery process for rare earths from used polishes has been investigated by using a chemical vapor transport method via the formation of vapor complexes RAl_nCl_{3+3n} (R = rare earth). The used polishes were chlorinated with N_2 + Cl_2 gas mixture at 1273 K, and the resulting rare earth chlorides were transported chemically with the vapor complexes along the temperature gradient. Most of rare earth chlorides, $AlCl_3$, and $FeCl_3$ were transported during 82 hours of heating. The rare earth chlorides were mainly condensed over the temperature range of 1263–903 K. On the other hand, $AlCl_3$ and $FeCl_3$ were deposited at temperatures below 413 K. The highest $LaCl_3$ and $CeCl_3$ purity of about 80% was obtained in the process.

Chapter 3. Surface modification of CeO_2-ZrO_2 solid solutions took place using formation

and transport of volatile vapor complexes such as $AlCl_3$-$CeCl_3$ and $AlCl_3$-$ZrCl_4$, which was denoted as "chemical filing." XPS analysis showed surface Ce enrichment, and transmission electron microscopy and Raman spectra revealed that defective phase was formed on the surface of the samples by the chemical filing. The reduction temperature of the samples after the chemical filing was about 50 K lower than that of the fresh sample, and further decreased by a reduction/reoxidation cycle. The redox property of the chemically filed sample was maintained even after the redox cycles at high temperatures, indicating its excellent durability compared to the solid solution prepared by a conventional procedure.

Chapter 4. Thermodynamics of dissociation of metal iodides into metal and iodine atoms in metal halide arc discharges was investigated for ScI_3/NaI/Hg, DyI_3/Hg, CsI/Hg, and TlI/NaI/Hg systems at the temperature range of 1000 to 3000 K. Densities of the metal vapors calculated in the systems with the common thermodynamic quantities of metal atoms and iodides in vapor phases were compared with those experimentally determined from spectroscopic measurements or model calculations. For CsI and TlI, the experimental and calculated density values were closed to each other. On the other hand, the experimental values were much smaller than the calculated ones for sodium and rare earth iodides because of diffusion of the iodides by chemical transport and convection in the discharges at high temperatures. Apparent Gibb's energy changes of the dissociation in the lamps were expressed as first-order equations of temperature containing the terms of the increments of the average enthalpy and entropy changes, which were dependent on the molecular weight of the iodides. The densities of metal vapors derived with the obtained equations were comparable to those experimentally determined for all the systems under investigation. A series of equations were applicable to estimating the vapor density distribution of the other metal iodides, whose partial pressure distribution had never been experimentally estimated.

References

[1] K. L. Nash, Separation chemistry for lanthanides and trivalent actinides, in K. A. Gshneider, Jr. and L. Eyring (eds.), Hand book on the Physics and Chemistry of Rare Earths, Vol. 18, Elsevier, New York, 1994, pp. 435.

[2] H. A. Øye and D. M. Gruen, *J. Am. Chem. Soc.*, **91**, 2229 (1969).

[3] (a) J. W. Hastie, High Temperature Vapors, Academic Press, New York, 1975. (b) H. Schäfer, *Angew. Chem. Int. Ed. Engl.*, **15**, 713 (1976).

[4] G. N. Papatheodorou, Spectroscopy, structure and bondings of high-temperature metal halide vapor complexes, in J. L. Gole an W. C. Stwalley (ed.), Metal Bonding and Interactions in High temperature Systems (ACS Symposium Series, Vol. 179), American Chemical Society, 1982, pp.309.

[5] K. Hilpert, *J. Electrochem. Soc.*, **136**, 2099 (1989).

[6] S. Boghosian and G. N. Papatheodorou, Halide vapors and vapor complexes, in K. A.Gshneider, Jr. and L. Eyring (eds.), Hand book on the Physics and Chemistry of Rare Earths, Vol.23, Elsevier, New York, 1996, pp. 435.

[7] J. Jiang, T. Ozaki, K. Machida, G. Adachi, *J. Alloys Compd*., **260**, 222 (1997), and references cited therein.

[8] K. Murase, K. Shinozaki, Y. Hirashima, K. Machida, and G. Adachi, *J. Alloys Compds*., **198**, 31 (1993).

[9] K. Murase, T. Fukami, K. Machida, and G. Adachi, *Ind. Eng. Chem. Res.*, **34**, 3963 (1995).

[10] Z.-C. Wang, J. Yu, and Y.-L. Yu, *Bull. Chem. Soc. Jpn.*, **69**, 2369 (1996)

[11] Z.-C. Wang, and Y.-H. Sun, *Chem. Lett.*, **1997**, 1113

[12] Z.-C. Wang, J. Yu, Y.-L. Yu, and Y.-H. Sun, *J. Alloys Compds*., **264**, 147 (1998).

[13] Y.-H. Sun, Z.-C. Wang, and L. Guo, *J. Alloys Compds*., **269**, 88 (1998).

[14] Y.-H. Sun, Z.-C. Wang, and L. Guo, *J. Alloys Compds*., **285**, 73 (1999).

[15] R. D. Shannon, *Acta Cryst.*, **A32**, 751 (1976).

[16] H. Schafer, Chemical Transport Reactions, Academic Press, New York, 1964.

[17] Z.-C. Wang and L.-S. Wang, *Inorg. Chem.*, **36**, 1536 (1997).

[18] L.-S. Wang, R.-J. Gao, Y. Su, and Z.-C. Wang, *J. Chem. Thermodynamics*, **28**, 1093 (1996).

[19] Z.-C. Wang and L.-S. Wang, *J. Alloys Compds*., **265**, 153 (1998).

[20] Z.-C. Wang, L.-S. Wang, R.-J. Gao, and Y. Su, *J. Chem. Soc., Faraday Trans*., **92**, 1887 (1996).

[21] Z.-C. Wang, Y.-H. Sun, and L. Guo, *J. Alloys Compds*., **287**, 109 (1999).

[22] D. L. Zagari, *Ceram. Eng. Sci. Proc.*, **16**, 302 (1995).

[23] D. Parton, *Glass*, **73**, 531 (1996).

[24] I. Gaballah, E. Allain, and M. Djona, *Metall. Trans. B*, **28B**, 359 (1997).

[25] I. Barin and O. Knacke, Thermodynamic Properties of Inorganic Substances, Springer, Berlin, 1973.

[26] I. Barin, O. Knacke, and O. Kubaschewski, Thermodynamic Properties of Inorganic Substances (Supplement), Springer, Berlin, 1977.

[27] O. G. Polyachenok, *Russ. J. Phys. Chem.*, **40**, 1203 (1966).

[28] I. Gaballah, M. Djona, and E. Allain, *Metall. Trans. B*, **26B**, 711 (1995).

[29] K. C. Taylor, Automobile catalytic converters, in J. Anderson and M. Bouder (eds.), Catalysis—Science and Technology, Springer-Verlag, Berlin, 1984, Vol. 5.

[30] H. C. Yao and Y. F. Yu. Yao,, *J. Catal*., **86**, 254 (1984).

[31] A. Trovarell, *Catal. Rev. Sci. Eng.*, **38**, 439 (1996).

[32] M. Ozawa, M. Kimura, and A. Isoga, *J. Alloys Compds*., **193**, 73 (1993).

[33] T. Murota, T. Hasegawa, S. Aozasa, H. Matsui, and M. Motoyama, *J. Alloys Compds*., **193**, 298 (1993).

[34] C. de Leitenburg, A. Trovarelli, F. Zamar, S. Maschio, G. Dolcetti, and J. Llorca, *J. Chem. Soc. Chem. Commun.*, **1995**, 2181.

[35] F. Zamar, A. Trovarelli, C. de Leitenburg, and G. Dolcetti, In 11th International Congress on Catalysis - 40th Anniversary, J. W. Hightower, W. N. Delgass, E. Iglesia, and A. T. Bell (eds.), Studies in Surface Science and Catalysis; Elsevier Science B. V., 1996, Vol. 101, p. 1283.

[36] A. Trovarelli, C. de Leitenburg, G. Delcetti, *CHEMTECH*, **27** (3), 32 (1997).

[37] G. Balducci, P. Fornasiero, R. Di Monte, J. Kaspar, S. Mariani, and M. Graziani, *Catal. Lett.* **33**, 193 (1995).

[38] P. Fornasiero, G. Balducci, R. Di Monte, J. Kaspar, V. Sergo, G. Gubitosa, A. Ferrero, and M. Graziani, *J. Catal*., **164**, 173(1996).

[39] R. Vidmar, P. Fornasiero, J. Kaspar, G. Gubitosa, and M. Graziani, *J. Catal.*, **171**, 160 (1997).

[40] R. Di Monte, P. Fornasiero, M. Graziani, and J. Kaspar, *J. Alloys Comp*., **275–277**, 877(1998).

[41] P. Fornasiero, R. Di Monte, G. Ranga Rao, J. Kaspar, S. Meriani, A. Trovarelli, and M. Graziani, *J. Catal.*, **151**, 168 (1995).

[42] G. Balducci, P. Fornasiero, R. Di Monte, J. Kaspar, S. Meriani, and M. Graziani, *Catal. Lett.* **31**, 193 (1995).

[43] R. T. Baker, S. Bernal, G. Blanco, A. M. Cordón, J. M. Pintado, J. M. Rodríguez-Izquierdo, F. Fally, and V. Perrichon, *Chem. Commun*., **1999**, 149.

[44] S. Otsuka-Yao, H. Morikawa, N. Izu, and K. Okuda, *J. Japan Inst. Metals*, **59**, 1237(1995).

[45] N. Izu, T. Omata, S. Otsuka-Yao-Matsuo, *J. Alloys Compds*., **270**, 107(1998).

[46] S. Otsuka-Yao-Matsuo, T. Omata, N. Izu, and H. Kishimoto, *J. Solid State Chem.*, **138**, 47 (1998).

[47] B. Jezowska-Trzebiatowska, S. Kopacz, and T. Mikulski, The Rare Elements—Occurrence and Technology, Elsevier, Amsterdam, 1990.

[48] T. Masui, Y. Peng, K. Machida, and G. Adachi, *Chem. Mater.*, **10**, 4005 (1998).

[49] M. Yashima, H. Arashi, M. Kakihana, and M. Yoshimura, *J. Am. Ceram. Soc.*,**77**, 1067(1994).

[50] D. Michel, M. Perezy Jorba, and R. Collongues, *J. Raman Spectrosc.*, **5**, 163(1976).

[51] P. Fornasiero, J. Kaspar, and M. Graziani, *J. Catal.*, **167**, 576(1997).

[52] V. Perrichon, A. Laachir, G. Bergeret, R. Fréty, L. Tournayan, and O. Touret, *J. Chem. Soc. Faraday Trans.*, **90**, 773(1994).

[53] J. Kaspar, *Catal. Today*, **50**, 285(1999).

[54] H. Permana, D. N. Belton, M. Rahmoeller, S. J. Schmieg, C. E. Hori, A. Brenner, and K. Y. S. Ng., SAE Paper 970462, 1997.

[55] F. Zamar, A. Trovarelli, C. de Leitenburg, and G. Dolcetti, *J. Chem. Soc., Chem. Commun.*, **1995**, 965.

[56] T. Higashi, *J. Illum. Engng Inst. Jpn.*, **73**, 566 (1989).

[57] J. F. Waymouth, *Proc. IEEE*, **59**, 629 (1971).

[58] W. J. van den Hoek and J. A. Visser, *J. Appl. Phys.*, **51**, 174 (1980).

[59] J. H. Waszink and L. G. M. de Greef, *J. Appl. Phys.*, **49**, 5150 (1978).

[60] R. J. Zollweg and R. W. Liebermann, In Proceedings of the symposium on High Temperature Metal Halide Chemistry, Atlanta; D. L. Hilderbrand and D. D. Cubiciotti (Eds.), The Electrochemical Society; Princeton, N. J.,1977; Vol. 78-1, p.52.

[61] W. J. van den Hoek and G. Rouweler, Philips Res. Repts. 31, 23 (1976).

[62] R. O. Shaffner, *Proc. IEEE*, **59**, 622 (1971).

[63] E. Fischer, *J. Appl. Phys.*, **45**, 3365 (1974).

[64] K. Skudlarski and J. Kapala, *J. Chem. Thermodynamics*, **16**, 91 (1984).

[65] K. Hilpert, L. Bencivenni, and B. Saha, *Ber. Bunsenges. Phys. Chem.*, **89**, 1292 (1985).

[66] C. Hirayama, J. F. Rome, and F. E. Camp, *J. Chem. Eng. Data*, **20**, 1 (1975).

[67] D. E. Work, *J. Chem. Thermodynamics*, **13**, 491 (1981).

[68] R. Viswanathan and K. Hilpert, *Ber. Bunsenges. Phys. Chem.*, **88**, 125 (1984).

[69] L. Gmelin, Gmelin Handbuch der Anorganischen Chemie, SE B3; Springer-Verlag; New York,1974.

[70] C. W. Struck and J. A. Baglio, *High Temp. Sci.*, **30**, 113 (1991).

[71] C. W. Struck and J. A. Baglio, *High Temp. Sci.*, **31**, 1 (1991).

[72] C. S. Liu and R. J. Zollweg, *J. Chem. Phys.*, **60**, 2384 (1974).

[73] T. Foosnæs and H. A. Øye, *Acta Chem. Scand.*, **A35**, 81 (1981).

[74] O. Kaposi, L. Lelik, and K. Balthazar, *High Temp. Sci.*, **16**, 311 (1983).

[75] K. Hilpert and M. Miller, *J. Electrochem. Soc.*, **136**, 2199 (1989), and references cited therein.

[76] M. M. Metallinou, O. Herstad, T. Østvold, and G. N. Papatheodorou, *Acta Chem. Scand.*, **44**, 683 (1990).

[77] K. Hilpert and M. Miller, J. Electrochem. Soc., **137**, 1618 (1990).

[78] S. Boghosian and O. Herstad, *Polyhedron*, **13**, 1639 (1994).

[79] H.-P. Stormberg, *J. Appl. Phys.*, **51**, 1963 (1980).

[80] K. Murase, G. Adachi, M. Hashimoto, and H. Kudo, *Bull. Chem. Soc. Jpn.*, **69**, 353 (1996).

[81] G. P. Dudchik, O. G. Polyachenk, and G. I. Novikov, *Russ. J. Inorg. Chem.*, **14**, 1669 (1969).

[82] G. P. Dudchik, O. G. Polyachenk, and G. I. Novikov, *Russ. J. Phys. Chem.*, **43**, 1203 (1969).

[83] R. Berjoan and P. Meubus, *Metall. Trans. B*, **8B**, 461 (1977).

[84] T. Omata, H. Kishimoto, S. Otsuka-Yao-Matsuo, N. Ohtori, and N. Umesaki, *J. Solid State Chem.*, **147**, 573 (1999).

[85] G. Meyer and P. Ax, *Mater. Res. Bull.*, **17**, 1447 (1982).

[86] G. Meyer, *Inorg. Synth.*, **25**, 146 (1989).

[87] D. Kim, *J. Am. Ceram. Soc.*, **72**, 1415 (1989).

Acknowledgments

The author would like to express his most sincere gratitude to Professor Dr. Gin-ya Adachi, Department of Applied Chemistry, Faculty of Engineering, Osaka University, for his continuous guidance, many invaluable suggestions, and his heartful encouragement throughout this work.

The author is also indebted to Professor Dr. Yasuhiko Shirota and Professor Dr. Toshikazu Hirao for their valuable comments and suggestions in the course of this thesis.

The author is sincerely greatful to Associate Professor Dr. Ken-ichi Machida for his constant guidance and stimulating discussion, and Assistant Professor Dr. Toshiyuki Masui for his encouraging suggestions and obliging help for carrying out this study. The author expresses his gratitude to Dr. Nobuhito Imanaka and Dr. Hiroki Sakaguchi for their valuable suggestions and heartful advice.

The author makes grateful acknowledgement to Dr. Jianzhuang Jiang, Shandong University, and Dr. Kuniaki Murase, Kyoto University, for their helpful guidance and assistance.

The author desires to express his sincere thanks to Dr. Hideki Yoshioka and Dr. Hirokazu Izumi, Hyogo Prefectural Institute of Technology, for their assistance with X-ray photoelectron spectroscopy measurements, Dr. Kuniaki Tatsumi, Dr. Tetsuro Jin, and Dr. Tetsuo Yazawa, Osaka National Research Institute, for their assistance with Raman spectra measurements, and Assistant Professor Dr. Masaharu Eguchi, Research Center for Environmental Preservation, Osaka University for his assistance with X-ray fluoresence spectrometry and ICP-AES measurements.

The author gratefully acknowledges supplying starting materials with Shin-Nippon Kinzoku Kagaku Co., Ltd.

The author wishes to thank the author's coworkers Mr. Ken-ichi Nishikawa, Mr. Toshiki Miyazawa, and Mr. Kousuke Nakano. I would appreciate Dr. Yasuyuki Kobayashi, Mr. Masahiro Ito, Mr. Kenji Noguchi, Mr. Yumin Peng, Ms. Misa Yamamoto, Mr. Ryo Hamada, and all the other members of the research group of the Adachi Laboratory for their kind help, occasional discussion, and friendships.

Research Fellowships of the Japan Society for the promotion of Science for Young Scientists is greatly acknowledged.

Finally, the author is particularly grateful to his father, Mr. Akinori Ozaki, his mother Mrs. Hiroko Ozaki, and his brother, Mr. Syugo Ozaki, for their perpetual support and encouragement.